DESIGN AND IMPLEMENTATION OF A NOVEL, FUEL-FLEXIBLE, LABORATORY-SCALE, PREMIXED COMBUSTOR

By

BENOIT FOND

A THESIS PRESENTED TO THE GRADUATE SCHOOL
OF THE UNIVERSITY OF FLORIDA IN PARTIAL FULFILLMENT
OF THE REQUIREMENTS FOR THE DEGREE OF
MASTER OF SCIENCE

UNIVERSITY OF FLORIDA

2009

To my parents and my sisters

ACKNOWLEDGMENTS

I am very grateful to Dr. David Hahn for his constant support and advisement throughout my master's degree at the University of Florida. His scientific knowledge and intellectual curiosity have been a very valuable inspiration for me. In addition, Dr Hahn has always shown an unlimited patience and provided me encouragement.

I would also like to thank Mark Harris for sharing his great experience in the design of gas turbine combustors.

I acknowledge my sincere thanks to Dr William Lear for serving as a co-chair in my committee and to Dr Nicolo Omenetto and Dr David Mikolaitis for their valuable teaching and advice.

I am also thankful to my labmates (Bret, Prasoon, Phil, Michael A, Michael B, Richard and Sarah) to their contribution in making the laboratory a very pleasant place for research and discussion. Finally, I would like to thank my parents and my five sisters for their constant encouragement in pursuing my studies across the Atlantic.

TABLE OF CONTENTS

page

LIST OF TABLES

LIST OF FIGURES

LIST OF ABBREVIATIONS

NOx	nitrogen oxides
PAH	polycyclic aromatic hydrocarbons
A	section (m^2)
C_p	specific heat at constant pressure ($J.kg^{-1}.K$)
k	thermal conductivity ($W.m^{-1}.K^{-1}$)
$\dot{m}$	mass flow rate ($kg.s^{-1}$)
M	Mach number
P	pressure (Pa)
Q	heat (J)
R	universal gas constant (8.314 $J.K^{-1}.mol^{-1}$)
T	temperature (K)
V	volume (m^3)
α	absorptivity
ε	emissivity
λ	wavelength (m)
μ	dynamic viscosity ($Pa.s^{-1}$)
ρ	density ($kg.m^3$)
Φ	equivalence ratio
g	gas (subscript)
i	inlet (subscript)
o	stagnation condition (subscript)
l	liquid (subscript)
w	wall (subscript)
*	sonic condition (subscript)

Abstract of Thesis Presented to the Graduate School
of the University of Florida in Partial Fulfillment of the
Requirements for the Degree of Master of Science

DESIGN AND IMPLEMENTATION OF A NOVEL, FUEL-FLEXIBLE, LABORATORY-SCALE, PREMIXED COMBUSTOR

By

Benoit Fond

December 2009

Chair: David W. Hahn
Cochair: William E. Lear
Major: Mechanical Engineering

Recent developments in the production of fuels from alternative sources such as biomass raise a global interest in burning these highly variable fuels in gas turbine combustors. However, current low emission burner technologies and combustor stability are very sensitive to fuel composition. The current study aims at designing a fuel flexible combustion system which can be used for kinetic investigations, as well as a future candidate for low purity fuels combustion.

A novel premixed burner design has been created based on a concept of a forced recirculation by jet impingement and a strong stirring. A numerical investigation of the combustion performance has been performed on a fully detailed model to define an operative range of interest. The entire system has been designed to provide this range of operation based on detailed heat transfer cooling and gas dynamics injector models.

Optical and physical diagnostics capabilities have been implemented in order to provide insight into the reactor chemistry. This will allow the characterization of the combustor performance and kinetic investigation of alternative fuel combustion on the

one hand, and of the kinetic effects of CO_2 and H_2O in flameless combustion on the other hand.

CHAPTER 1
INTRODUCTION

Environmental awareness has been a leading force for gas turbine development in the recent years. The economic value of energy no longer includes only the processing cost from the fuel source to the fuel but attributes a real part to pollutant emission upon power generation. This latter part could take different forms such as the carbon tax on CO_2 emissions in Scandinavian countries, or the emission trading with the cap and trade policy in the United States. Since most of the pollutants are being initiated in the combustor, developments of this component have been crucial for emission abatements. In addition, with the progressive change in the fuel sources landscape, burners should now meet the challenge of the adaptability to promising alternative fuels along with a decreasing pollutant generation.

On future gas turbine combustors, different objectives should converge. The emissions abatement is of primary importance for both power generation and aircraft propulsion systems. Single digit nitric oxides and carbon monoxide emissions are becoming a reality in combustors, including new flameless configurations. Another motivation comes from scaling down the combustion systems. Having the highest heat release in the smallest volume is a priority in aircraft propulsion systems. This would reduce the weight, and so the overall fuel consumption. Reduced fuel consumption could also go along with improved efficiency requirements. In addition to these conventional trends, changes in the way we consider the fuel sources bring new considerations. Even though stability in the combustion system has always been a crucial point on aircraft combustors in which a flame should be anchored over a wide range of conditions during the flight, the localization and diversity of the alternative fuel

source candidates in ground power generation also calls for a need in developing stable fuel-flexible combustion systems.

Emission abatement has been mainly done in the last decade through the dry low NOx technology [1]. Different mechanisms have been identified in the generation of Nitric oxides such as the Zeldovich or thermal NOx mechanism and the Fenimore or prompt NOx mechanism. Overall, NOx emissions are strongly linked to the flame temperature. Therefore the main concept would be to operate in a lean regime so that the excess of air will lower the flame temperature. In addition, the mechanism of soot formation is very dependent on the local fuel to air ratio in the flame. Large gradients in the composition of the fuel air-mixture will lead to the formation of soot precursors. By mixing the air and the pre-vaporized liquid fuel upstream of the injector, a premixed combustion system delivers a nearly homogenous mixture decreasing significantly the amount of soot formed. However premixing flames offers a narrow range of stability compared to diffused burners, which makes lean premixed technology difficult to use in aircraft propulsion system.

In terms of emissions, significant decreases have been observed in dry low NOx systems burning natural gas, presenting a mole fraction of CH_4 varying from 70 to 90%. The current energy context offers a promoting force for investigation of alternative sources of fuels such as biomass and coal. However coal-derived synthesis gas, mainly syngas composed of hydrogen and carbon monoxide present combustion characteristics quite different from the well-investigated methane. Moreover, fuel supply may become more and more local as the diversification of sources become a reality, and therefore the composition of the syngas is expected to be highly variable. The

premixing concept used in dry low NOx systems is particularly sensitive to the composition of the fuel used. Currently; their performance is restrained to methane and their adaptability to the future fuel changes still needs to be assessed. Changes in fuel composition not only affect the emissions and heat release performance, but the other components of the air path such as the compressor and the turbine. Increase in air flow rate due to a lower heating value of the burning mixture may affect the compressor performance. Also, corrosive products could also be a major issue in material wear. Concerning the combustion itself, the oxidation chemistry plays a very important role, especially in premixed systems. Operability and emissions performance are therefore greatly influenced by the fuel composition. In premixing systems, the mixture of air and fuel is flammable far upstream of the injection point meaning that if the ignition delay is not sufficiently controlled, ignition could occur in an unexpected section of the system and could have some critical effects. An even more critical phenomenon would be a flashback on the air supply lines. Finally, if the chemistry dynamics are not sufficiently investigated, combustion limits could suddenly be reached (i.e. flameout) within small changes in operating conditions. A lot of efforts are now being done in order to investigate the oxidation of these exotic fuels through different experimental set ups in parallel with computer simulations. Information on the oxidation and pollutant formation kinetics could be extracted from different measurements, such as ignition delay, laminar flame speed, and flame blowout.

Shock tube experiments have been studied extensively and ignition delay correlations have been extracted for several fuels over a wide range of conditions using these systems. The ignition delay is also greatly influenced by fuel composition. These

experimental times could be compared with computer simulated values in order to develop a mechanism or a reactor model. Practically, auto-ignition at an undesired place could also damage the combustor. Kalitan and co-workers have studied ignition delays of CO/H_2/air mixtures behind reflected shockwaves at atmospheric conditions and elevated pressures [2]. They compared their experimental results to current kinetic models. This step is a critical precursor of the use of synthesis gas in power generation plant. Indeed, H_2 and CO have particularly low flammability limits and the combustion rates of a synthesis gas mixture are strongly related to the H_2/CO ratio. Shock tubes are actually based on a transient process but ignition delays can also be obtained from continuous flow devices and rapid compression machines.

The laminar flame speed is a concept based on premixed laminar flame combustion. It contains information on the kinetics of the combustion of the mixture but also on the diffusivity of its species, and related thermo chemistry [3]. Natarajan and co-workers burned CH_4/H_2/CO mixtures in Bunsen burner and wall stagnation flame reactors. They performed flame speed measurements with a charge coupled device (CDD) camera on the Bunsen flame, and laser Doppler velocimetry on the stagnation reactor. Premixed mixtures went from 5-95% for H2 and CO and up to 40% for CH4, and measurements have been done on preheated mixtures up to 700K, and at pressures ranging from 1 to 5 bars. Measurements could then be compared with some detailed methane oxidation mechanism such as the Gas Research Institute mechanism version 3 (GRI Mech 3.0). Detailed mechanism provides with kinetic rates of elementary reactions such as thermo chemistry of the species involved. The GRI 3.0 describes a

detailed mechanism appropriate to gas natural combustion. It includes the NOx formation and reduction but does not describe soot formation [5].

In addition, lean blowout measurements are often done on premixed pre-vaporized swirling flame combustor devices. Based on the concept of chemical time limited reaction, the residence time of the reaction at blowout could be linked to the reaction rates and compared with a reactor network model. Zhang et al. studied the effect of the composition of H_2/CO/CH_2 mixtures on lean blowout in a premixed gas turbine combustor (Zhang et al. 2007). However in this type of device, the lean blowout theory holds as long as the reaction time is larger than the mixing time scale. A non-homogeneous reaction zone will yield to other combustion regimes such as flamelets into eddy. In order to uncouple the convective and diffusive physical processes from the chemical reactions, a very strong mixing should be achieved such as in a well stirred reactor (WSR).

The well-stirred reactor theory has been extensively used as a modeling tool to investigate reactor behavior. The first experimental device considered as approaching the well-stirred reactor concept has been designed by Longwell and Weiss in 1953. Their primary motivation was to extract global reaction rates over different air/hydrocarbon mixtures [6]. In a well-stirred reactor, the composition inside the reactor is homogeneous. Therefore the exhaust composition is identical to the composition inside the reactor. The idea is that a residence time of the gases inside the reactor could be extracted which would put together the influence of the incoming flow, the temperature, the pressure inside the reactor and the volume of the reactor. This residence time could be given by the expression below:

$$t_{res} = \frac{\rho V}{\dot{m}} = \frac{PV}{\dot{m}RT}. \quad (0.1)$$

This time would represent in theory the time allowed for the chemical reaction to progress toward completeness. Just before blowout the maximum reaction rate is obtained.

The well-stirred reactor developed by Longwell and Weiss was brick insulated and a premixed pre-vaporized air-fuel mixture entered the reaction zone through central orifices creating sonic jets. The mixing forces created by these high velocity jets provided a strong homogeneity. Blowout measurements were performed for rich and lean mixtures. Later, some other well stirred reactors have been designed such as the hemispherical stirred reactor developed by Wright [7], and then Blazowski [8], or some conical reactors [9-10]. A significant advance has been made by the development of the toroidal jet stirred reactor developed by Nenniger [11]. In his device, a plug flow reactor was used in line with the WSR. An investigation of the mixedness of the reactor has been carried over this device and revealed some very small mixing times of 2×10^{-4} s for a reactor residence time of 5ms. Nenniger ran fuel rich air/acetylene and air/toluene mixtures in his 250mL reactor. Soot, PAH, light hydrocarbons and oxygen were probed over the length of the plug flow reactor corresponding to different residence times. This reactor was then extensively used by different researchers, for examples, to study the stability and emission of gaseous fuel [12], the emission characteristics of different liquid fuels [13], and later to characterize soot inception on ethylene/air mixtures [2004] .Well-stirred reactors have been a useful tool to understand emissions and soot formation. They represent an advanced combustion system that is primarily limited to kinetic

investigation purposes. The brick material and the shape of the combustor are not yet suitable to practical system for power generation. Moreover, the sonic stirring is not possible on high power system with considerable flow due to important pressure drops and material buckling limits.

The work presented in this thesis aims at developing a system which is inspired by the well stirred combustor systems but which may also be applicable to actual combustion systems, a micro turbine system used for semi cycle experiments. This system would need to be highly fuel flexible so to obtain combustion data over a wide range of mixtures and conditions and accurate control should be possible over a range of equivalence ratios, the air flow rates, and the temperatures. Also the combustor flow path should be simple enough to enable combustion modeling by reactor neural network so that reaction mechanisms can be investigated. And of particular importance, a state of art diagnostic should be implemented for combustion products characterization.

CHAPTER 2
STATEMENT OF SCOPE

Objectives of the combustion Rig

Reaction limited operation.

In liquid fuel combustion, three consecutive processes have to be considered. The breakout and evaporation of the liquid fuel into small droplets comes first, then the mixing between the fuel and air over the combustion volume and finally the oxidation reaction. In most of the practical systems, one of these three processes limits the consumption of the fuel. The coupling between these processes makes the chemical mechanism very difficult to investigate in a traditional non-premixed flame where composition varies throughout the flame.

Indeed in order to estimate reaction rate parameters, the concentration of the reactant and the temperature have to be known. The collision theory and empirical results provide the reaction rate expression for a bimolecular elementary reaction step:

$$A + B \rightarrow C + D, \tag{0.2}$$

in which the rate of reaction is:

$$\frac{d[A]}{dt} = -k[A][B], \tag{0.3}$$

and k is expressed by:

$$k(T) = AT^{b} \exp(-E_a / RT), \tag{0.4}$$

where A and b are some constants and E_a is the activation energy.

If the equivalence ratio, flow of the reactant, and temperature varies significantly in the flame, the access to kinetic rates would be very difficult. The ideal for fundamental

understanding would be to have an homogeneous mixture of vaporized fuel, air, diluents and products at a controlled temperature all over the reactor volume, so that one can compare the product composition (emissions) to a zero-dimensional set of inputs (temperature, flow of air, equivalence ratio, dilution ratio, pressure) for a given fuel. The values obtained could then be compared to computer simulation results based on a chemical mechanism and the well-stirred reactor theory. The reaction should be reaction rate limited. An ideal combustor would have its mixture instantaneously vaporized and mixed as soon as it enters the reactor volume. This objective has been approached by preheating the fuel and then spraying it into a vaporization chamber where it mixes with the air at an elevated temperature. Within a sufficient time between the spray and the injection, the liquid fuel should vaporize completely. Then the mixing into the combustor chamber is achieved in Jet Stirred reactor through a significant number of small orifices creating some sonic jets, stirring the reactor vigorously. In a gas turbine system, the sonic condition is hardly achievable. In fact the negative pressure gradients on the compressor liner wall due to a negative relative pressure would lead to wall buckling. In fact, the liner is generally very thin for weight reasons and the buckling limit is reached before the sonic regime.

Stability

The stability could be defined as the ability of a system to maintain combustion over a certain range of conditions. The stability performance can be considered either as the range of fuel air ratio over which a combustion regime could be sustained in the system, or either as the maximum air rate the system could accept without extinction at a given composition. This characteristic of the burner would be an objective for fuel flexibility. For example, the wider the operation range, the better the oxidation chemistry

could be understood. The phenomenon of blowout in which the flame is no longer attached to the injector and is “blown out” of the burner occurs at the limit of the often called “static stability” range It is opposed to dynamic stability or instabilities describing pressure oscillations which created damages in the combustor materials due to heat release rate variations [15]. In an ideal well-stirred reactor, the stability loop would be the widest for a given premixed mixture compared to all practical systems. Longwell and Weiss have published stability loops for a variety of fuels using their spherical reactor [16]. There are two dimensions in a stability loop. To understand the “static stability” concept, the energy balance in a well stirred reactor is illustrated on Figure 2-1, in which the curve trends are extracted from Nenniger’s PhD dissertation [11]. The heat generation is a complex function of the reactor temperature which depends on the complete reaction mechanism. The heat losses curve is a straight line if we consider an adiabatic reactor and a constant heat capacity mixture. To solve the energy equation in steady state means to equalize the heat generation and the heat losses so that the solution of the system is given by the intersection of the two curves. The lowest point corresponds to the case of a non-reactive mixture and the highest correspond to a flame regime. The intermediate point does not provide a stable solution as it is located on the decreasing rate of the heat generation so that steady state could not occur.

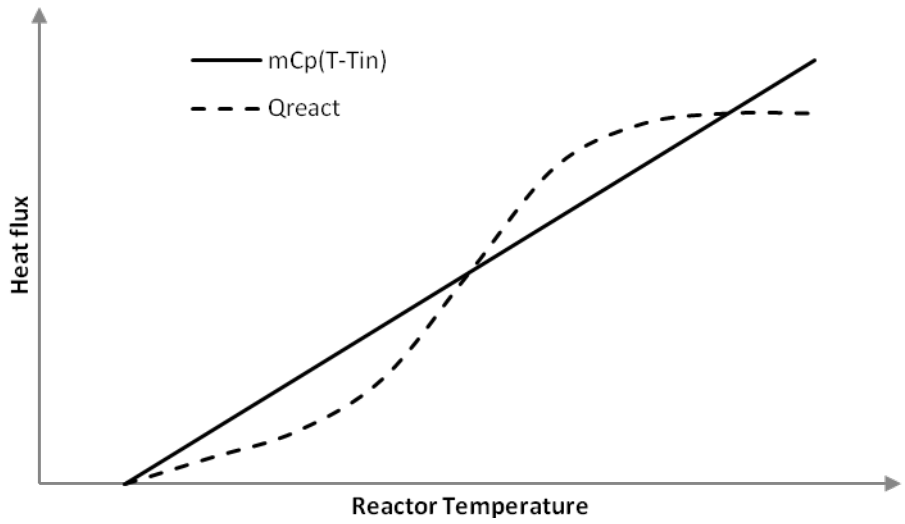

Figure 2-1. Heat balance in a Well Stirred reactor

The first dimension is the equivalence ratio. For a given mass flow rate, combustion could occur only between two equivalence ratio limits. On the lean side, the dilution of the air/fuel mixture with some additional air will decrease the reactor temperature, having a negative effect on the reaction rates. Indeed, the dilution effect will increase the slope of the heat loss curve and the higher intersection point will decrease on temperature. It can be seen on Figure 1-2 that in theory, there will be a point in which a further rotation of the heat generation curve will prevent the crossing of the two curves and so the only solution for the reactor will be at the feed temperature. On the rich side, blowout is still under active investigation, but the formation of soot and polycyclic aromatic compounds enhance the heat transfer to the wall due to blackbody radiation of the burning particles and the heat losses are getting significant. However, rich blowouts are more complex due the water-shift gas equilibrium and the fast reaction rate of H_2, the main product of the breakout of a rich hydrocarbon air mixture.

Another dimension for static stability is the one associated with the mass flow rate. For a given equivalence ratio, if one increases the air flow rate, the time allowable for reaction or residence time will decrease. The reaction will not be complete, thereby decreasing the reactor temperature, but in the same time the concentration in reactant will be more important. The concentration effect will outweigh the temperature drop, and the overall reaction rate will be faster and the flame will sustain. If one keeps increasing the flow, there will be a point where the temperature decrease effect on the reaction rate will be more important than the reactant concentration increase, and combustion will no longer occur.

Computer-based kinetic simulation can also be used in parallel with blowout data. Computer simulation will provide the steady state-energy equation solutions over a range of flow rate and equivalence ratio. If one is able to detect blowout with precision, one is provided with a valuable data set. Blowout is highly dependent on reactor pressure. The larger the pressure, the larger the air flow will be at blowout. Indeed the reaction rates are directly related to the concentration of the reactant given by the pressure and the mass fraction. The easiest way to get blowout data would be to maintain a low pressure in the combustor volume so that blowout occurs at the minimum flow rate without being limited by the compressor or other devices. Moreover, by running close to the blowout point means also running at lower temperature. These non equilibrium temperatures are also called kinetic temperatures. Therefore a direct access to the flame temperature by means of insulated thermocouple is simplified.

On a practical system, the stability loop is narrower. This is actually due to the heat losses on the one hand, and to the incomplete back mixing between the incoming

flow and the combustion product on the other hand. These two phenomena prevent the fresh mixture from reaching a sufficient temperature, which would for a given residence time lower the completion of the reaction. Inside the flammability limits a mixture will blow out if not enough heat is transferred to raise the incoming mixture to the auto ignition temperature. Different techniques have been developed in order to stabilize the flame in a practical gas turbine combustor evolving in a premixed mode. Bluff body flame holders and swirling vanes are used in ground based burners. In fact, a low velocity region would help the flame to sustain, as it would transfer heat to the fresh mixture by means of the recirculation of the hot combustion gases. In the aircraft industry, sequential burners are used as a way to provide better stability. A first burner is fuel rich and the incomplete combustion products go into a second burner provided with fresh air to terminate combustion. In addition, staged-combustion in which two or more mixtures of different equivalence ratios are injected at different positions, has shown significant stability improvements. In diffusion flames where eddies of fuel burn surrounded by air, the overall lean operation hides local rich-fuel regions which stabilize the flame. However, this type of combustion produces more pollutants and the reaction is vaporization-rate limited. Actually the stability and stirring criteria are one, hence a good mixing and a control over the heat losses is very important in the design.

Control and diagnostics

As discussed in the introduction, there are different ways of obtaining the kinetic parameters involved in the oxidation mechanism using some experimental devices. For all of them the accuracies on both the control over the inlet conditions and the measured variables (product composition, ignition delay) are critical to extract valuable data. The supply lines of air and fuel should be independently metered for mass flow

and temperature. As the equivalence ratio played a very important role in the oxidation chemistry, only small errors can be tolerated.

Also, an access to the reactor temperature would be very valuable. It would allow calculating the global residence time defined in Equation 1-1. However, an ideal well-stirred reactor could reach a very elevated temperature which is the adiabatic flame temperature of the mixture if the reaction evolves toward completion. Indeed adiabatic flame temperatures for air-fuel mixtures can reach more than 2000K at stoichiometric condition, with a peak for acetylene-air mixture at 2773K. Techniques for flame measurements include direct thermocouple measurement with a sheath insulated probe of platinum/rhodium which could be used up to 2600K. It also includes laser-based techniques such as coherent anti-stokes Raman spectroscopy (CARS). CARS involve the interaction between the laser wave and the vibrational spectrum of a molecule in a coherent manner and a directed signal could be collected. The difficulty of this technique stems from the fact that the pump and probe wave (often the same signal) should be finely tuned to be resonant with a single vibrational transition of the sample. In addition, the classical concept of WSR implies an adiabatic reactor. Even though this condition is approached well using brick insulation, this material is not acceptable in a practical system. Indeed fusing and crumbling of the liner would damage the turbine blades. In the Longwell's study of high temperature combustion rates [6], the liner had to be changed every 10 runs at very rich and very lean conditions, and every 2 runs for near stoichiometric equivalence ratio. As nickel-based alloy cannot stand more than 1400K, active cooling would be required in a system adaptable to a real gas turbine

system. Since heat losses could be implemented in a computer well-stirred reactor model, heat losses could be tolerated as long as they are precisely evaluated.

In a well-stirred reactor, composition at the outlet is supposed to be identical to the composition inside the reactor. Based on the inlet flow's composition and temperature on the one hand, and on the reaction mechanism and kinetic rates in the other hand, composition within the reactor volume could be evaluated using a computer-based model. In order to understand oxidation chemistry, an iterative process could be done in order to match the computer simulation to experimental results under different conditions. Therefore, diagnostics over the product composition is crucial. Also the product composition should not change considerably between the reactor volume and the position of the probe or this change should be controlled. Nenniger's toroidal jet stirred reactor includes two sections, a well stirred reactor and a plug-flow reactor [11]. Indeed, the well-stirred reactor was followed by a tube in which combustion kept evolving toward completion. In that case different sections over the length of the P.F.R will correspond to different residence times. A sequence of W.S.R and P.F.R could be simulated as well as a sequence of several WSR. Moreover, species composition diagnostics could be of different natures depending on the processes one wants to understand. These are generally of two types, real-time or gas sampling. Gas samples could be extracted from the reactor and composition analyzed by different methods such as gas chromatograph-mass spectrometer (GC-MS). The development of laser-based diagnostics has provided different real time techniques, especially on soot diagnostics such as Laser Induced Incandescence (LII) which can provide with particle size distribution and soot volume fraction [17].

Fuel and gases

The development of a reactor for kinetic investigation of exotic fuels includes a certain number of steps. Before running this fuel into the new system, the reactor characteristics themselves have to be investigated. Apart from the aerodynamics of the combustor, often studied for practical systems with planar laser induced velocimetry or using cold flow techniques, the kinetic model created for the combustor has to be adjusted on the basis of a reference fuel. Detailed oxidation mechanisms of several fuels have been developed at Lawrence Livermore National Laboratory (LLNL) or by the Gas Research Institute (GRI).

The current interest in liquid fuel oxidation and the publication of two versions of a detailed mechanism for n heptane by Lawrence Livermore laboratory led our choice for n-heptane as reference fuel. Indeed, Curran and coworkers at LLNL developed this mechanism based on rapid compression machine experiments, reflected shock wave ignition delay in shock tube, and well-stirred reactor experimental results [18]. The range covered by this mechanism goes from 1 to 42 atmospheres, temperature from 550 to 1700 K, and equivalence ratio from 0.3 to 1.5 and the nitrogen-argon level of dilution from 75% to 99%. Recently, Herzler and co-workers listed different experimental studies performed on n-heptane [19]. However most of the experimental studies presented here have been done relevant to high charge compression ignition engines (HCCI) and diesel engine by their range of pressure and temperature.

A second step of the implementation would concern some gaseous fuel. As for liquid fuel, the reference fuel, methane has been chosen. The GRI 3.0 Mechanism developed originally by the Gas Research Institute, provides a detailed mechanism for methane [4]. In addition LLNL provides two mechanisms on straight chain hydrocarbons

to respectively model NOx production with the first one, and soot and polycyclic aromatic hydrocarbons formation with the second one [20, 21].

A third step would be the test of exotic fuels and the investigation of different levels of dilution. Liquid fuel testing could include some synthetic fuel, for example from a Fisher-Tropsch (F-T) Process. By this process, synthesis gas obtained from biomass or coal gasification and composed mainly of CO and H_2 are transformed into mainly straight-chain hydrocarbon. For selectivity reasons, F-T synthesis takes place at low temperatures (150-300°C) and catalyst such as cobalt and Iron are used [22]. This process was invented in the 1920's by the two researchers of the Max Planck Institute who gave their names to it. At that time, Germany was very poor in petroleum product compared to other foreign nations (U.S.A, U.R.S.S, United Kingdom), but very rich in coal and lignite. Then with the militarization of the third Reich in the 1930's, a lot of effort was put in order to process liquid fuels for the military. Therefore, production of F-T fuel culminated during the war before the bombing of a large part of German oil factories. The United States showed in recent years a great interest in this process as part of the CO_2 capture technology. The Energy and Gas Dynamic System Laboratory at UF tested some F-T synthetic fuels and their operability has been demonstrated on a micro-gas turbine system [23]. This process is closely linked to the gasification process upstream and raises a huge scientific interest. Indeed, in the scope of reducing the CO_2 emission and so the human signature on global warming, the development of solar powered plant, and the investigation of catalysts such as Iron could increase significantly the energy content of syngas using the water-shift equilibrium. Therefore, an interest in syngas oxidation chemistry is raised and has been investigated through different studies

[3, 5, 15]. For these reasons above, runs with mixtures of $CO/H_2/CH_4$ and air representing different qualities of syngas is planned and especially low H_2 content mixture with a CO/H_2 ratio greater than 5.

In the current low emission research, the concept of vitiated combustion has been investigated for its NOx and soot emission reduction. In fact, a high level of dilution, in parallel with a high air inlet temperature creates a combustion regime characterized by a non-luminous flame, a homogeneous temperature, and a distributed reaction in the primary zone [24-29]. The inlet conditions could be in theory achieved with a recirculation of the hot exhaust gas. However in most system, the cooling of these exhaust gases has a detrimental effect on cycle efficiency. W.E Lear developed an innovative micro-turbine cycle where the cooling of the exhaust gases is provided by an absorption refrigeration plant [30]. This semi-closed cycle micro turbine has been derived to give the power water extraction and refrigeration system (PoWER) offering the advantages of a simultaneous generation of electricity, water steam, liquid water and refrigeration in parallel with lower emissions. On this system, a sharp decline in luminosity of the flame has been observed with the transition to the flameless combustion regime [31]. However, the studies carried on soot emission were conducted with commercial low-resolution optical equipment. The system designed in this thesis could be used for the development of state of art diagnostics technique on soot. Indeed the laboratory scale and the instrumentation would give a more flexible control over the combustion conditions, and the optical access at the exit of the primary zone would offer an interesting position for soot characterization. Also, in the gas turbine combustor system, a lot of physical processes are coupled such as vaporization of the fuel, mixing

and reaction. If one is able to uncouple these processes, one could be able to investigate the fundamental effect of dilution on the combustion regime. Therefore, the dilution of the flammable mixture with gases will be implemented. The products of hydrocarbon combustion at equilibrium are mainly composed of nitrogen, carbon dioxide, water vapor, carbon monoxide (for very lean or rich mixture), oxygen (lean mixture), and hydrogen (rich mixture) due to the water-gas shift and nitric oxide. Using a CANTERA reactor model developed by Singh [32], a reproduction in an open system of an exhaust gas recirculation could be achieved setting the inlet composition close to the simulated results.

As a summary, the fuel and gases that will be implemented in this burner are:

- Air, as the oxidizer
- N-heptane (C_7H_{16}),as a reference liquid fuel
- Natural Gas (mainly CH_4), as a reference gaseous fuel and a synthesis gas component
- Carbon Monoxide (CO), as a synthesis gas component and a diluent
- Hydrogen, as a synthesis gas component and a reference fuel
- Carbon Dioxide (CO_2), as a diluent
- Water vapor (H_2O) as a diluent
- Nitrogen (N_2) as a diluent and liquid carrier for water vaporization

From the considerations above, one can define the guidelines of the combustion rig. The combustor geometry and the injection system has to provide a fair amount of mixing giving a good homogeneity of the mixture inside the combustor zone under investigation. Comparison between the combustion characteristics of the actual system on a given fuel and the results from a widely investigated kinetic model representing this

combustor should be possible through adequate diagnostics techniques. Finally, the investigation of the combustion of the different fuels and gases listed before should be possible over the widest possible range of controlled inlet conditions (temperature, composition, flow rates).

Constraints and Limitations

The burner to be implemented is this study is integrated into a bigger system involving the fuel delivery, the air delivery, and the exhaust. Some technical limitations due to the other devices, which are part of the entire combustion system, will have to be considered in the design. The important parameter that must be determined for the design will be the reactor volume. In fact, given a volume of reaction and a range of residence time of interest, one can calculate the air flow needed for combustion and the quantity of liquid fuel needed.

Flow rates

The current laboratory cannot power an electrical device which requires more than 7.5 horse power. The compressor and the air heaters are the electricity consumers. A compressor of 7.5hp could in general deliver 24.2 ACFM (Actual Cubic Feet per Minute) at 175psi corresponding to 284 SCFM (Standard cubic feet per minute) using standard conditions at 60°F and 1 atmosphere. A dryer could be used to get rid of humidity .The SCFM units are in fact a mass flow rate as one can convert a volume into a mass given the temperature and the pressure so that 284 SCFM would be around 130g/s using the equation

$$\dot{V}_{ACFM} = \dot{V}_{SCFM} \left[\frac{P_{std}}{\left(P_{act} - P_{sat}\,\Phi\right)} \right] \left(\frac{T_{act}}{T_{std}} \right), \qquad (0.5)$$

where Φ is the relative humidity and P_{act}, P_{sat}, P_{act} respectively the actual, saturation and standards pressures.

As discussed before, one will also need some fresh air for cooling the hot material of the combustor. A heat transfer model must be programmed in order to estimate this flow at a given volume. The flow rate may be also limited by the fuel consumption. In fact by safety reason, one cannot store more than a certain volume of fuel. For this reason, the reference fuel consumption in continuous operation is limited to 1 gallon per hour.

Pressure

In combustion, the pressure has a very important role on the oxidation reaction rates. In fact the probability of collision between two molecules will increase considerably with a shorter mean free path due to a pressure rise, and so a rise in number density. However the effect on an elementary step will depend on its molecularity defined as the number of colliding molecular entities. In terms of blowout and stability, if one decreases the pressure on a given system, there will be a limit where the flame will blow out. By setting the pressure at a low level, one will need less air flow to reach an incomplete reaction regime and then a blowout. However, as the pressure decreases, the flow required gets smaller and smaller and so the bulk effect of the heat losses becomes very important.

If one recalls the energy equation in steady, one can get the expression:

$$\dot{m}C_p \frac{\partial T}{\partial x} = -\dot{q}'_{losses}, \tag{0.6}$$

where $\dot{q}'_{losses}$ is a linear heat flux. This latter term includes a constant term with respect to the mass flow of air representing the radiation heat flux and a power function of the

mass flow rate through the convective effects. The convective heat transfer rates in a gas turbine combustor are described in more detail in the heat transfer section of the Chapter 3. By decreasing the mass flow rate, the temperature gradient will get larger according to Equation 2.5 since there is a fixed part of the heat losses and a variable part in which the dependence on the mass flow rate is elevated to a power less than one. Moreover a negative relative pressure would raise some technical difficulties. Indeed, in this case, we would need to use a vacuum pump downstream of the combustion system to raise the pressure to the ambient and so drive the flow to the exhaust. This type of system is shown in Figure 2-2 A) with an arbitrary ¼ atmosphere pressure in the combustion primary zone. The exhaust gases being very hot, the control over the exhaust will need some expensive temperature resistant devices with a large volume flow rate rating. For these reasons, the design will try to get the smallest but positive relative pressure as possible in the combustion chamber. In this case, the system will be similar to the one in Figure 2-2 B). A compressor will alternatively drive the flow from the ambient to a tank on the basis of a duty cycle. The pressurized tank at a pressure up to 180 psia will deliver the air to the injection system at a decreased pressure using an expansion valve. The combustion pressure will be over the ambient so that the exhaust flow could be driven to the outside. Now, the combustion pressure will be dependent of the volumetric air flow and the pressure drop coefficient induced by the downstream exhaust pipe. It could even be controlled through a valve. Some advantages in this system would be the possibility to use the pressurized tank receiver to provide air to a small machine shop. The laboratory in which the combustion rig will

be installed is new and without compressor so the choice of the compressor and the design of the air supply is also part of the work realized in this thesis.

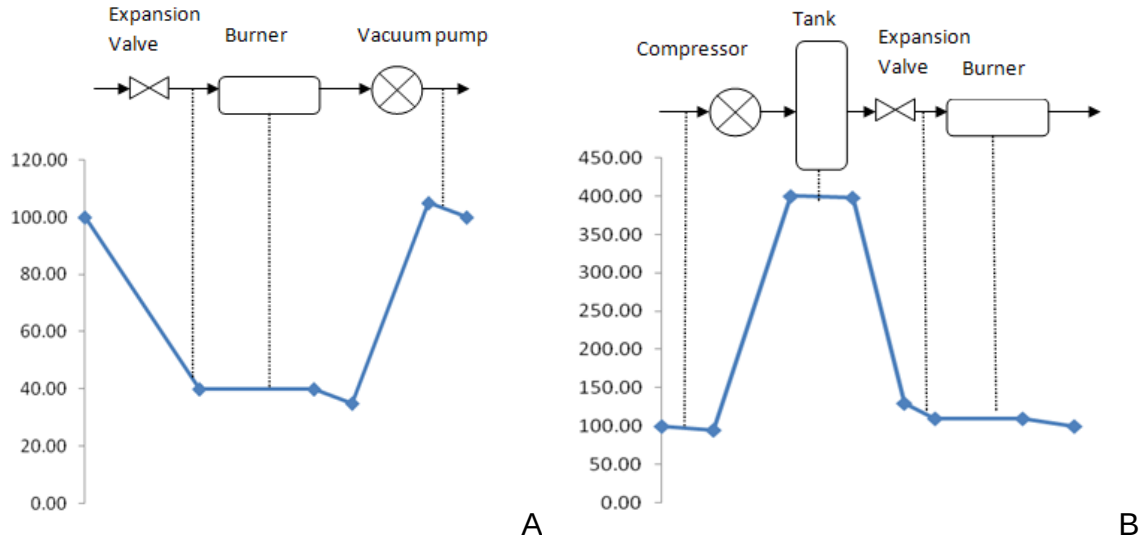

Figure 2-2. Absolute pressure evolutions (in kPa) along the flow path of a combustion system burning at negative pressure A) and a positive pressure B).

Volume

On the large size, the volume will be limited by the maximum flow delivered by the compressor. The minimum volume limit comes from the heat exchange are-to-volume ratio. As the diameter decreases, this ratio increases for an annular reactor. Moreover, there is a point where machining gets very difficult as the combustor is miniaturized. A kinetic simulation is presented on the following chapter in order to set the maximum volume size. In addition, a heat transfer model developed in Chapter 3 will estimate the heat losses on the combustion gas bulk temperature and determine if whether or not a volume is acceptable.

Inlet and reactor temperature

The inlet temperature is an important parameter for the stability of the reactor as well as the flame temperature or reactor temperature in a well-stirred system. Indeed, in

a WSR, the composition is homogeneous and so is the temperature. This is an idealized concept; however, in reality it can depend on heat transfer calculations to predict the limitation in terms of wall cooling and heat losses. Indeed the higher the flame temperature, the higher the heat transfer rates and the better the cooling should be to maintain the material of the combustor at a reasonable temperature. As an ideal, normal stainless steel alloy (SS 304) could in general hold a continuous 900K, a nickel-based alloy such as Inconel or Hastelloy could stand up to 1100K, and Molybdenum has a melting point at 2880 K. Considering the benefits of higher temperature, the hotter the inlet mixture, the more stable will be the flame. However for an air/fuel mixture in an ideal W.S.R, the increase in inlet temperature would imply an increase in flame temperature. In theory, within a sufficient residence time, a well-stirred reactor should reach the adiabatic flame temperature. Considering the reaction as adiabatic and that chemical equilibrium is reached, the entire heat release should raise the mixture to the adiabatic flame temperature. In Figure 2-3, the adiabatic flame temperature is plotted at constant pressure for $CH_4/O_2/N_2$ mixture for different mixtures and inlet temperatures.

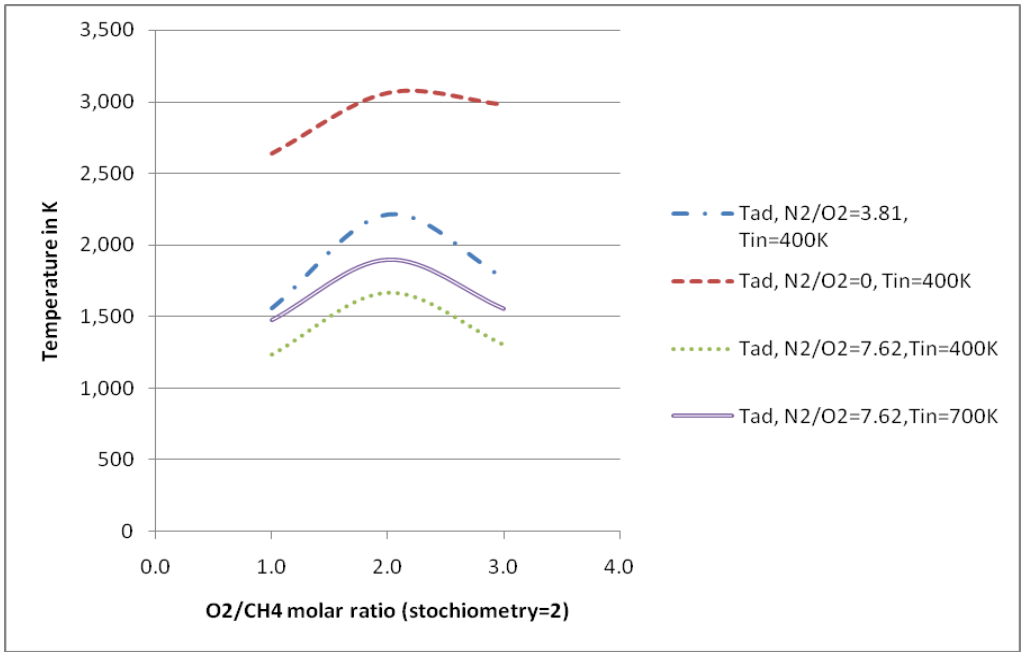

Figure 2-3. Adiabatic flame temperature for mixtures of $CH_4/O_2/N_2$

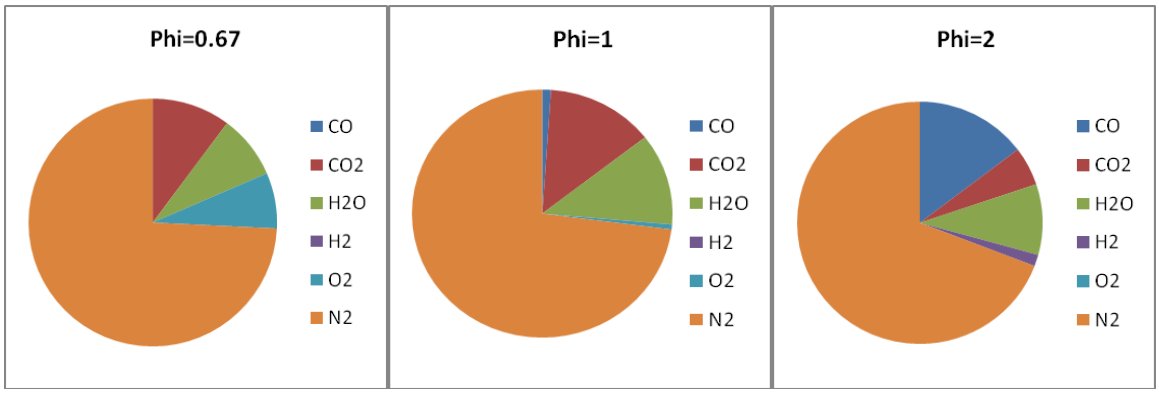

Figure 2-4. Composition at equilibrium for different methane-air mixtures at initial temperature of 400K and a constant pressure of 1 atmosphere.

These calculations were done using Cantera, on a GRI3.0 mechanism by fixing the enthalpy and the pressure. For a given oxygen-to-nitrogen ratio, the adiabatic flame temperature is maximum at a near stoichiometric mixture (O_2/CH_4=2). Indeed, the maximum heat of reaction per unit mass is obtained as almost all of the reactants are consumed to give CO_2 and water. Therefore the flame temperature versus equivalence

ratio curve is a bell whose top is near the stoichiometric point. The composition of the equilibrium mixture is shown on Figure 2-4. One can observe that for a stoichiometric mixture the products are essentially CO_2 and H_2O and N_2, and so the heat of reaction is maximized. On the lean side, one sees that a good part of the oxygen remains in the products, and so the inert oxygen consumes some of the reaction enthalpy to reach the adiabatic flame temperature. As one goes toward rich mixtures, the concentration of CO which enthalpy of formation is lower than CO_2 becomes predominant. For this reason, the combustion could be considered as incomplete as not all the CO is completely oxidized in CO_2 following the reaction:

$$2CO + O_2 \rightarrow 2CO_2. \tag{0.7}$$

The water-gas shift equilibrium is also involved on rich combustion leading to the formation of H_2 in the products. The reaction involved is:

$$CO + H_2O \rightarrow CO_2 + H_2 \tag{0.8}$$

Even though the mass fraction is low, the lightness of hydrogen hides a large molar fraction of 17.2% on Figure 2-4.As one goes toward a pure oxygen/fuel mixture, there is little or no inert species, and so less heat is needed to raise them to the final temperature, and therefore the remaining reacting species are heated to a higher temperature.

On the other side, as level of dilution by inert gases such as nitrogen is increased, the adiabatic temperature drops directly linked to the thermal effect of dilution. This type of combustion is of particular interest since the reactor is at a reasonable temperature and the gradient between the inlet temperature and the adiabatic flame temperature is

fairly small promoting a homogeneous reaction zone. This is one of the ideas behind flameless combustion or moderate and intensive low oxygen diluted combustion (MILD) as it is named in Italy. However the kinetic rates are very slow at 400K in a diluted regime, which could not be observed from adiabatic temperature results. Therefore, the flameless combustion concept is also called high temperature air combustion (HTAC) in Japan. The objective is to have a high inlet temperature together with a small temperature rise due to combustion. This high inlet temperature is typically obtained by an exhaust gas recirculation as mentioned above and the hot exhaust gases are cooled down to 700-800K mix with the fresh air and are injected back into the combustion chamber.

Most studies performed on WSR based their measurements on an air/fuel mixture inlet temperature of about 400K. For a premixed system, the advantages of this 400K is that this is below the auto ignition temperature of most of the fuels, which prevents ignition in the premixed section, and over the boiling point of the fuel, ensuring a pre-vaporization of this latter. Indeed the fuel in injected in the air stream and then the two mixes before being injected. If the air is at a temperature higher than the boiling point, heat will be transfer to the fuel to start its vaporization in the mixing section. Moreover, we want to prevent ignition upstream of the combustion chamber which would have damaging effects on the materials, so we do not want the air to reach the auto ignition temperature of the fuel. We will target a 400K temperature for the air over the entire range of flow rate achievable. Concerning the vitiated combustion regime (dilution with N_2 and other gases), we want to raise the inlet temperature to 700K but we will limit the

total flow rate so that no additional heating power will be required compared with the fuel/air combustion regime.

In Table 2-1, some important physical properties are listed for the different fuel planned to be implemented in the system. These results are extracted from International Chemistry Safety Cards (ISCS) and are more oriented on safety than on fundamental combustion properties. However, they could indirectly provide information applicable to premixed combustion systems design. For liquid fuel, the flashpoint is defined as the temperature at which the vapor pressure of the liquid fuel will provide in the gas-phase a concentration of fuel molecules high enough so that it forms a flammable mixture with the surrounding air. Practically, it would be the minimum temperature at which one can ignite a liquid fuel under ambient pressure using an ignition source. When the ignition source is removed, combustion would stop. Another temperature, important for both gaseous and liquid fuel is the auto ignition temperature. It is defined as the minimum temperature at which a flammable of air and gas mixture ignites spontaneously under a standard pressure (1 atmosphere). One should keep in mind that these concepts are empirical and of practical sense more than being fundamental values. Theory will tell that under ideal conditions, a mixture of air and fuel will always react after an infinite amount of time. In addition, safety standards organizations often relate to flammability limits. These tests are carried on vessels that contain a gas of a given composition. A spark plug is then used to ignite the mixture and if the mixture is inside the flammability limits, the flame propagates within the vessel volume. The energy that is provided to the mixture for ignition by the plug is called ignition energy. This ignition energy is also function of the temperature and composition of the mixture.

Table 2-1. Some physical and chemical properties of the different fuels involved. (NA: Not applicable)

Flammable fluid	ISCS 0001 Hydrogen	ISCS 0023 Carbon Monoxide	ISCS 0251 Methane	ISCS 0657 N-heptane
Boiling point	-253°C	-191°C	-161°C	98°C
Density (liquid phase/water)	NA	NA	NA	0.68
Vapor pressure at 20°C	NA	NA	NA	4.6kPa
Density (vapor phase/air)	0.07	0.97	0.6	3.46
Flashpoint	NA	NA	NA	-4°C
Flammability limits (in % vol)	4-76	12.5-74.2	5-15	1.1-6.7
Auto ignition temperature	500-571°C	605°C	537°	285°C

CHAPTER 3
DESIGN OF THE BURNER

System approach

As described in the previous chapter, the design of this entirely new combustion rig in a new building space will include all the gases and fuel supply lines and the exhaust. The air will be compressed, metered, and heated. The liquid fuel will be pumped, metered, heated and sprayed into the combustion air stream. The mixture of fuel and combustion air will be injected in the combustor primary zone. Some of the air will go directly to cooling passages, and then will mix with the combustion products. After combustion, these two streams will be exhausted outside. The different systems to design are represented in Figure 3-1. The first step in the design will be the combustor itself, because its performance defines all the other components of the system.

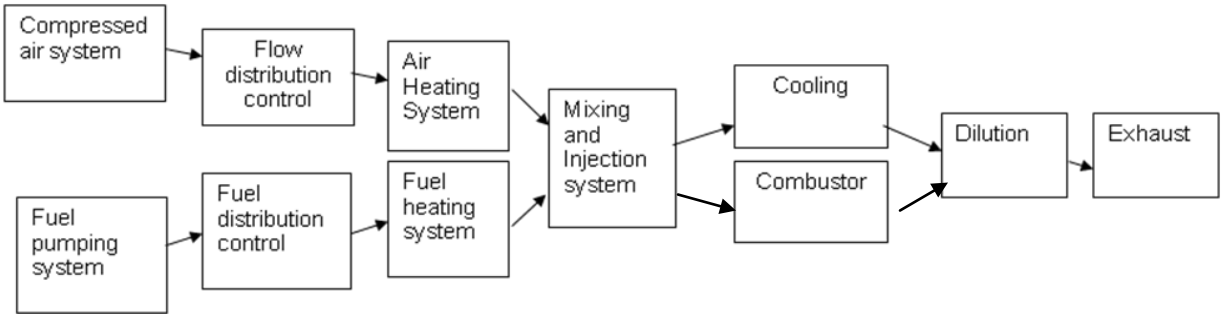

Figure 3-1. Combustion System approach for premixed liquid fuel/air mixture

Combustor Geometry

As described in the objectives, the geometry should allow a sufficient amount of back mixing in order to stabilize the flow and to provide a better homogeneity. Premixing of air and fuel in combustion has been seen in the past decades as a significant way to create low CO and NOx emissions in gas turbine combustors. Significantly low gradients in Fuel/air fraction of the mixture entering the primary zone prevent the formation of hot spots responsible for the formation of thermal NOx. For the same reason, a significant decrease in polycyclic aromatic hydrocarbons (PAH) production is obtained. Studies on premixed laminar flames showed that soot occurred only above a highly rich equivalence ratio [14]. However, premixing also brought stability issues in homogeneous mixtures, particularly as they operate near lean blowout. Stabilization techniques, such as bluff body and swirlers have been seen as a way to achieve significantly stable operation at low equivalence ratio. Re-circulating combustion gases transfer heat to the cool mixture, raising it to the auto ignition temperature. Longwell, and then Ballal and Lefebvre, have seen the recirculation zone as a homogeneous reactor [33,34]. The stabilization performance depends on the time for the cold mixture to enter the shear layer limiting the recirculation zone, the rate of entrainment of fresh mixture into the recirculation zone, and the residence time of gases inside the recirculation zone. However, in swirl-stabilized flames, vortex precession and breakdown phenomenon would be an important source of combustion instabilities so that active boundary control and Helmholtz resonators are often employed in current dry low NOx technologies [1]. The idea behind the current design is to provide back mixing based on jet impingement and flow split rather than large vortices structures.

The combustion zone geometry created in this project has been elaborated to provide this low velocity recirculation zone. This geometry is shown on Figure 3-2 and Figure 3-3. The annular combustor presented here is made of a hollow cylinder liner with a wall on one side and the exhaust on the other side. A smaller tube is mounted and the mixture is injected almost radially somewhere along the length of the liner. The fresh mixture will impinge at a fairly high velocity into the central tube so that part of it will be entrained toward the rear wall and the other part will go toward the exhaust where it will be later diluted with the liner cooling air. This design will provide a cross flow between the injection stream and the combustion products coming from the back of the reactor and so the heat transfer and mixing will be enhanced.

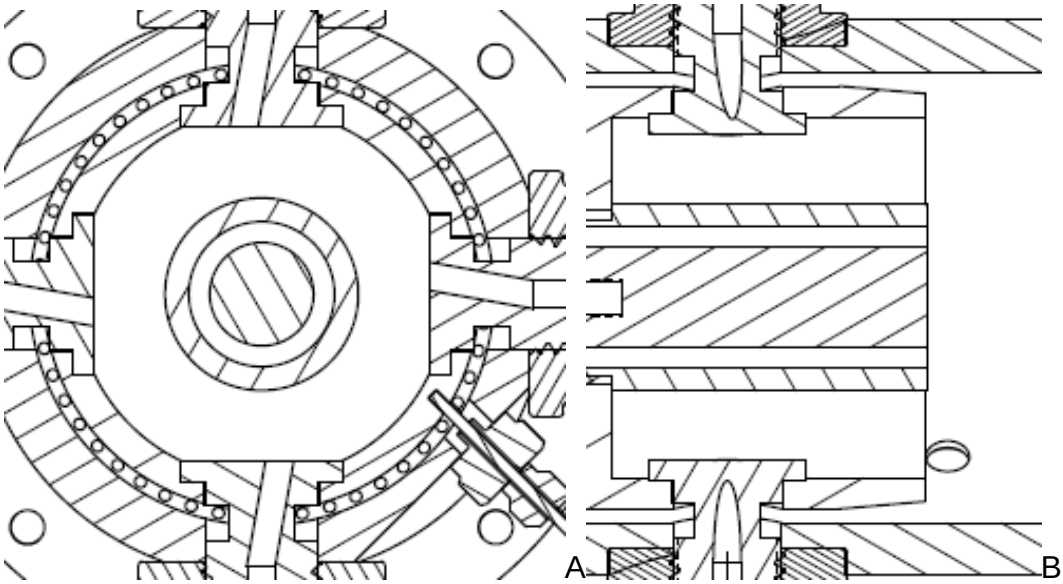

Figure 3-2. Normal A) and axial B) cut of the burner

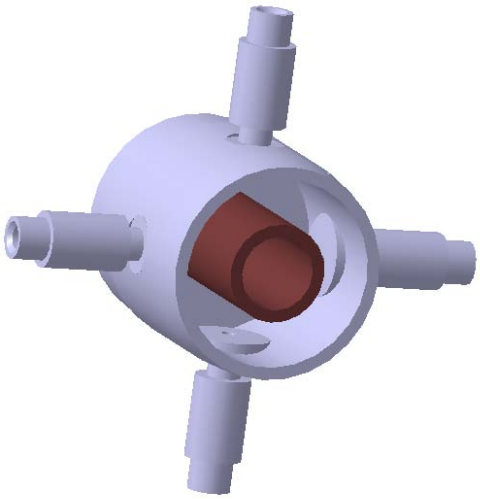

Figure 3-3. CAD view of the primary zone of the burner

In this design two parameters were incorporated to address geometry influences. The inner tube can be replaced, changing considerably the jet impingement configuration as well as the combustor volume. In addition, the injectors are cylindrical and incorporate a slight 10° injection angle with respect to the radial direction so they can be rotated to act on the flow split as show in figure 3-4.

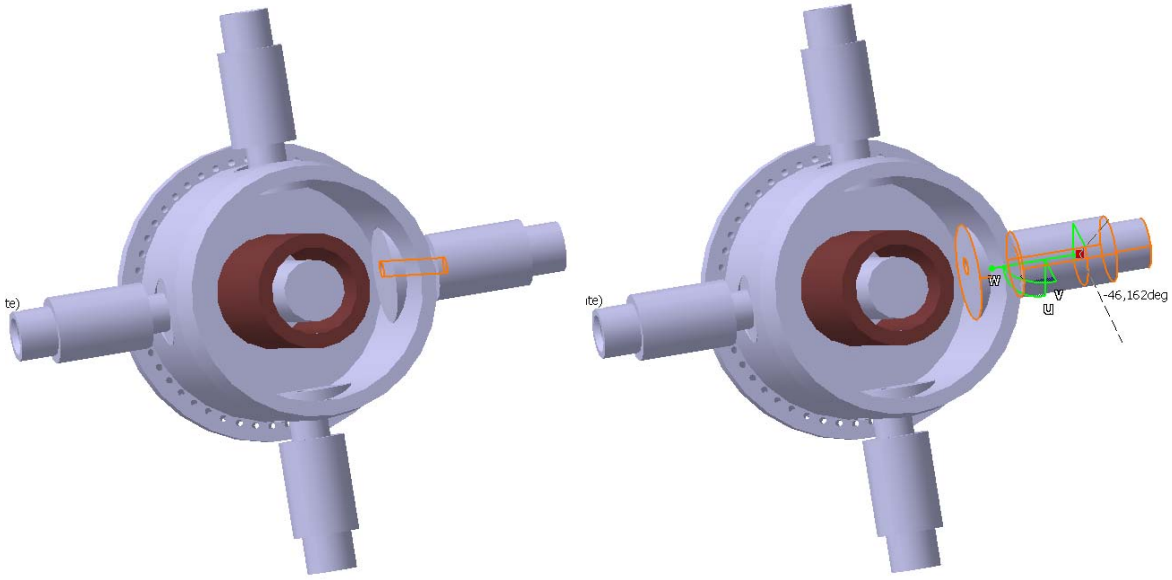

Figure 3-4. Flexibility in the injector design

The injection angle is chosen as a compromise between a good tangential distribution of the flow and a jet impingement speed. The swirl number has been calculated as defined in the equation:

$$S = \frac{\int_{r_i}^{r_o} \rho U_\theta U_z r^2 dr}{\int_{r_i}^{r_o} \rho U_z{}^2 r^2 dr}, \qquad (0.9)$$

where U_ϑ and U_z are respectively the tangential and axial velocities, r_i and r_o the inner and outer radius of the annular space. Considering the cold gas injection velocity and the combustion product axial velocity, the swirl number could be approximated at 10. However, the high velocity of the cold mixture jet imply a stirred reaction zone more than a swirling flow.

In this design, air and fuel are injected at four different points around the circumference and the jets are directed toward the center tube. The number of injectors has been seen as the simple way to provide a good homogeneity and a good control over the reactor composition by opposition to a liner with holes. A future step in the implementation could include injection of air trough 8 additional radial injection holes. This would provide an orthoradially staged combustion. Staging has been a central concept in the COSTAIR® burner development for NOx reduction in gas turbine combustors [35]. The pressure drop could be metered to ensure the same jet impulsion at the injection. This geometry has been inspired from a system designed at Florida Turbine Technology by Mark Harris for non premixed-combustion [36]. It revealed a very good stability performance. Once the idea of the design is defined, some main parameters have to be fixed. These are the ratio between the diameter of the liner and

the diameter of the center tube influencing the jet impingement, and the position of the injection circle with respect to the length of the combustor acting on the size of the primary zone and secondary zone.

Kinetic modeling

The objective in this part is to determine a volume of the reactor which would allow reach of the targeting operation points. Indeed, the goal is to be able to control the residence time as much as possible in order to reach the regimes of interest. A parameter has been used for many years in order to correlate mass flow rate, pressure, temperature volume and is named the loading parameter θ. This parameter provides a partly non-dimensionalized variable which is used in gas turbine combustor design to describe the combustion efficiency. Indeed Greenhough and Lefebvre correlated experimentally heat released rates to a loading parameter θ defined in the equation:

$$\theta = \frac{\dot{m}_a}{P^n \cdot V_c \cdot e^{(\frac{T}{300})}} \tag{0.10}$$

where P stands for the reactor pressure, V_c the reactor volume, T the inlet temperature [37]. The value of n was first correlated by Longwell and Weiss equal to 1.8, and used by Lefebvre and Greenhough as 1.75 [6,37].

In order to determine the proper flow rate or residence time of interest, it is useful to model the combustor behavior so that one can get estimation in terms of blowout limits, combustion efficiency, and emissions over the different inlet conditions for the reference fuel. As the combustion process involves aerodynamics, heat transfer and chemical kinetics, the modeling might be very complex numerically. Turbulent flow modeling is already a challenge but reacting turbulent flow adds a lot more complexity.

Turbulence modeling has been investigated through different approaches such as the k-Epsilon model, the Reynolds Stress Model (RSM), the large eddy simulation (LES), or Direct Numerical Simulation (DNS). Combustion modeling often uses these turbulence models along with some simplified reaction mechanism in order to have a reasonable computational time. Indeed, detailed mechanism such as GRI 3.0 involves more than 200 species and 3000 reactions and the calculation time becomes enormous if it is implemented on each cell of a CFD model. Eaton and co-workers achieved a review of the different comprehensive combustion models established [38]. However, for emission and stability research, detailed mechanism are unavoidable to understand the pollutant formation and especially the chemistry of P.A.H. Modeling with a detailed mechanism often implies working with ideal reactors of different kinds. The continuously stirred tank reactor (CSTR) model is defined under the same assumptions than a well-stirred reactor which are a continuous flow of products and reactants (steady state), a uniform composition throughout the tank and an exhaust composition identical to the tank composition. In a CSTR, the residence time varies with the flow of reactants, and the reactor is considered zero dimensional. In a plug flow reactor (PFR) model, the flow is one-dimensional, steady, and frictionless as well as no mixing is allowed in the axial direction. In a PFR, the farther from the inlet the longer the residence time is. Even though most of the practical combustors are very far from these ideal models, some zones of a combustor could be more and less linked to one or the other of these models

Modeling of a practical combustion system is often achieved through a reactor network approach. It consists in doing a first CFD simulation on a fine mesh with basic chemistry of the combustor. Then depending of the goal of the model, some zones of

similar properties are defined such as velocity, temperature and composition. Then these zones could be modeled as a CSTR with defined a parameter, and the flow between these zones can be estimated from integration of the velocity extracted from CFD results. A network of ideal reactors is so constructed and detailed chemistry model could be computed on each of these reactors. More details on the reactor network approach for combustor modeling could be found in a paper from Falcitelli [39]. In addition, Lebedev and co-workers modeled a gas turbine combustor for emission research with a reactor network approach [40].

For the current project, in a first step, a simple reactor network model is based on a physical model more than on a CFD approach. Mark Harris has highly contributed in both programming a useful tool that provides an easy to use interface, and sharing his experience in running combustion rigs when setting a combustion model [36]. Actually if one observes the reactor geometry, on Figure 3-2 and Figure 3-3, one can separate the combustion zone of the burner in three zones represented on Figure 3-5. Indeed, the flow will impinge on the central tube, creating a flow split. Some of the flow will go toward the back wall and come back to mix with the fresh mixture. Then it will move downstream and start to be diluted with the cooling air. The primary reaction zone corresponds to the annular reaction volume located from the rear wall to the injection. The secondary zone will correspond to the annular reaction volume located between the injection and the end of the liner. Finally, a short dilution zone is considered out of the liner and which shape is also annular. It is important to notice that in this CTSR network model, the dilution of the cooling air with the combustion products does not appear. Indeed, diagnostics were implemented to probe right at the exit of the liner. The cooling

passages have been designed to minimize the interaction and mixing between the cooling air and the combustion products close to this zone. There may be some reactions downstream as the combustion may be incomplete in the liner, and some of the intermediates products may keep reacting while mixing with the cooling air. However the current focus is primarily on the reaction occurring in the annular reaction zone.

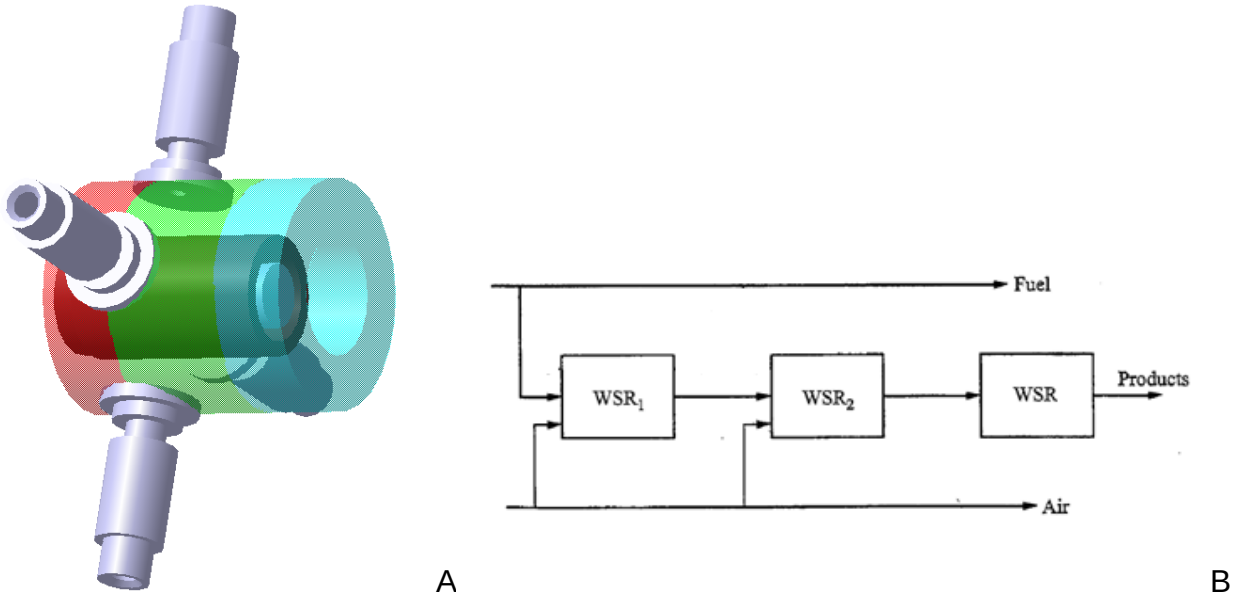

A B

Figure 3-5. Primary (red), secondary (green) and dilution zone (blue) used in the reactor network model A) and flow transfer between WSR according to the model 1 B).

In the simulation process, the flow rate of air, the inlet temperature, and the pressure are set to a certain value and a reactor total volume is also defined. A CSTR network simulation is performed for a given flow rate of fuel. After, the fuel flow rate is raised by a fixed amount and a new computation is performed. The process stops when a simulation results gives a reactor temperature equal to the inlet temperature. This means that the flame blew out. Two sets of computations were performed. The first one was done at a loading parameter of 1moles/s/liters/atm$^{1.8}$ and a second one at two times

this value. It should be noticed that for these runs, a total reactor volume had to be fixed as required by the simulation, and so was set to a 1L. However this volume does influence the calculation only by its ratio with the mass flow rate. Therefore, one can extract the loading parameter and use this one to evaluate which volume would produce the same condition (exit temperature, and composition) given the mass flow rate available in the laboratory. Concerning the reactor model used, the flow distribution was set as described in Figure 3-5. Again, the way the flow is split comes from a good correlation between this model and the experimental results observed on a gas turbine combustor whose geometry was close [36]. The term exhaust is not really appropriate as the combustion gases will be further diluted downstream of the liner with the cooling air.

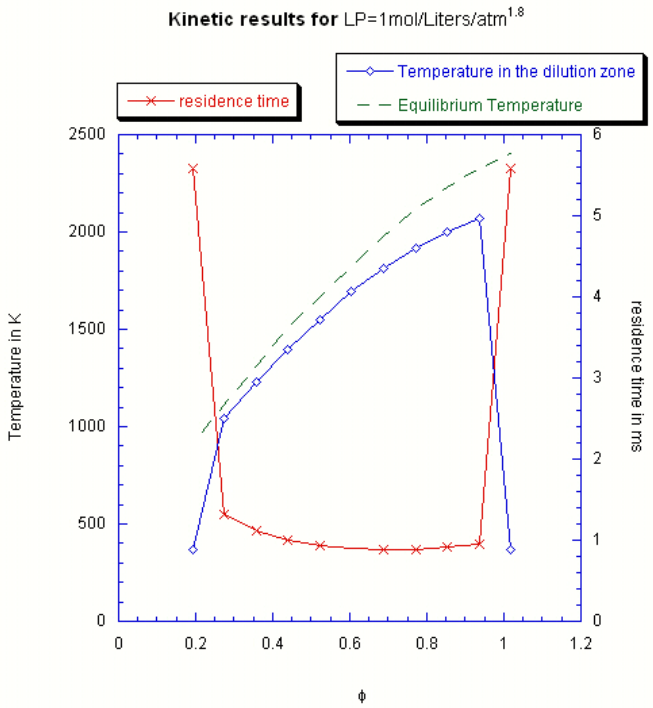

Figure 3-6. Temperature and residence time obtained at LP=1 (model 1)

The results of these simulations are plotted in the Figure 3-6 and Figure 3-7. The equivalence ratio is based on the fuel-air ratio defined with the injection air only (excluding the cooling air). The exit temperature was the temperature of the third CSTR. It is important to notice that this temperature will not be equal to the exhaust temperature as the combustion products are further diluted with the air from cooling passages of the liner and the tube. Finally the residence time in the primary zone is calculated using Equation 1-1. As the flame blows out the reactor, the temperatures drops and therefore the residence time jumps due to the fact that the density of a cold mixture is low. In fact the mixture being no longer ignited, no significant reaction occurs, and the only solution available will be the one of non-reacting flow with the exit temperature equal to the inlet temperature. In addition, the equilibrium temperature is plotted, which represents the temperature that would be obtained if an infinite residence time is allowed. This latter was computed using CANTERA commanded by Matlab. The gas properties were set as followed: the temperature was set at 367K as in the CSTR network, the pressure at one atmosphere, and the composition was varied over the equivalence ratio range of interest. The solution corresponds to equilibrium reached at constant enthalpy and pressure. The constant enthalpy condition accounts for the adiabatic condition of the reactor.

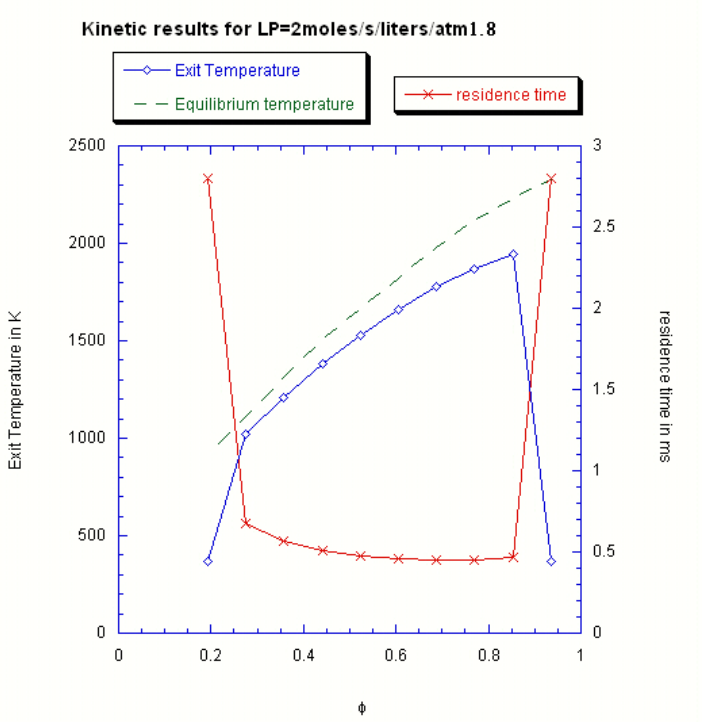

Figure 3-7. Temperature and residence time obtained at LP=2 (model 1)

In the Figure 3-8 and Figure 3-9, one can notice that the range of global equivalence ratio goes from 0.25 to 1 for a LP equal to unity, and from 0.25 to 0.8 for a LP of 2. As expected the stability limits get narrower as one increases the load, and so a decrease in the residence time. However it is noted that this narrowing affects almost exclusively the richer side. In addition, the two kinetic or exit temperatures remain close between the two regimes at lean mixture, and then the gap between them grows steadily as the data moves toward richer mixtures. There are two important remarks that one should raise concerning these figures. The stability limits of the reactor for a LP of unity ranges from 0.35 to near stoichiometry. It was expected that these blowout equivalence ratios would be much larger on both the lean and rich side with similarity with a single CSTR model. This may be explained by the fact that these results were obtained with a model in which 100% of the fuel is going to the primary zone so that the

local equivalence ratio in the primary zone will be doubled compared with the global equivalence ratio. Hence, the rich blowout would be around 2 considering the local equivalence ratio for and a L.P of 1.

In addition, the results do not have the bell shape for the exhaust temperature as one would expect if one thinks of the shape of the adiabatic flame temperature for n heptane. In the results, the temperature keeps increasing as the equivalence ratio goes up. The effect of decreasing a short residence time is not the same for the two edges of the stability limits. This could be explained if one considers the breakdown of straight chain hydrocarbons into carbon monoxide and hydrogen. Indeed, a tool to model hydrocarbon combustion consists of breaking down the fuel into CO and H_2, and then to consider the oxidation mechanism of the two fuels formed. The breakdown of fuel will often be considered as the limiting step, since its time scale is usually larger than those of CO and H_2 oxidation reactions. The global fuel breakdown reaction could be modeled by:

$$C_x H_y + xO_2 \rightarrow xCO_2 + \frac{y}{2} H_2. \qquad (0.11)$$

In this equation, one could intuitively consider that as the hydrocarbon-to-oxygen ratio is increased, the breakdown will give more H_2. The oxidation chemistry of hydrogen being faster than the one of CO, this could explain the smaller effect that a decrease of residence time would have on reaction completeness.

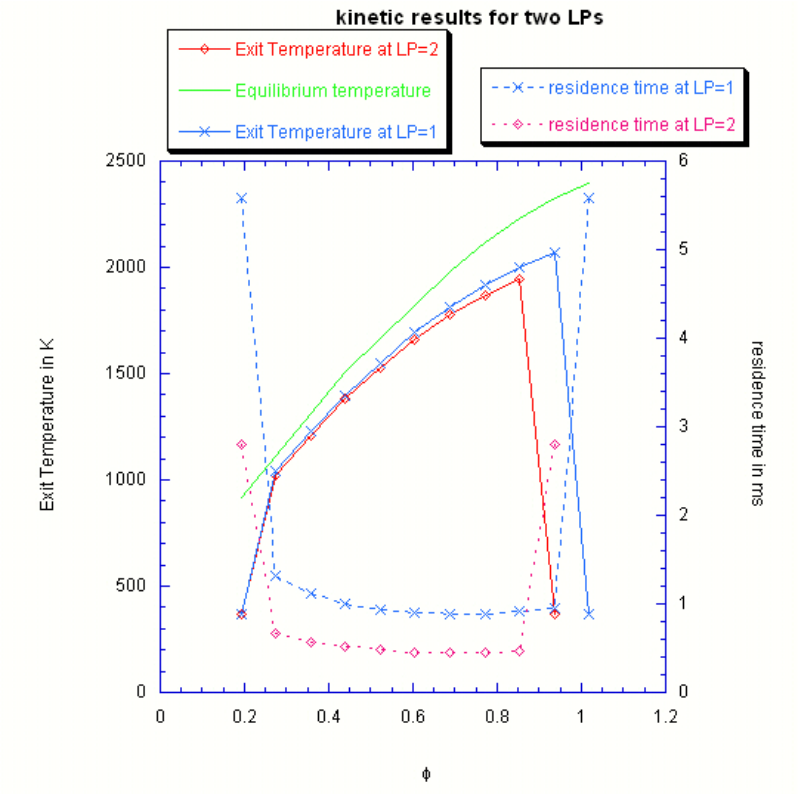

Figure 3-8. Exit temperature and residence time in the primary reactor for two different loadings simulated using the model 1).

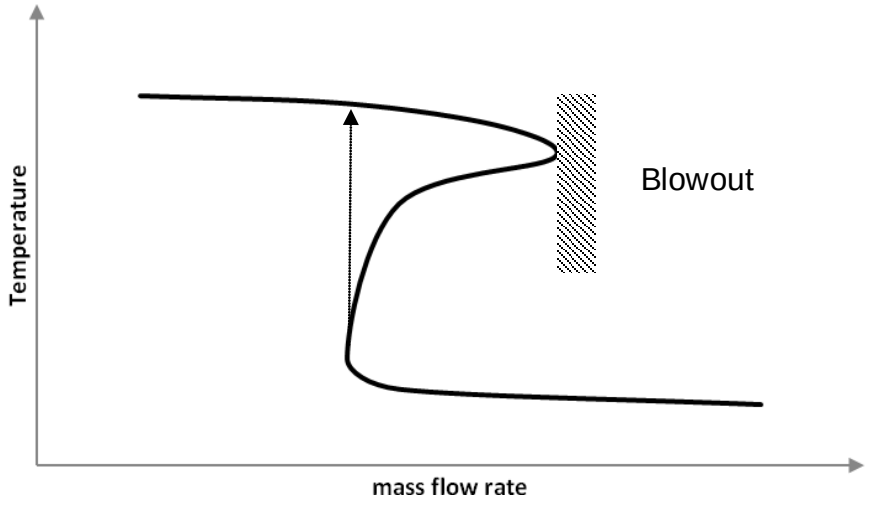

Figure 3-9. Temperature evolution in a WSR for a given composition

However, the sharp decline in temperature is not easily explained and should be investigated. Indeed, obtaining accurate results near the blowout limit is a delicate task since one has to go through a region in which 3 solutions exists at the same time, two of them are stable and one is unstable as shown on Figure 3-9. If one considers a given mixture of air and fuel, and starts at very low mass flow of air, the temperature will decrease as the mass flow rate is increased until the flame blows out. Starting on the other hand, if one considers an infinitely small residence time; the temperature of the reactor will be close to the inlet temperature. As the mass flow rate is increased, the temperature will increase very weakly. The mixture will stay fairly low even for mass flow rate larger than that at blowout on the forward approach. A minimum residence time is reached where the temperature jumps suddenly to the upper section. The portion of triple solution complicates the approach of the blowout since this unstable solution may either jump into the hot side or the cold side. Indeed, the unstable solution being fairly close to the upper solution, an inappropriate first guess could easily lead to an extinguished flame even if a real solution exits. One may have to adopt a scheme in which the results from one simulation are used as a first guess for the next simulation. This approach has to be considered in the future when the experimental results will be compared to that of the numerical model. However, we will consider these preliminary results as satisfactory for our purpose here, which is to provide the exit temperature and some first stability limits. Indeed, a more sophisticated solving scheme may give wider stability limits.

A third set of computations were performed at a higher loading, i.e. 4 moles.s^{-1}.$liters^{-}1.atm^{-1.8}$. This time the scheme was changed to the one defined in Figure 3-11

where half of the fuel is injected in the primary reactor and half of the fuel is in the secondary CSTR. In Figure 3-10, one can see that the results are quite different from the previous reactor network model. This time the stable regime goes from 0.5 to 1.7 and is more centered on the stoichiometric condition. The residence time goes down to 0.3ms in the primary reactor. The exit temperature presents the same trend as in the other model, and is monotonically increasing with the equivalence ratio. The stoichiometric flame gives a temperature of about 1500K at stoichiometric condition and a temperature difference of 550K with the equilibrium temperature at an equivalence ratio of 1.3. However, these results raise the question of an exit temperature higher than the adiabatic flame temperature which needs to be further investigated to determine if this computationally-related or if the reaction is actually under a super-adiabatic regime when exiting the reactor.

The current interest in having the possibility of running at low residence time is of two orders. First, the stability of this burner can be characterized. Then, if the reactor appears to be very stable, the strength of this geometry in stabilizing the flame will be demonstrated. Indeed, combustion of low heating value gases raises some static stability issues which make their use in gas turbine combustor very challenging. For instance, running low H_2 syngas (fraction of hydrogen less than 15%) is difficult due to the very low chemical time scale or auto ignition delay [15]. This means that the mixture needs a large residence time in order to ignite and transfer the heat of combustion.

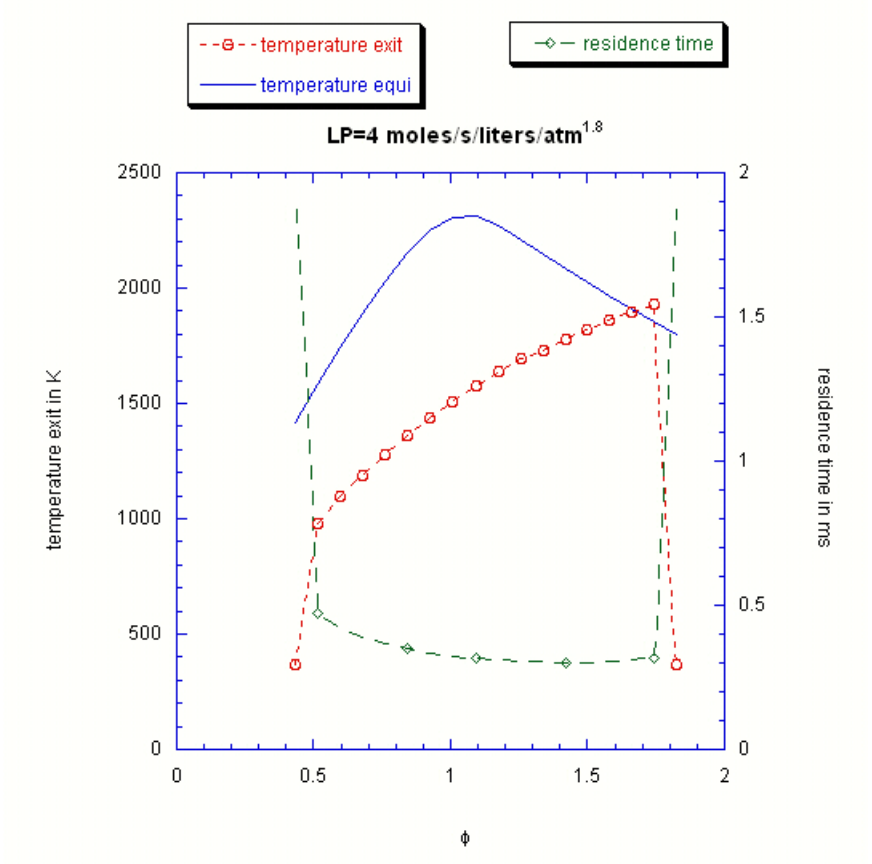

Figure 3-10. Temperature and residence time obtained with computer simulations (model 2)

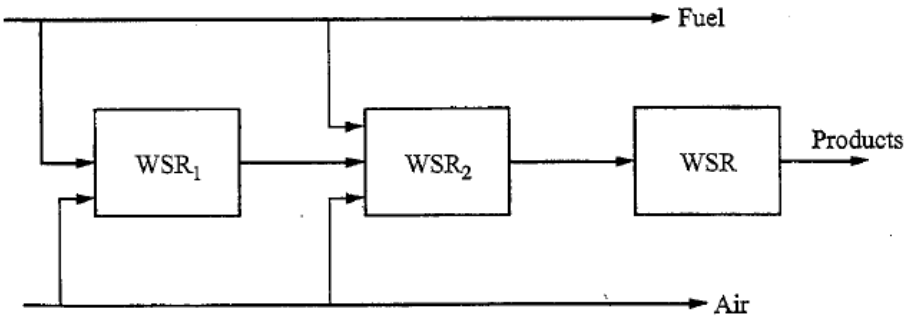

Figure 3-11. Flow transfer between CSTRs according to the model 2.

The second motivation in reaching low exit temperatures at stoichiometric conditions is in the fact that the reaction does not reach equilibrium, and some intermediate products exit the combustion zone of the reactor and can be probed. This would provide insight into oxidation chemistry of the fuel tested and data to retro feed a

reactor network model. At a large reactor residence time, the inefficiencies of the reaction are mainly due to the lack of mixing, to the heat losses, and to the poor vaporization of the fuel as described in the W.S.R emissions study of Zelina and Ballal [12]. In contrast, at low reactor residence time, or higher loadings, the inefficiencies of the reaction will be also due to the slow chemistry part of the oxidation mechanism, which reduces the completeness of the reaction. Moreover, the higher the flow, the lower the impact of the heat losses and the better the mixing is. A third interest consists in running at lower temperatures, offering the possibility of direct probing of the flame temperature. As mentioned before, a sheath insulated probe of platinum/Rhodium could be used up to 2600K, and with even further reduction in temperature, type K thermocouples could even be used since they have a 1600K rating. In addition, low temperatures will make species probing easier using extractive gas sampling connected to gas chromatograph-mass spectrometer systems, or a commercial gas analyzer for hydrocarbons detection as a cheaper technology.

Flame temperature together with combustion products composition will provide very important data in order to understand the reactor behavior. Comparison of the results with some values obtained using a neural reactor network model may allow for a retro feed of the model, and then may help to understand the flow split. The best agreement a model will have with the experimental data extracted from the laboratory reactor, the more useful this latter will be for the understanding of exotic fuel kinetics and pollutant formation mechanisms. According to these considerations it is desired to be able to reach a loading parameter of at least 4 in a first implementation basis, and to reach 10 on the long term. However, the base load or design condition is based on a

Loading parameter of 1. This means that the fuel flow consumption of 0.5gal/hour will be based on this regime. This gives a total air flow rate of 7g/s at this condition and for the stoichiometric mixture. Using the equation below,

$$V = \frac{\dot{m}_{\max}}{\theta_t P^{1.8} e^{T_i/300} M_a}, \tag{0.12}$$

with θ_t being the targeted loading parameter, and $\dot{m}_{\max}$ the maximum flow rate available in g/s, one can evaluate the volume of a reactor in which this combustion conditions may be approached within our limitations, yielding.

$$V = 60mL. \tag{0.13}$$

In Table 3-1, the different loads and the corresponding air flow are given. One must take into account that it is necessary to pump some additional air for the cooling, which may be at least equal to the combustion air. Therefore the next step in the design would be to design the cooling system and evaluate the air flow needed. This means that the overall combustion volume targeted is an iterative process.

Table 3-1. Combustion air flow rates

Loading parameter (mol/s/liters/atm$^{1.8}$)	1 (design point)	4 (full load short time)	10 (full load long term)
Air flow rate (%of compressor capacity)	7g/s(5%)	28g/s(21%)	70g/s(54%)

Heat transfer model

As mentioned before, the current reactor stands between a gas turbine combustor and a well-stirred reactor. Experimental well-stirred reactor shells are made of ceramic materials which can sustain really high temperatures. The toroidal jet reactor developed by Neniger [11] or the spherical reactor by Longwell and Weiss [6] are some examples of this type of design. The materials used provides a good isolation and the reactor could be considered as nearly adiabatic. Even though ceramic thermal barrier coatings have been developing a lot in the past years to protect, for example, the blades of turbines, the development of 100% ceramic combustor raises some issues. Indeed fusing and crumbling of the ceramic shell could easily occur and give debris which would damage the turbine blades. In addition, using refractory material will limit the geometry and dimensional tolerances of the combustor which is primordial for sealing considerations. Therefore, the use of pure ceramic material for the current system is not considered and instead an actively cooled metal is used. In the absence of cooling, the pieces that would be subject to an important heat transfer from the combustion gases are the liner and the inner tube. They will need to be cooled by a flow of air or other coolant. To design the passages and chose the material, a program modeling the heat transfer inside the combustor is developed.

The program could solve either for the cooling flow required giving the input parameters given in Table 3-2, and setting the wall temperature to an appropriate value**,** or it could solve the wall temperatures giving the cooling flow rates. It solves a system of non-linear equations representing the energy equation for the metals in steady state. Assuming a one dimensional radial and steady state model, fluxes should equalize at a given wall, giving 2 equations for 2 wall temperatures per wall. The resolution is made at

a given location on the liner length. To obtain a temperature distribution along the liner, a step could be chosen and the cooling air temperature at a shifted position could be obtained integrating the heat flux along the length step, and using the energy equation for the gas.

Table 3-2. Input parameters of the heat transfer model

Input Parameters	symbol	Equations concerned
Combustion		
Gas flow rate	$\dot{m}_g$	3.14
Fuel air ratio	q	3.9
Flame temperature	T_g	3.11,3.14
Materials		
Thermal conductivity liner	k_l	3.15
Thermal conductivity tube	k_t	3.15
Thermal conductivity casing	k_c	3.15
Emissivity liner	ε_l	3.16
Emissivity tube	ε_t	3.16
Emissivity casing	ε_c	3.16
maximum temperature liner	T_t	3.11,3.14,3.15
maximum temperature tube	T_l	3.11,3.14,3.15
Geometry		
Cross section Combustion	A_g	3.14
Cross section Central cooling	A_c	3.14
Cross section Annular cooling	A_a	3.14
Thickness liner	t_l	3.15
Thickness tube	t_t	3.15
Thickness casing	t_c	3.15

For each wall, the steady state energy equation provides the equations below:

$$C_1(T_{w1}) + R_1(T_{w1}) - K_1\ (T_{w1}, T_{w2}) = 0, \tag{0.14}$$

$$C_2(T_{w2}) + R_2(T_{w2}) - K_2\ (T_{w1}, T_{w2}) = 0, \tag{0.15}$$

where C_i and R_i are, respectively, the convective and radiation heat transfer flux received by the wall through the side i, K_{ij} being the conductive flux directed from the i side to the j side.

The three modes of heat transfer are important in gas turbine combustion. First, the gases from the combustion zone transfer heat to the wall by radiation. The rate of transfer will be highly dependent on the luminosity of the flame. A non-luminous regime will be characterized by the absence of soot particles. In that case, the gas will emit and absorb in narrow emission bands. The surface of the wall could be considered as a grey surface with a corrected emissivity compared to a blackbody. The net radiant heat flux from the gas to the wall is given by

$$R_{gw} = \sigma(\varepsilon_g T_g^{\,4} - \alpha_g T_w^{\,4}), \tag{0.16}$$

in which σ is the Stefan constant, ε_g the gas emissivity and α_g the gas absorptivity.

Lefebvre and Herbert investigated the emissivity and absorptivity values which are respectively dependent on gas and wall temperature, and provided the approximation [41]:

$$\frac{\alpha_g}{\varepsilon_g} = \left(\frac{T_g}{T_w}\right)^{1.5}. \tag{0.17}$$

In addition, values for the non-luminous flame absorptivity can be obtained using the formula provided by Reeves [42],

$$\varepsilon_g = 1 - \exp\left[-290 P (q l_b)^{0.5} T_g^{\,-1.5}\right], \tag{0.18}$$

where q is the fuel air ratio and l_b the beam length. The beam length varies with the shape and the size of the gas volume. Fishenden and Saunders provided an expression for this beam length for most practical combustion situations [43]:

$$l_b = 3.4\frac{V}{A}, \tag{0.19}$$

where V is the flame volume, and A the limiting area between the flame and the wall.

Considering all the equations above and using a correction factor of $(1+\varepsilon_w)$ for the fact that the liner surface is grey, Equation 3.7 gives:

$$R_{gw} = 0.5\sigma(1+\varepsilon_w)\varepsilon_g T_g^{1.5}(T_g^{2.5} - T_w^{2.5}), \tag{0.20}$$

where ε_w is the emissivity of the wall.

In the case of luminous flames, soot particles present in the flame are very hot and emit in the visible spectrum. Particularly important in high pressure combustors, as the soot particles can get larger, this luminosity may need to be accounted in these cases using a luminosity factor as described by Lefebvre [44].The soot formation process in atmospheric flames is a complex mechanism highly dependent on the atomization and vaporization processes of the fuel. Some studies have been done on the soot formation process in well-stirred reactors at high equivalence ratio by Nenniger and Manzello among others [11,14]. However, caution must be exercised in using correlations obtained from practical gas turbine combustor, which might not be pre vaporized and which geometry could be very different from our design. The mechanism of soot formation by droplet burning is very different soot regimes from that occurring in a rich premixed flame. In addition the adiabatic temperature of the combustion gases peaks at an equivalence ratio around 1.05 for the n heptane mechanism provided by Lawrence

Livermore National Laboratory [20, 21]. Works on toroidal well stirred reactors in series with PFR showed the absence of flame generated particles in ethylene flame below an equivalence of 1.9 [14]. Overall, neglecting the luminosity of the flame will not underestimate the heat transfer rate as long as this phenomenon does not occur at the critical thermal conditions. The soot formation and oxidation mechanism will be discussed in detail in Chapter 6.

The convective effects are harder to characterize in this combustor design due to the complexity of the aerodynamics. The configuration of the injection is radial by opposition to the axial swirler in conventional gas turbine combustor, so that correlations used in gas turbine cooling could not really apply in this case. The model widely used for estimation of the Nusselt number in gas turbine combustor is based on a fully-developed flow with constant surface temperature in a circular tube give the following approximation:

$$Nu = 0.021 \mathrm{Pr}^{0.5} \mathrm{Re}^{0.8}. \qquad (0.21)$$

This is valid for a range of Prandtl number between 0.5 and 1 [45]. The assumptions of constant temperature or constant heat flux may be questionable in gas turbine combustion. However the effect of peripheral heat flux variation could be accounted using heat flux functions as described in the same book. Some calculations have also been carried by Kays and Leung on fully-developed flow in concentric circular tube annuli [46]. In the current system, a jet of fresh mixture impinges on the inner tube and mixed with the combustion gases. One can evaluate a worst case in which it is assumed that the gases are at a uniform adiabatic flame temperature in the combustor.

In that case, one may use the fully developed constant temperature model on a turbulent duct. The Reynolds Number will be estimated using:

$$\mathrm{Re} = \frac{\rho_g U_g d_h}{\mu_g} = \frac{\rho_g}{\mu_g}\left(\frac{4\dot{m}_g}{\rho_g \pi (d_i^{\,2} - d_o^{\,2})}\right)(d_i - d_o) = \frac{4\dot{m}_g}{\pi \mu_g (d_i + d_o)}, \tag{0.22}$$

and the convective heat flux from the gas to the wall could be given using Equation 3.12:

$$Cgw = 0.022 \frac{k_g^{\,0.5} Cp_g^{\,0.5}}{\mu^{0.3} d_h^{\,0.2}}\left(\frac{\dot{m}_g}{A_s}\right)^{0.8}(T_g - T_w). \tag{0.23}$$

If one neglects axial heat flux, the radial conductive heat flux along the thickness of a liner or a tube is given by:

$$K_{12} = \frac{k(T_{w1} - T_{w2})}{t_w}. \tag{0.24}$$

On the cooling side, the radiation heat transfer can be expressed as the heat transfer between two gray surfaces of a given emissivity:

$$R_{12} = \frac{\sigma(T_2^{\,4} - T_1^{\,4})}{A_1\left(\frac{1-\varepsilon_1}{\varepsilon_1 A_1} + \frac{1}{F_{12} A_1} + \frac{1-\varepsilon_2}{\varepsilon_2 A_2}\right)}, \tag{0.25}$$

where F_{12} is the geometric shape factor between the surface 1 and the surface 2. This one could be estimated equal to unity for a long annular space. One can extract values for the emissivity of Nickel based alloy from Greene at various temperatures and level of oxidation [47]. Machined stainless steel emissivity would be considered equal to 0.14. Finally, the convective heat flux due to the air flowing into the cooling passages could be estimated using the same constant surface temperature fully developed flow

described in Equation 3.15, considering the gas as cooling air and the temperature of the exterior wall of the liner or internal wall of the inner tube. The heat transfer processes neglected in this model are the radiation heat flux from the liner to the tube, assumed to be negligible compared to those due to the combustion gases, the convective heat flux from the ambient on the casing assuming a quiet atmosphere, and all the axial conduction heat fluxes.

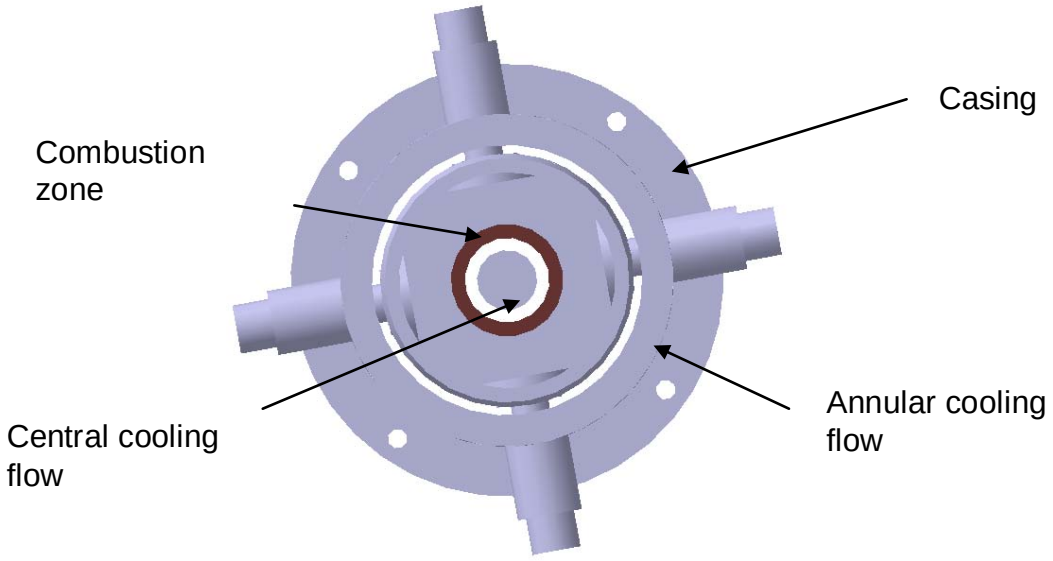

Figure 3-12. Representation of the cooling passages

One can notice in the equations above that the Equations 3.5 and Equation 3.6 will be non-linear. Therefore a solver which is based on a Newton-Gauss method is used that is included in the function fsolve of Matlab 7.5.0. In addition, the heat transfer fluxes are integrated over the length of the combustor in order to evaluate the heat losses from the combustion volume and the temperature rise of the cooling air.

Some constraints have to be considered when using this model. First if one considers the size of the cooling passages, one might be attracted to reduce them to 1/16". Indeed, if one considers only the system of Equation 3.6 and Equation 3.7 at a

single position over the length, the velocity of the cooling flow being very large, the cooling convective heat flux will be very large and the wall temperature low for a given heat flux. However using the energy equation for the gas over the length of the cooling passages, it could be noticed that the cooling air temperature will rise significantly, and that the constant temperature model will not be valid. Also, the velocity should stay under the sonic level for wall buckling limit reasons and because the correlations used at a given point for heat transfer calculations consider the flow as incompressible. Changes of density are not neglected and have been evaluated using the gas dynamics model developed and which will be presented after. In addition, it is desired to limit the interaction between the cooling flow and the combustion gases in the dilution zone, and so prevent the flame to attach inside the cooling passages. For this reason the momentum of the cooling flow, at the exit of the passages should not be lower than the momentum of the hot flow from the combustion zone. In addition to these aerodynamics considerations, reducing the wall thickness to the minimum could be attracted since it increases the conduction fluxes and decreases the temperature difference across the wall. The injection system designed in this project seals with the liner wall. The machining of the liner sealing surfaces would be very difficult on very thin walls. In addition the wall buckling limit will be lowered. Therefore, the thickness of the liner was set at 0.2 inches. The constraints are summed below:

$$\begin{aligned} & M_a \le 0.3 \\ & \Delta T_g \le 100K \\ & \rho_a V_a \ge \rho_g V_g . \end{aligned} \tag{0.26}$$

The choice of material is very important in heat transfer considerations. Indeed, as noted in Table 3-2, the thermal conductivity in the conduction flux and the emissivity in

the radiation flux will depend on the material chosen. Other machining and cost considerations should also be taken into consideration. Therefore, the objectives and constraints have to be described in the research of an adequate material. It is desired to maximize the maximum service temperature in air or the melting point of the metal. Increasing the service temperature will reduce the need for cooling, and so decrease the overall heat transfer. If one thinks of a global Newton's law of cooling, the heat transfer is a monotonic function of the temperature difference. The higher the metal temperature, the lower the heat losses induced by the cooling and so the closer the system is from the adiabatic condition. The maximum service temperature does not depend only on the melting temperature, but can take into consideration other parameters as the mechanical strength at high temperature or the resistance to corrosion. The resistance to corrosion is a more complex criterion giving the different forms of corrosion mechanical failure modes. It is particularly important when injection of water is used as a NOx reducing strategy and for marine propulsion system. The thermal conductivity may have an important role in keeping the axial component of the heat flux low, and so reducing the temperature gradient. However the direct influence on the radial heat transfer could be less than expected. The results for a given geometry and some different heat conductivities are plotted in Figure 3-13.

Plotted below are the wall temperature for a reference conductivity set at 10W/mK, and comparisons to the temperature obtained for two other conductivities. We can observe that the conductivity plays an increasing role with an increase in the cooling flow rate, and that the role declines with an increase in the heat conductivity.

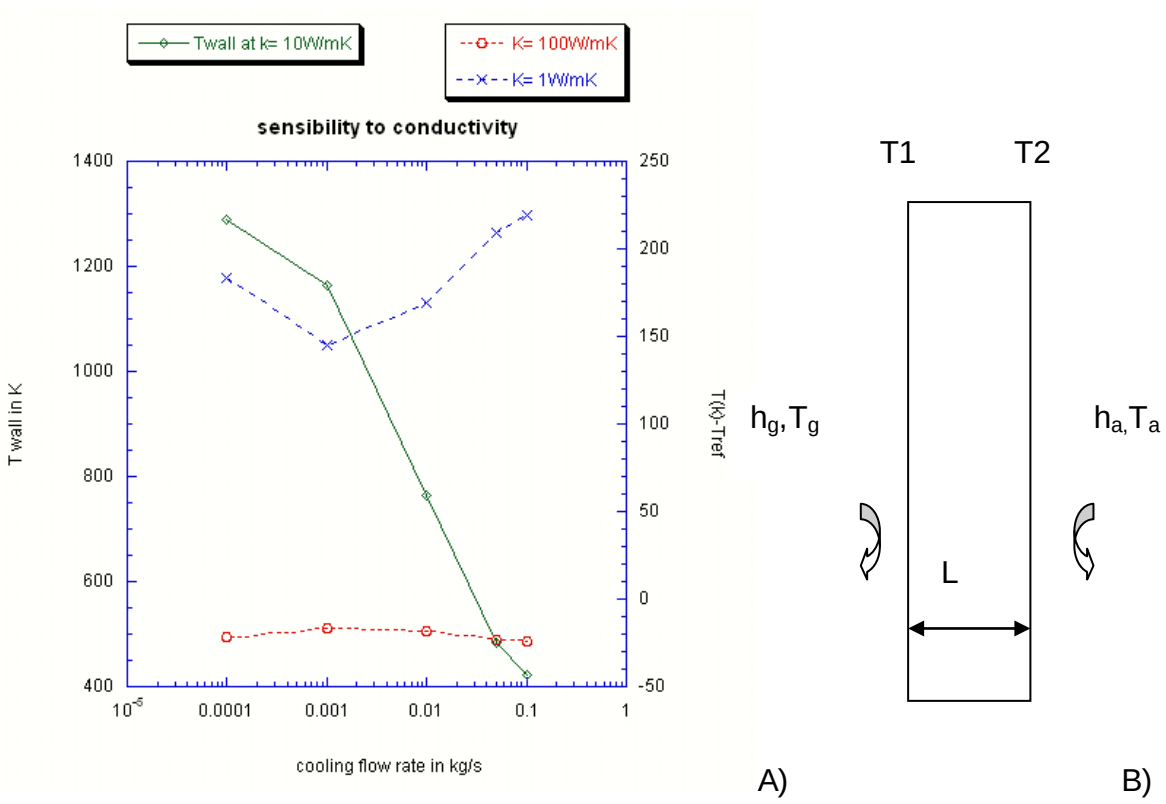

Figure 3-13. Influence of the conductivity in the heat transfer, experimental results (A) and steady state wall model (B)

The interpretation could be easily done based on a steady state wall model represented above. An electrical analogy would give:

$$\dot{q}'' = (\frac{T_g - T_a}{R_T}), \tag{0.27}$$

where R_T is given by:

$$R_T = \frac{1}{\frac{1}{h_g} + \frac{L}{k} + \frac{1}{h_a}}. \tag{0.28}$$

The effect of the ratio of L and k is not significant unless the convective coefficient grows or the ratio of the conductivity to the length becomes really large as demonstrated in the sensibility expression below:

$$\frac{\partial R_T}{\partial (L/K)} = -\frac{1}{\left(\frac{L}{K}+\frac{1}{h_a}+\frac{1}{h_g}\right)^2}. \qquad (0.29)$$

One can notice that the effect of K is the exact inverse of the material thickness when considering only the radial heat flux.

Table 3-3. Performance functions for material choices.

Functions	symbol	objective	extreme value
1.Melting Temperature	T_m	to maximize	1000K
1'.Maximum service temperature (air)	T_s	to maximize	1000K
2.Thermal conductivity	K	to maximize	15W/mK at 298.15K
3.Resistance to Corrosion at 1000K		to maximize	
4.Machinability (Hardness Vickers)	H_v	to minimize	200 at 298.15K
5.Density	ρ	to minimize	15g/cc
6.Cost of material	C_m	to minimize	15$/lb

The extent to which the material is easy to machine is also very important. In the current case, the sealing surfaces being critical on the injection surface, one cannot tolerate large errors in clearance due to machining difficulties. The hardness of the material could be used to determine its machinibility index as described by Thiele [48].

In addition, the materials involved in the heat transfer calculation do not have the same order of priority for the functions described in the Table 3-3.

Indeed, the liner and the injector have to be machined precisely and sustain fairly high temperature. The rig casing does not see high temperature so the mechanical strength and the cost are also important as it is the larger piece.

The inner tube will see a very high temperature due to the jet impingement. Indeed, the velocity used to determine the convective heat transfer rate is based on the

total mass flow rate. However due to the turbulent jet, this velocity will be higher. Correlations for axisymmetric turbulent jets could be are given by Turns [48], and the mean velocity components respectively in the radial and axial direction are:

$$\overline{v}_x = \frac{3}{8\pi}\frac{J_e}{\rho\varepsilon x}\left(1+\frac{\xi^2}{4}\right)^{-2}, \tag{0.30}$$

$$\overline{v}_r = \left(\frac{3J_e}{16\rho_e\pi}\right)^{1/2}\frac{1}{x}\left(\xi-\frac{\xi^3}{4}\right)\left(1+\frac{\xi^2}{4}\right)^{-2}, \tag{0.31}$$

with J_e being the initial jet momentum and

$$\xi = \left(\frac{3J_e}{16\rho_e\pi}\right)^{1/2}\frac{1}{\varepsilon}\frac{r}{x}, \tag{0.32}$$

and the eddy viscosity is:

$$\varepsilon = 0.0.285 v_e R, \tag{0.33}$$

where v_e is the initial jet velocity.

The axial and transverse axes of the axisymmetric jet are based on the initial jet position. As described in the geometry, the rotation of the injectors between runs is possible and offers a variation into the jet direction and the impingement angle. Assuming no cross flow and no reflection, the impingement velocity could be estimated as a direct function of the distance and the direction. To do so, some coordinate systems changes can be done using a rotation matrix. For an injector angle of 10° and the direction of the jet into the tube normal plan, the velocity was estimated at 100m/s. The temperature of the jet at impingement will also be very important. However, the determination could be fairly complex due to cross mixing with the combustion gases. It is evident that the temperature should be fairly lower than the reactor temperature of

2400K used in the model. In front of these unknowns, it was decided to implement first a very high temperature resistant and conductive metal. The simplicity of the inner tube does not require high precision machining and its low volume will decrease the large price of the raw material so that one can think of purer materials while controlling cost.

On Figure 3-14 are positioned different metals with their service temperatures and their thermal conductivities. For pure material, the melting point is considered. One can observe three main groups on the graph. First, molybdenum is far apart with outstanding melting point and thermal conductivity respectively at 2617 °C (2890K) and 138 W/mK (at 300K). Then one finds Platinum, Zirconium and Titanium with elevated melting point but small conductivities. That justifies their use in rocket and aircraft design since they also present an excellent mechanical strength and a low density. Then, in a third group are the different alloys including Nickel based alloy, Cobalt based alloy and Stainless steel. Their thermal conductivities are comparable. Inside this latter group one finds on top the nickel and cobalt-based alloys which ally high service temperature with a strong resistance to oxidation. They have been extensively used for decades in gas turbine combustor design. The properties of some of these alloys together with Molybdenum are presented in Table 3-4. These data have been extracted from Matweb (www.matweb.com). It must be noticed that the thermal conductivity varies with the temperature, with some correlation available for Nimonic 75 and Inconel 600 [50].

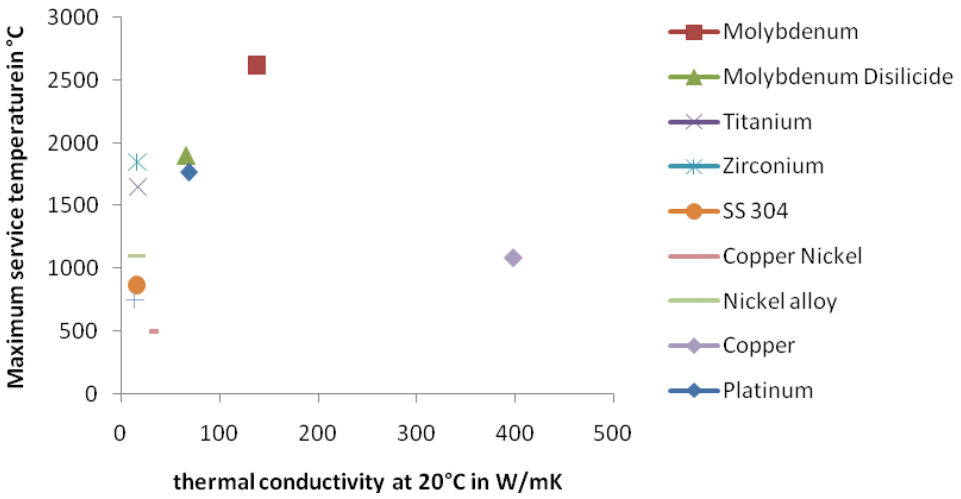

Figure 3-14. Thermal properties of different materials

Table 3-4: Properties and composition of some tentative materials

Properties	density (g/cc)	k (W/mK) at 20°C	k (W/mK) at 800°C	Ts (°C)	Ni (%)	Co (%)	Mo (%)	Cr (%)
Haynes 230	8.97	8.9	28.4	1095	57	<5.0	2	22
Haynes Hastelloy X	8.22	9.7	24.8	1095	47	1.5	9	22
Haynes 188	8.98	10.4	24.8	1095	23	42	0	22
Nimonic 75	8.37	11.7	NC	1095	72	0	0	19.5
Molybdenum	10.22	138	112 (727°)	2600	0	0	100	0
Inconel 600	8.47	14.9		1095	73			15.5

When choosing the material for this laboratory scale system, one should keep in mind that even though some properties such as mechanical strength or price may not be as important as it would be in a gas turbine combustor, ignoring them will prevent the adaptation of the system to a future industrial use. Even though thermal properties of molybdenum are excellent, it suffers from two disadvantages which are its elevated hardness (HV=230) and the stability of its oxides. Its hardness restrains the machining processes so it could not be a good candidate for the liner, but would suit the inner tube

requirements. Concerning the liner and the injector, copper could be a candidate if its melting temperature would be higher. It cannot t be used for temperature over 700K. Zirconium, platinum and titanium present fairly high melting temperature, platinum offering in addition a good conductivity. However the price of the pure material is enormous. Finally, nickel and cobalt-based alloy offers a high service temperature, a good resistance to corrosion, and a fair machinability. The choice has been made toward Hastelloy X for its excellent resistant for corrosion due to its molybdenum content for the liner and the injector. Concerning the tube, molybdenum is a good option in the short term.

The results of the heat transfer calculations are presented in Figure 3-14. First, the temperatures of the wall on the combustion sides have been set to a target value and the program solves for the mass flow rate at a given geometry. The central air cooling and the annular air cooling versus the flow of combustion air are plotted on Figure 3-14 A. As expected, an increase in the combustion air flow will enhance the convection heat transfer so that a higher cooling flow rate is needed to keep the wall temperature constant. The different results are attached in the appendices. From a controlling point of view, the temperature of the liner could be kept nearly constant by measuring the liner wall with a thermocouple and feeding the flow controller using a (Proportional Integral Derivative) PID or another type of regulator based on both the results and a proportional integral action. In order to characterize a range of operation, one has to consider the heat losses in the combustion chamber. On Figure 3-14 B, the heat losses are plotted in terms of axial bulk temperature drop along with the axial cooling air temperature rise.

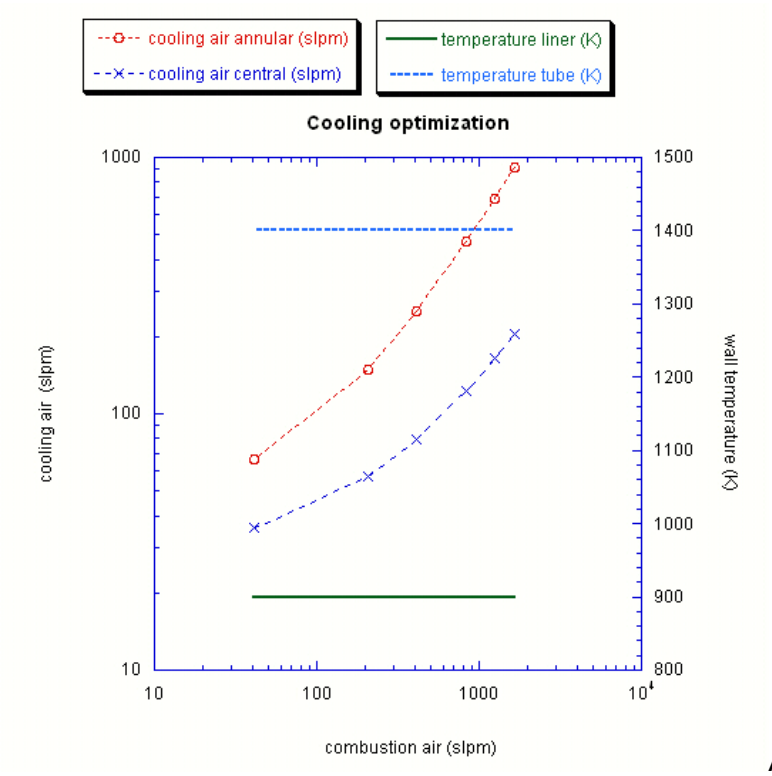

A

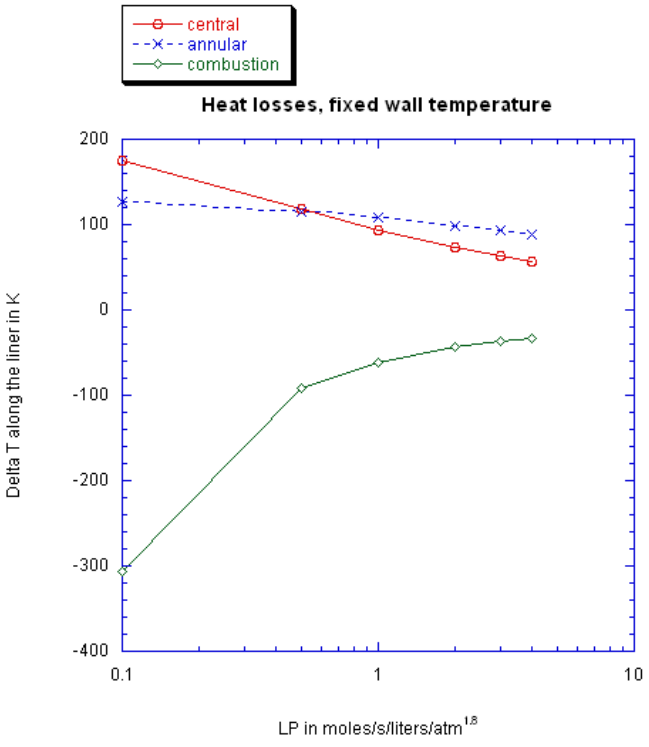

B

Figure 3-15. Cooling flows required A) and axial temperature changes B)

These are the results of heat rate integration along the length of the liner and the tube. These results have been obtained fixing the wall temperature for different flows here expressed in terms of loading parameters. It is seen that above a loading parameter of 0.5 moles.s^{-1}.liters^{-1}.atm$^{1.8}$, the axial temperature changes are within a 100K range. As expected the changes are decreasing with an increase in the load. Indeed, as the convection coefficient increases, the ratio of the total losses over the mass flow decreases, and so does the change in bulk temperature as described in Chapter 2 with Equation 2-5.

Gas dynamics model

As defined in the overall objectives of the rig, the flexibility of the system is a priority, which means that the rig should stand a large range of flow rates, gas composition and temperature. In order to achieve a sufficient mixing of the air and the fuel, and then to provide a good stirring in the reactor under the targeting range of operation, the evolution of the pressure, temperature and velocity in the supply lines and cooling passages should be estimated using a gas dynamics model. The stirring criteria in the combustion zone will be highly dependent on the injection jet velocity or pressure drop. Indeed, Kumar and co-workers investigated some scaling criteria for designing a mild burner, including keeping a pressure drop of 600mm of water gauge [51]. The injectors should be designed in order to provide at least this pressure drop over the targeted range of operation. In addition, the pressure drop along the supply lines could bring the flow to an unexpected sonic regime if it is not correctly estimated.

The model developed here is a one-dimensional gas dynamics model which accounts for geometry change, singular and regular pressure drops, and heat transfer. Between each node, four consecutive objects are used to evaluate Mach number,

pressure, temperature and density at point n+1 giving the values of this set of variables at point n. These four objects are the isentropic flow model accounting for area change, the Fanno flow in constant area duct accounting for friction effect, the pressure drop due to the singularities of the flow, and the Rayleigh flow accounting for heat transferred to the fluid. These are shown on Figure 3-15.

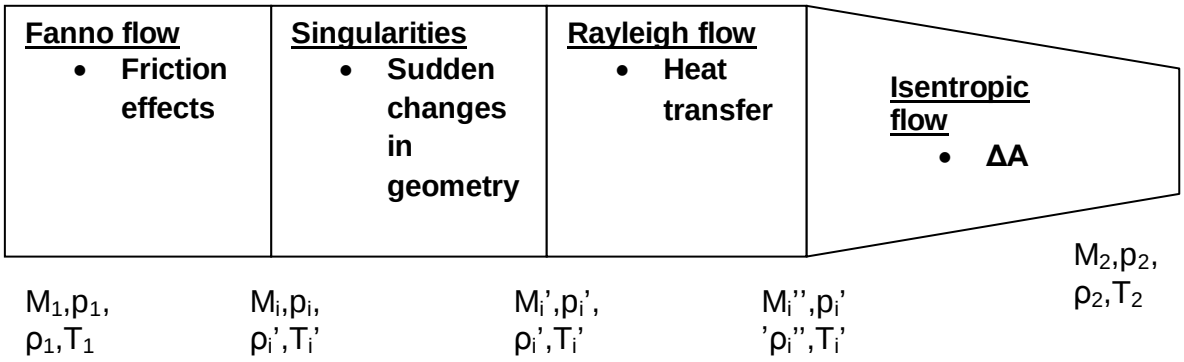

Figure 3-16. Gas dynamics model programming scheme

The isentropic flow model assumes the gas to be perfect and the flow to be adiabatic. The Mach number of the gas flow will be directly related to the ratio between the section of the duct and the critical section noted A^* at which the flow is exactly sonic. In this isentropic flow, the stagnation properties T_0, P_0 and ρ_0 stays constant. Therefore one can estimate the set of properties knowing the area change and the Mach number downstream using:

$$M_2 = f^{-1}\left(\frac{A_2}{A^*}\right) = f^{-1}\left(\frac{A_2}{A_1}\frac{A_1}{A^*}\right) = f^{-1}\left(\frac{A_2}{A_1} f(M_1)\right). \qquad (0.34)$$

The pressure drop module is made of two parts. The first one representing the friction effect and the model is called Fanno flow. A one dimensional flow of constant specific heat perfect gas through a perfectly insulated constant area duct is named

fanno line flow. The program here is based on the Fanno coefficient of friction. The friction makes the flow moving toward the sonic condition. If the flow is subsonic, the Mach number increases as one moves downstream. The stagnation and static pressure, temperature and density that the gas would reach at the sonic condition (downstream of the duct) will be noted with the superscript *. At a given position 1, one can evaluate the quantity below knowing M,

$$\left(\frac{fL_{\max}}{D}\right)_1 = f(M_1). \tag{0.35}$$

in which D is the diameter and L_{max} is the length downstream of this point that would be needed to raise the flow to the sonic condition. By the same way the Mach number could be evaluated at a position N+1 separated from N by the length L using the equation below,

$$\left(\frac{fL_{\max}}{D}\right)_2 = \left(\frac{fL_{\max}}{D}\right)_1 - \left(\frac{fL}{D}\right). \tag{0.36}$$

The Mach number at 2 is obtained using Equation 3.27. Between these two points, there will be a loss in stagnation pressure but no loss in the stagnation temperature. The temperature increases, while the pressure and the density decrease. The friction effect could lead a deflagration travelling inside a duct toward a detonation. It is fundamental in combustion to control this pressure drop in order to prevent damaging explosions. To use these equations above, one needs to evaluate the Fanno coefficient of friction. For laminar flow, concerning Reynolds Number less than 2000, the Fanno coefficient could be described the equation:

$$f = \frac{64}{\mathrm{Re}}. \tag{0.37}$$

For turbulent internal flow in a duct, with Reynolds number more than 2000, the Colebrook equation can be used:

$$\frac{1}{\sqrt{f}} = -2\log\left(\frac{2.51}{\mathrm{Re}\sqrt{f}} + \frac{k}{3.72 d_h}\right), \qquad (0.38)$$

where k is the roughness of the pipe, and d_h the hydraulic diameter. To solve Equation 3.29 a trial and error iterative scheme has been programmed in the Fanno module.

The flow path includes some singularities; hence an additional module has been programmed to take into account their effect on the flow properties. Three types of singularities have been taken into account:

- Sudden widening of the duct section
- Sudden restriction of the duct section
- Sudden change of direction of the flow (elbow…)

For each of these cases, a coefficient K of pressure drop is calculated based on the geometry. The equations for its calculation are given in Appendix B. Knowing these; one can calculate the loss of stagnation pressure through a singularity using the equation:

$$P_{02} = P_{01} - K\left(\frac{\rho U^2}{2}\right), \qquad (0.39)$$

where the points 1 and 2 are respectively located upstream and downstream of the singularity and U is the mean flow velocity.

Finally, the effect of heat transfer from the gases is accounted using a Rayleigh flow model. If one considers a one dimensional frictionless perfect gas in a constant area duct, the heated flow will move the Mach number toward the sonic condition (M=1). The opposite effect occurs when one cools the flow. So for subsonic flow, the Mach

number increases as the flow is heated. In a Rayleigh line flow, both stagnation pressure and stagnation temperature are affected by the heat transfer. Therefore, the superscript * is used for the properties that the fluid would have at the sonic condition. The ratios between the properties at a given point and this * properties are functions of the Mach number. By knowing the heat flux, one can calculate the difference in stagnation temperature using the energy equation:

$$\dot{m}C_p\left(T_{02}-T_{01}\right)=\int_1^2 \pi q'' D dl, \tag{0.40}$$

where q'' is the heat flux per unit area from the surroundings to the fluid. Therefore, the Mach number at point 2 can be evaluated using:

$$M_2=g^{-1}\left(\frac{T_{02}}{T_0^*}\right)=g^{-1}\left(\frac{T_{02}}{T_{01}}\frac{T_{01}}{T_0^*}\right)=g^{-1}\left(\frac{T_{02}}{T_{01}}g(M_1)\right). \tag{0.41}$$

The relations between the properties of the flow for the 4 types of flows are given in Appendix A. Finally, one can notice than in the current rig, the pressure is set by the downstream pressure as the gases exhaust to the atmosphere. It is desired to calculate the pressure downstream that would provide the desired flow rate to the combustor. A trial and error method has been programmed for the upstream pressure that would equalize the downstream pressure to the ambient for a desired flow rate. A simulation is presented in Figure 3-17. Two peaks of Mach number can be observed corresponding to the air nozzle for the premixing at point 2 and to the injector at point 5. The pressure drops are also significant at these two points. A small pressure recovery could be noticed as the flow is injected in the combustion zone at point 6 due to the larger section which is counterbalanced by the heat transfer from the combustion gases.

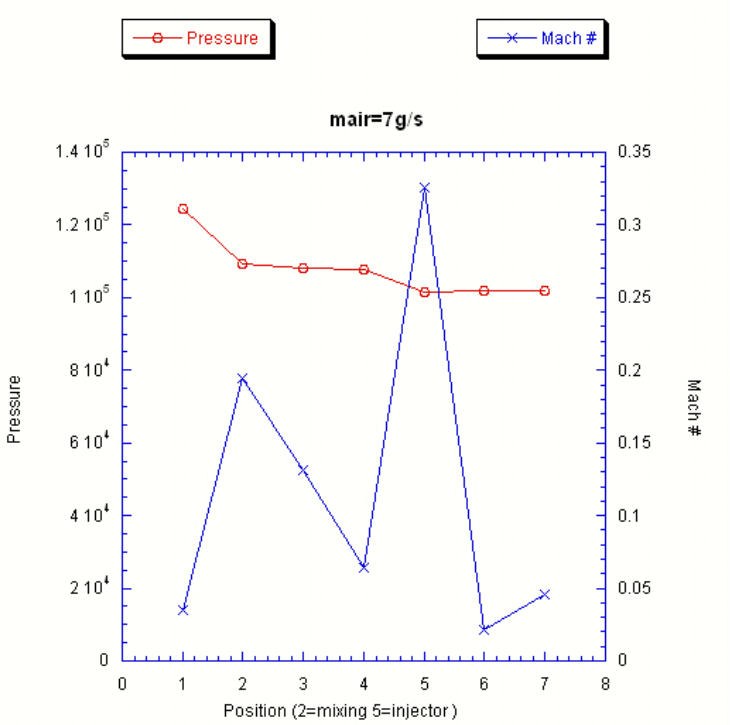

Figure 3-17. Pressure and Mach number evolution in the combustion air flow path

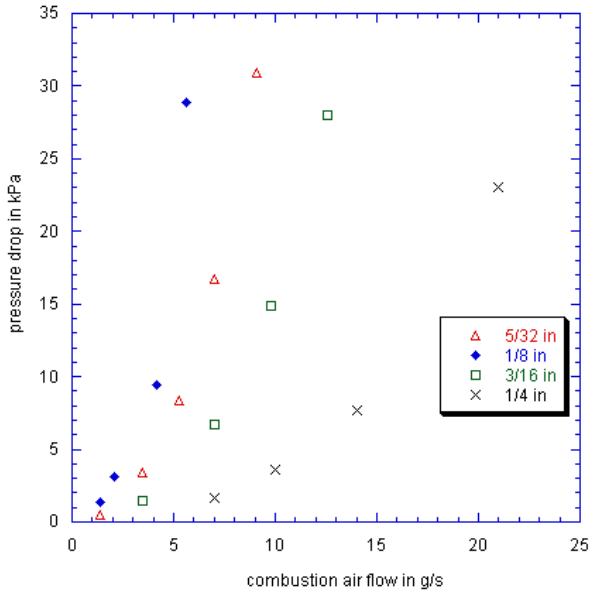

Figure 3-18. Pressure drop across the injector for different injectors

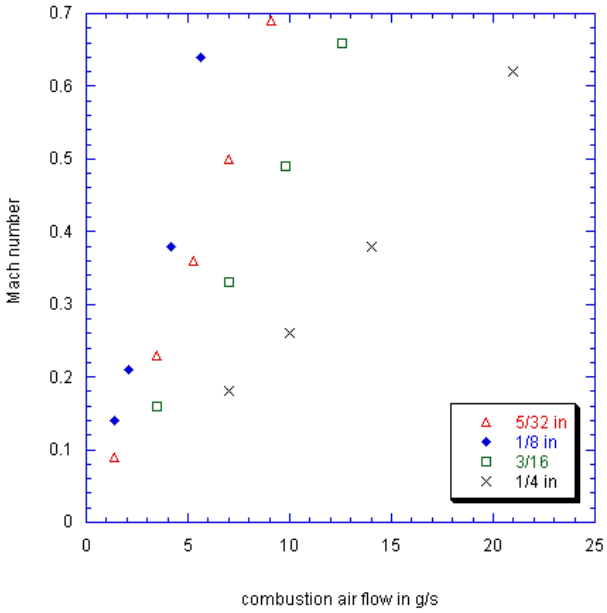

Figure 3-19. Jet Mach number for different injectors

Using this gas dynamics model, one can design the injector that would satisfy the condition of a high pressure drop across the injection to ensure a good mixing. Simulations have been done for 4 different diameters and are presented below in Figure 3-18 and Figure 3-19. From the results presented, we see that with a 3/16", one may be able to cover the range 5-18g/s. In addition, it is plan to add another set of injector at 1/4" so that we can cover in the long term higher range of flow rates.

In this chapter, the geometry of the burner and the different models used to obtain get the design parameters were considered. The geometry investigation gave the shape of the burner and the concept of radial multiple injections. The kinetic simulation determined the volume of the reaction zone, the heat transfer model provided with the size of the cooling passages such as the flow rate needed, and finally with the gas dynamics model the injectors were designed.

CHAPTER 4
FINAL DIMENSIONS OF THE RIG

In the previous chapter, the geometrical concept of the burner was provided and the different geometrical parameters were determined using different simple simulation approaches. From the results of the simulations and based on some criteria established, appropriate dimensions were selected. The final values of these dimensions were also determined from an economic viewpoint, which means that standard tubing and standard drill sizes were used as much as possible. The final design is presented on the next pages on Figure 4-1 and Figure 4-2. The rig is made of 7 main pieces whose quantities and material is presented in the Table 4-1. The liner is actually originally made of two pieces, which is the cylindrical body and the swirling vane, which is an annular piece, tapped and then pressed into the main body.

Table 4-1. List of the main parts of the combustion rig

Number	Piece	Material	Quantity
1	Liner	Haynes® Hastelloy X	1
2	Injector	Haynes® Hastelloy X	4
3	Casing	Stainless steel 304	1
4	Inner liner	Molybdenum	1
5	Tube	Stainless steel 304	1
6	Cooling air liner	Stainless steel 304	1
7	Distribution plate	Stainless steel 304	1

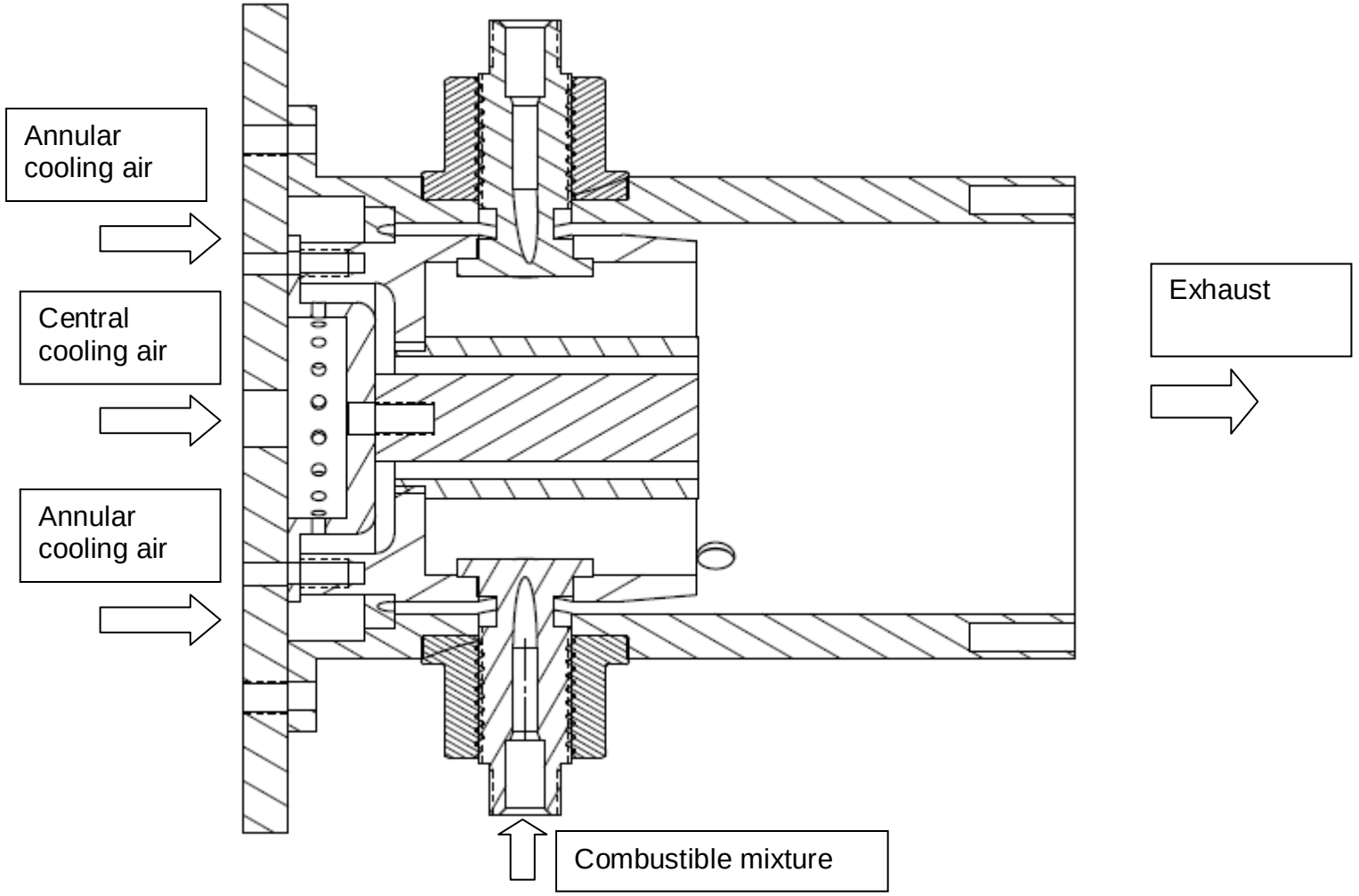

Figure 4-1. Axial view of the rig (Scale1/1)

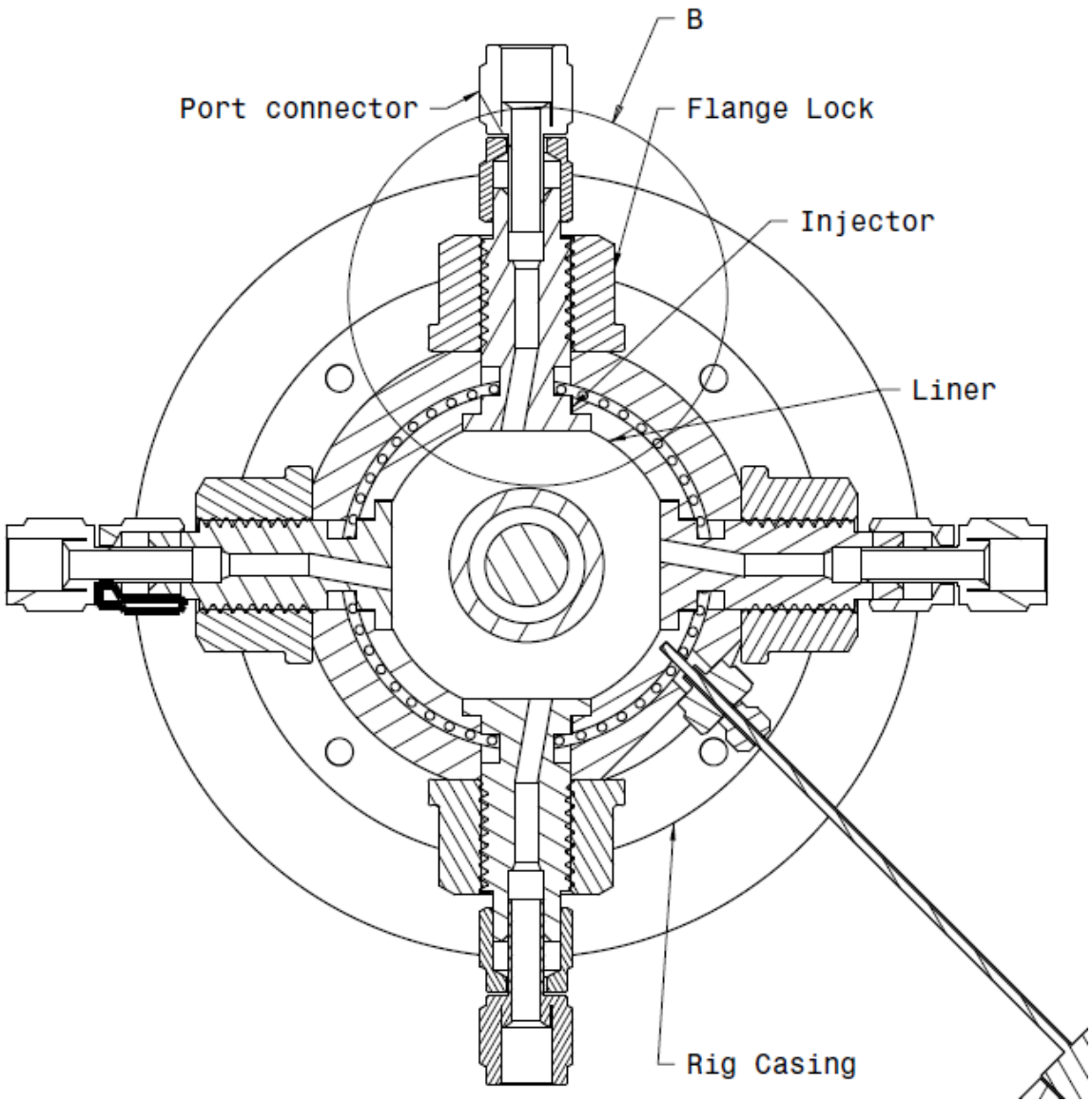

Figure 4-2. Normal view of the rig (resized)

The figures above being at scale 1/1, the dimensions could be read directly from the figure. Concerning the volume of the combustor, this is an annular shape of dimensions: 1.08”(27.4mm) of internal diameter, 2.076”(52.7mm) of external diameter and 1.8” (45.7mm) of length. Therefore, the total volume of the primary and secondary reaction zone (see Figure 3-5) is about 4.5 cubic inches or 75mL.

One can notice that a rod has been mounted inside the molybdenum tube to increase the cooling flow velocity. The cooling flow path enters the rig trough a central hole in the distribution plate shown in Figure 4-4, and flows to a pre-chamber in which the liner is tapped 20 times. The function of this large volume chamber is to equalize the flow and therefore provide a good distribution around the circumference. The air flows radially and then cools the rear part of the liner before entering the molybdenum tube at the end mixing with the combustion gases. Concerning the annular flow, the air is provided through 4 holes in the distribution plate (Figure 4-4). It enters an annular volume of large section before flowing through 50 holes of 1/16” diameter to enter through cooling section of the liner presenting a 0.08” clearance. The 50 holes are set at 20 degree angles with the axis of the liner and in the tangential plan. The function of these holes is to provide an important pressure drop between the annular pre-chamber and cooling passages so that a good distribution of the flow is obtained. In addition the angle provides a swirling effect, with the effect to increase the absolute velocity in the cooling passages.

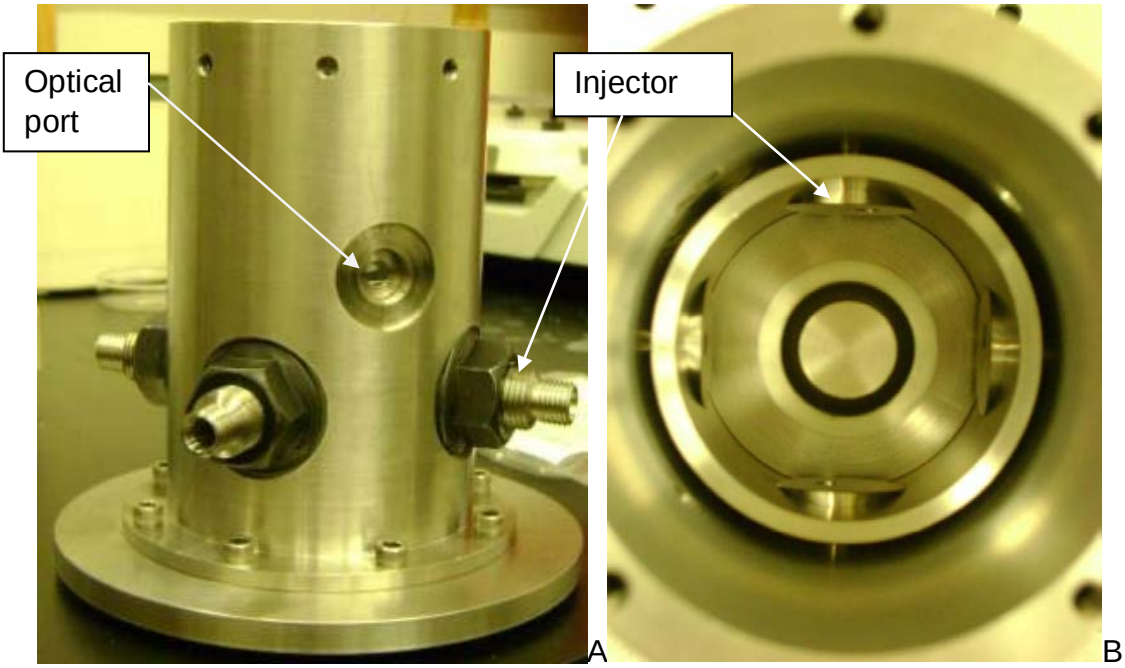

Figure 4-3. Rig assembled, outside A), and combustion zone B)

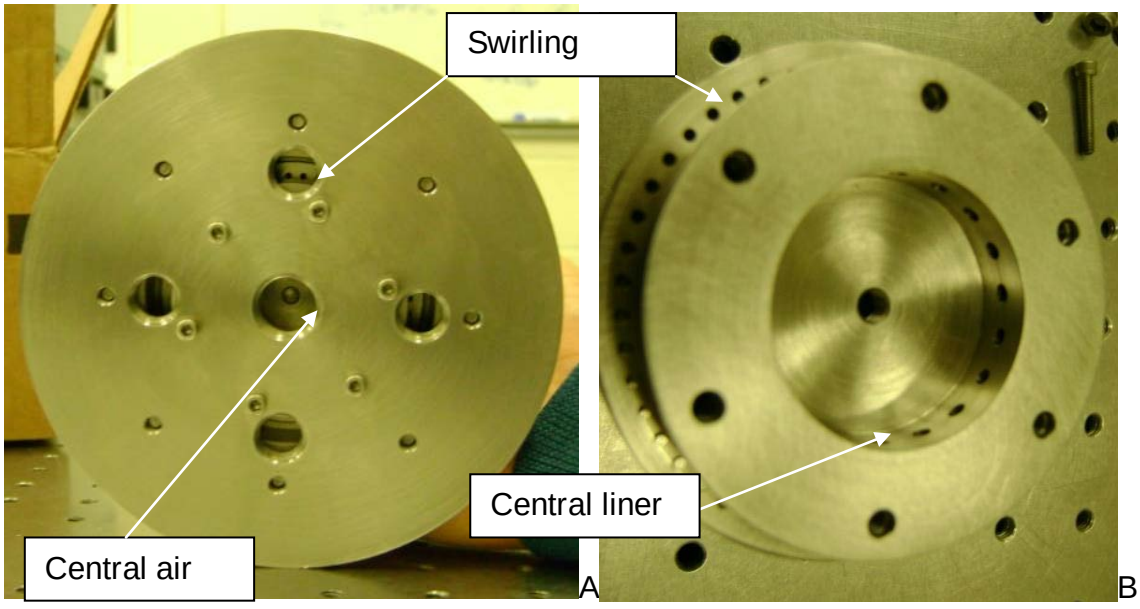

Figure 4-4. Back view of the rig with distribution plate A) and without B)

The critical parts in the current design are the injectors. The radial injection includes a slight 10° angle, hence designing a shape of an injector which would not significantly

perturb the flow was a challenge. A previous tentative design with no injection angle and intrusion into the injection chamber is compared to the current design on Figure 4-3. In the final design the injector is a cylindrical part with a neck for cooling reasons. The sealing is made with a plane to plane contact and an axial constraining stress was used with a flange lock nut pressing a counter sink on the casing.

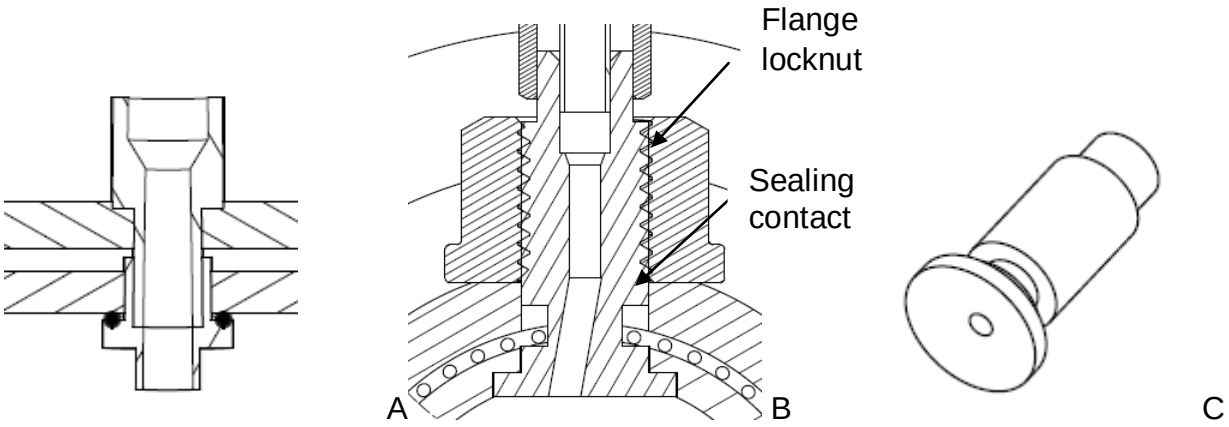

Figure 4-5. Injector design: previous invasive design A) and final design with normal B) and C) isometric views

If one considers the small size of the liner diameter, one can figure out how a high precision machining will be critical in the performance of the combustor. The clearance between the liner and the injector was specified at 0.005” for the smaller diameter. Figure 4-3 shows that in addition there are injector ports on both the liner and the casing so that geometric tolerances should be accurately addressed. Indeed, the cylindricity will provide a reduced clearance for additional sealing and a possible rotation for flexibility. The coaxiality of holes and their perpendicularity with the countersink on the liner and the rig are essential to the main plane-on-plane sealing. To get good sealing surfaces, the casing and the liner have been assembled during the final machining and corrections have been made to match the clearance requirements. Considering the

geometrical constraints and the discussion in Chapter 3 concerning the pressure drop across an injector, it was decided to machine a set of blank injectors. This set of injectors has the same functional surfaces with the liner and the casing than the tapped one, but no hole has been drilled. The latter has been based on a 1/4” outside diameter but the exact diameter can be decided based on the preliminary experimental observations. In addition, given the small size of the assembly, the threads are mainly British fine thread. The complete machine drawings with the specifications are provided in Appendix B.

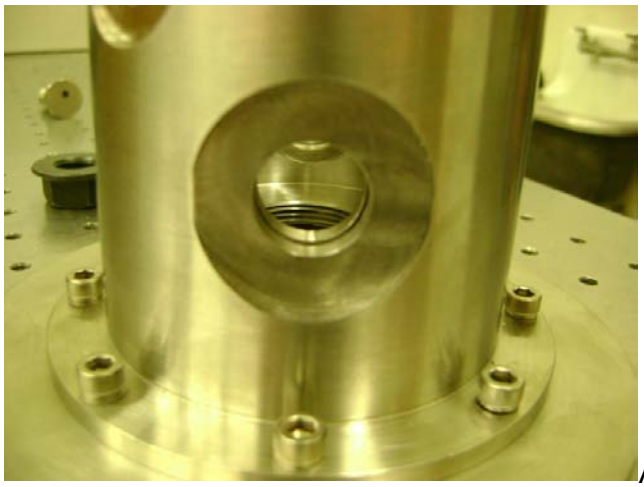
A

B

Figure 4-6. Injector ports on rig casing and liner A) and injector B)

The machining operations have been performed by T.M.R. Given the complexity and the precision required for this combustion system, a continuous contact has been maintained with the machinist supervisor. All the operations have been done manually. The tool and the rotation speed are given in Table 4-2. No real difficulties have been encountered on the different parts. Molydbdenum needs a soft tungsten carbide due to its tendency to crack and chip. For Haynes° Hastelloy X, no more than 0.05” could be cut in one pass. Very good sealing have been obtained on the injector ports which was

critical in this design. In addition, a very good coaxiality could also be observed for the molybdenum tube, the rod and the liner which was challenging given their mounting scheme. On an economic point of view, computer manipulated control of the drilling and turning operation would be viable starting at a series of 4 rig assemblies.

Table 4-2. Machining parameters used:

Material	Tool	Rotation speed (rough
Stainless steel 304	C5 Carbide	500rpm
Haynes® Hastelloy X	C2 Carbide	220rpm
Molybdenum	C1&C2 Carbide	220rpm

CHAPTER 5
DESIGN OF THE DELIVERY SYSTEM

Air supply

The air supply should be designed in order to provide a combustible mixture whose composition, temperature and pressure is accurately controlled. In addition for premixed combustion, the fuel and air should be mixed before entering the combustion zone. As mentioned before, premixed combustion raised the problem of the presence of a flammable mixture downstream of the injector. Auto ignition and flashback in unexpected sections of the system could be very damaging. This is particularly true in flow controllers which are expensive material and cannot stand temperatures above 70°C. As summary of the conditions that the delivery system has to accomplish, the list below has been established:

- Delivery of the combustion air flow to the four injectors (2-20g/s)
- Delivery of the cooling air to the cooling passages
- Heating of the injection air to the desired temperature (400-700K)
- Atomization, Vaporization and mixing of the fuel in the air mixture
- Precise control over the four injector mixture composition.

Compressor, dryer, filters and receiving tank

A compressor pumps the air from outside to pressurize a tank. The maximum pressure the tank could support is 175psi. The compressor has been chosen according to the maximum power available on the laboratory site corresponding to 7.5hp. The pressurized air could serve for other activities in the laboratory such as air powered machine tools. The idea here is to work on a duty cycle. Indeed, the compressor will be turned on as soon as the pressure in the tank is lower than a specified value pressure. When the pressure is reached the compressor will be turned off. During operation of the rig, air will be drawn from the tank on a continuous basis. Therefore, the pressure will

keep decreasing in the tank until a specified minimum pressure is reached and then the compressor will be turned on. When selecting the compressor technology, consideration was given to the cost, but also the fact that the compressor will have a discontinuous duty. Large current are drawn from the network when starting a compressor and so electrical starters are employed. For these reasons, a splash lubricating reciprocating engine was selected. A more silent apparatus such as rotary screw compressor are more expensive and not designed to be started many times per day. For a reciprocating engine, the compressor and tank were investigated under various loads from the combustion system in order to minimize the starts and to calculate the switch pressures.

The compressor could be modeled as a volumetric pump which means that the volumetric flow rate is constant and the pressure determined by the receiving tank pressure. The tank could be represented as a constant volume system undergoing change in pressure. An explicit Euler scheme could be used to represent the pressure evolution in a tank described below,

$$P\left(t+\delta_t\right) = P(t) + \frac{(\dot{m}_{in} - \dot{m}_{out})RT}{V_T}\delta_t, \tag{0.42}$$

$$\dot{m}_{in} = \frac{P(t)}{RT}\dot{V}(t), \tag{0.43}$$

with V_T being the total volume of the injector and $\dot{V}$ (t) being equal to the volumetric flow rate of the pump when turned on or zero if turned off. A simulation of the pressure evolution in the tank is shown on Figure 5-1, which shows that the compressor could be turned on only 8 times when 35SCFM are drawn to the combustor assuming a 200 gallons tank. The manufacturer advises to keep an average amount of starts below 6

starts per hours on a continuous operation. The maximum pressure in the tank is set to 180 psi, which is the tank constructor rating and the minimal pressure at 80psi, so that the equipment downstream does not see too large of pressure variations. A dryer is used in line with the compressor to remove moisture and cool down to 50°F along with two high efficiency filters to remove small particles.

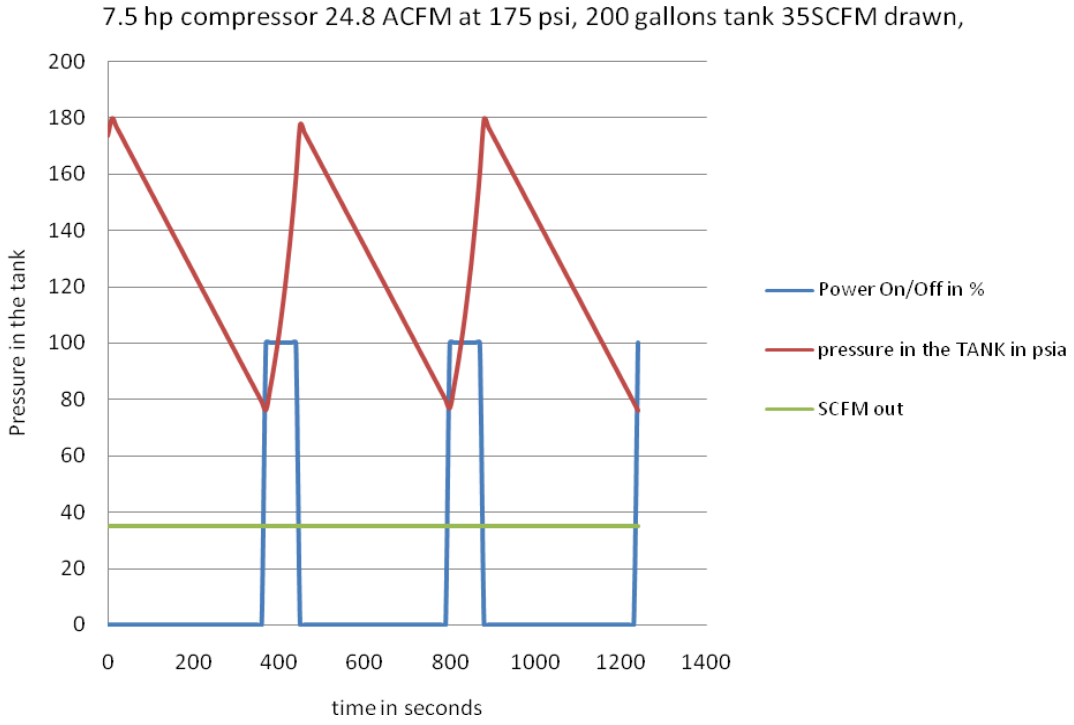

Figure 5-1. Pressure evolution in the tank at 35 SCFM.

Table 5-1. List of products for the air supply

Product	Supplier	Description
QT 7.5-7.5.80	Quincy	Simplex air reciprocating compressor 24.2 CFM at 175psi, mounted on an 80 gal. vertical tank
QPHT 50	Quincy	High inlet temperature refrigerated air dryer 40°F 40SCFM with aftercooler and coalescing air filter.
CPNT 00030	Quincy	Standard coalescing filters at 30SCFM and 100psig, 99% at 0.02 micron and with pressure difference gauge.
5018260-200	Quincy	120 gallons receiver tank

Air Heaters

Design specifications for the combustion system include preheating the combustion air to a temperature up to 700K for partial load (7g/s) and 400K for all loads as mentioned in the Chapter 2. With the four injectors being separately controlled, and the flow controllers not being able to withstand these temperatures, four independent heaters need to be used. The energy equation could be used to estimate the power required:

$$\dot{m}C_p\left(T_{in}-T_{out}\right)=\dot{Q} \tag{0.44}$$

Based on a 283K inlet temperature (from the dryer), the required load at 700K requires 732W and the full load at 400K, 587W. The heaters are controlled on an ON/OFF basis using an auto tunable PID CN132 from Omega. This latter items considers the difference between the set point and the signal of a type K thermocouple at the exit of the heaters. This controller being auto-tunable, it sets automatically the 3 constants of the proportional integral derivation action.

Fuel and air mixing system

The reference fuel, C_7H_{16} is mixed with the air upstream of the four injectors. The objective in this part is to provide a good control and mixing of the fuel and air mixture. That means the goal is to control the fuel-to-air ratio independently for the four injectors, and to minimize the radial distribution of the mixture composition at the injection. Recall that, premixed combustion offers large advantages in NOx reduction. However, this regime is difficult to achieve with liquid fuel. In gas turbine combustion, auto ignition of the fuel limits the residence time in the premixing section so that the processes of

atomization, vaporization and mixing should be quickly done. The mixture should be as homogeneous as possible to limit the fuel rich zone, with higher flame temperature and therefore higher NOx formation.

As this rig aims at being very flexible, runs should be possible over a wide range of flow and inlet conditions. Therefore, the range of fuel flow of interest has to be defined. As considered before, the minimal air flow rate that would lead to an adequate mixing could be estimated at 3.5g/s. The lowest fuel rate would so be obtained at the leanest flammable mixture at this flow rate. Weiss and co workers investigated the limits of heptane in a well stirred reactor and provided with a lean blowout equivalence ratio of 0.5 for a loading parameter equivalent to the current 3.5g/s and 0.6 at 20g/s (Weiss et al. 1958). As noted in the Chapter 3, given the geometry of the set of injectors, the system is limited concerning the maximum flow rate of air. Knowing the air flow rate, the mass flow rate could be calculated directly on the equivalence ratio basis:

$$m_f = \Phi \cdot m_a \cdot (F/A)_{stoch} \tag{0.45}$$

From Equation 1, the lowest flow of fuel can be estimated at 0.11g/s .Concerning the highest limit, the mass flow of air is limited to 20g/s. This is the limit the first set of injectors but a second set gives the opportunity to go up to 30 g/s. The equivalence ratio is limited for the highest flow to the stoichiometry.

Table 5-2. Range of total air and fuel flow rates

Air flow rate	Lower Fuel flow	Upper fuel flow
3.5g/s (LP=0.5)	0.11g/s	0.40g/s
20g/s (LP=3)	0.76g/s	1.3g/s

It was previously discussed that the air temperature would be set around 400K and up to 700K in the diluted regime. The objective is to get complete vaporization of the fuel in the premixing section so that the mixture could be considered as homogeneous at the injection. The boiling point of the reference fuel n-heptane is 371.58K. One could achieve complete vaporization of the fuel in a heat exchanger separately, but then the power to be transferred to the fuel by the heater would be very large, which may require a very large heat exchange area. In order to still favor vaporization, the fuel could be heated upstream of the premixing point, so that the total heat that has to be transferred from the air to the fuel to reach the evaporation curve is lowered, and the mixing length could be diminished. In the current design, a liquid fuel heater is designed to raise the fuel temperature just below the boiling point. The range of fuel flow rate being wide, a controller has to set the temperature of the fuel to the desired value. As the four injectors are independently controlled and the flow metered, 4 heaters have to be designed. Indeed the peristaltic pump could not stand 370K due to their polypropylene fittings, so the pumping and metering of the flow has to be done upstream of the heating system.

The heaters are made of a tube coated with a flexible heater. Two parameters have to be chosen, the diameter and the length of the tube. In order to design the heat exchanger, we use a constant surface temperature model for internal flow is used. In fact, a flexible heater in a duty cycle controlled by a P.I.D action is used to keep the liquid exit temperature at the specified value.

The heat transfer at a given section of the heater is given by:

$$\dot{q}_{conv}(x) = h\left(T_s(x) - T_l(x)\right). \tag{0.46}$$

Integrating the heat transfer rate over the entire length of the heater one gets:

$$\frac{(T_S - T_{l2})}{(T_S - T_{l1})} = \exp\left(-\frac{PLh}{\dot{m}C_p}\right), \tag{0.47}$$

where 1 and 2 are respectively the inlet and outlet liquid temperature. Inverting this relation to get T_s as a function of L gives:

$$T_s = \frac{T_{l2} - T_{l1}e^{\left(-\frac{PLh}{\dot{m}C_p}\right)}}{1 - e^{\left(-\frac{PLh}{\dot{m}C_p}\right)}}. \tag{0.48}$$

Using the energy equation and assuming steady state for the metal tube, one gets:

$$\dot{Q}_{conv} = \dot{m}C_p\Delta T_l \tag{0.49}$$

To be able to work in duty cycle and also fix the surface temperature, one wants that the power transferred to the fluid be less than the maximum power of the heater,

$$\dot{Q}_{conv} \leq P_{heater}. \tag{0.50}$$

In our case, the maximum Q_{conv} needed to raise the maximum flow rate to the boiling point is 150W per heater. The area covered by the heater tape for is 149 cm^2. The above equation is then used to calculate the surface temperature that this system would need. To get an estimate of the heat transfer coefficient, the correlation of the Nusselt number defined for an internal flow is used as:

$$Nu = \frac{hk}{D}. \tag{0.51}$$

Considering the low flows under investigation (down to 1mL/min), it is crucial to perform a proper dimensional analysis and so be able to use the relevant correlation. Some non-dimensional numbers are of importance when qualifying a flow of fluid.

The Reynolds number is the ratio of the inertia forces to the viscous forces,

$$R_e = \frac{\rho \cdot U \cdot D}{\mu}. \tag{0.52}$$

The Grashof number is the ratio of the buoyancy forces to the viscous forces,

$$Gr = \frac{g \cdot \beta \cdot (T_s - T_\infty)}{\upsilon^2}, \tag{0.53}$$

The Prandtl number measures the ratio of the viscous diffusion to the thermal diffusion,

$$\Pr = \frac{\nu}{\alpha} = \frac{\mu \cdot C_p}{k}. \tag{0.54}$$

At very low Reynolds number, the regime is referred as creeping flow, and the inertia term becomes negligible compared to the viscous effects. In the case of a heating duct, free convection due to buoyancy forces will appear as a consequence of the temperature gradient between the hot duct and the cold fluid. Mori and Futagami examined heat transfer on horizontal heated tubes with air [52]. They found that the Nusselt number started to increase compared to forced convection when the product of the three numbers above exceeds 10^3. Then it increases by 50% with a 10^5 increase of the latter product. On Table 5-3, are presented the values of the different non-dimensional numbers. In the current work, the Gr.Re.Pr product is well above this limit, so one can consider that the convection coefficient will be defined in a laminar regime.

Indeed, for a fully developed flow with constant temperature, Nu=3.56. For a 3/8" diameter, the length of heated tube will be 50cm and for a 3/16" it will be 100 cm. Using Equation 5-8, one can calculate the needed tube temperature for a heating of 150W to be transferred to the liquid. For an inlet temperature of 293K, a surface temperature of 394K for the 3/8" tube, and 376K for a 3/16" tube, are obtained. As 3/8" needs less length, provides an enhanced heat transfer coefficient (higher Gr Pr Re product), and a reasonable surface temperature, it was adopted.

Table 5-3. Non-dimensional numbers value for the creeping flow discussion

Tube	Re	Gr	Gr Pr Re (10^7)	$GrRe^{-2}$
3/16"	8.65-346	$1.49\ 10^6$	3.5-142	12.5-20000
3/8"	4.32-173	$1.19\ 10^7$	14.2-568	400-640000

In pre-vaporized, premixed system, the objective is to get a homogeneous gaseous mixture of fuel and air. As one will not reach vaporization of the fuel before the premixer, it is desired to spray the liquid fuel jet into the air stream so that atomization takes place. The atomization process in fuel injection is the one consisting of disrupting the consolidating surface tension by the action of an aerodynamic force. Indeed the surface tension is an effect of the intermolecular forces on the surface of a liquid and it tends to reduce the surface area of a liquid sheet or droplet. The minimum surface area/volume ratio being a sphere, this explains why the droplet from a faucet tends to be spherical. Using a model of a droplet breakup, the two forces should be equal so

$$\frac{1}{2}\rho_A U_R{}^2 C_D(\pi/4)D^2 = \pi D\sigma, \qquad (0.55)$$

where C_D is the drag coefficient of the droplet, σ the surface tension, D the droplet diameter, and U_R the relative velocity between the droplet and the air flow.

Atomization is generally seen as a sequence of two processes, the primary atomization which breaks the fuel sheet or jet into shreds and ligaments, and the secondary atomization which leads to smaller droplets. Two mechanisms have been distinguished to describe the fuel jet breakup process depending on the intensity of the disruptive force, which is a direct function of the intensity of the relative velocity between the air and the fuel bulk velocity. In the classical mechanism investigated by Rayleigh, small disturbances creates waves, which form a neck that which further lead to breakup due to surface tension effects. In this mechanism, the droplet size is of the order of the jet diameter and time scale of atomization remains large. When the relative velocity is further increased, the prompt atomization regime is reached in which breakup takes place very rapidly, and the final droplet size has no dependence with the jet initial size. This latter regime will be of primary interest for this work. This regime will be achieved if the jet of air is of sufficiently high velocity to promptly atomize the fuel jet, and this parameter will be critical in the design.

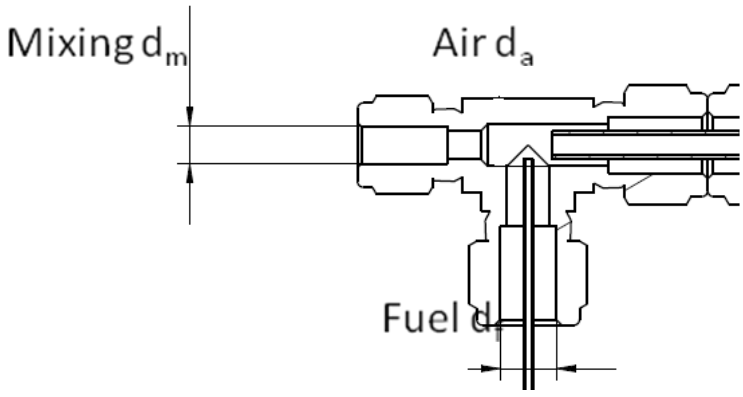

Figure 5-2. Mixing system

The system has to be able to guarantee the homogeneity of the air/fuel mixture over the entire range of flow rate. Using the one-dimensional gas dynamics model presented in Chapter 5, the diameters of the different passages were chosen that would accomplish a strong atomization, but also provide the necessary mixing and vaporization. Below are listed the important parameters and their function:

- 1. Air nozzle diameter: determines air jet velocity and so the atomization process (Equation 5.14).
- 2. Fuel nozzle diameter: determines the fuel jet penetration and the rate of atomization
- 3. Premixing section diameter: determines the rate of mixing by the turbulence intensity

The air nozzle diameter will be designed to provide the largest velocity without reaching a sonic flow anywhere in the air supply. In fact, the viscous effect on the air due to section narrowing will push the Mach number toward 1 since it could be considered as a Fanno flow. If the pressure drop is too great across an element, this may cause a sonic condition downstream at this injection. Given the range of mass flow of air targeted, one must yield:

$$\max_i(M(\dot{m}_{\max}, i)) \leq 1, \tag{0.56}$$

where i designates any cross section of the flow.

This shows the interest in programming a one dimensional gas dynamics model described in Chapter 3. The fuel nozzle is limited to the smallest tube possible. Indeed, the low flow of fuel involved in a continuous delivery by opposition to ICE (internal Combustion Engine) leads to very small velocity of the fuel. The maximum velocity will so be obtained with the smallest tube adaptable to the assembly, which is a 1/16”

stainless tube with a thick wall. Heating of the fuel upstream will lead to fairly high temperature, preventing the use of Polyethylene tube. The premixing section diameter consisting of a flexible hose is also of critical importance. In fact the amount of mixing and the residence time in the premixing section will guarantee the homogeneity of the injected mixture even though there is a poor fuel jet penetration. It is desirable to satisfy the following condition:

$$\tau_{mixing} \leq \tau_{res}. \tag{0.57}$$

The mixing could be estimated trough the turbulence intensity. A rule of thumb for turbulent developed flow (ReD greater than 4000) in a duct consists of:

$$\frac{(u'_{rms})}{U} = \mathrm{Re}_D^{-1/8}, \tag{0.58}$$

where U and u'_{rms} are respectively the root mean square of the fluctuating component and U the time average of the velocity

Then, one can very roughly approximately use a mixing time scale as the ratio between the diameter of the tube and the fluctuating component of the velocity. Indeed, the turbulent mixing wanted would be the radial one. The residence time is the length divided by the bulk velocity, so that the following is maximized:

$$\frac{\tau_{mixing}}{\tau_{res}} \approx \frac{\overline{u'}}{\overline{\frac{U}{L}}} \approx \mathrm{Re}_D^{-1/8} \frac{L}{D} \tag{0.59}$$

The maximum turbulence intensity would be achieved, in a developed flow, for the smallest Reynolds Number in the turbulent region. If Re=4000, the turbulence intensity reaches 35.4%. For a first implementation, a 6” length and 3/8” tube is used between

the mixing point and the injection. This tube could be changed afterwards, in order to study some partially or very well mixed premixing regime. The ranges of the different parameters discussed above are presented in Table 5-4. In Table 5-5, one can find the list of devices used in the fuel preparation/mixing system. 6 auto-tunable PID controllers are used for temperature control, four for the lines of air, one controlling simultaneously the four liquid fuel heaters, and 1 controlling the water heater for water steam injection fairly close to the liquid fuel heater.

Table 5-4. Parameters for the mixing system:

Condition	Dimension	Value (d_{in})	Lower flow	Upper flow
Air velocity	Air tube diameter	0.20”	49.6m/s	261.1m/s
Fuel velocity	Fuel tube diameter	0.0035”	0.02m/s	0.25m/s
Turbulence intensity in mixing tube	Premixing tube diameter	0.25”	32.6%	26.3%

Table 5-5. List of material used in the air/fuel mixing system:

Device	Supplier	Model	Description
Air Heater	Omega	AHP 7561	4 T-Type heaters (750W)
Thermocouple air	Omega	KQSS-116G-6	4 Type K thermocouples
Peristaltic pump	Fisher Scientific	13-876-2	5 Medium flow peristaltic pumps(0.8-85mL/min)
Flexible Heater-Liquid fuel	Omega	STH051-020	5 Heavy insulated heater tapes (156W)
Thermocouple fuel	Omega	TMQSS-040G-6	Type T thermocouple
Heater controller	Omega	CN132	6 PID Controllers
Controller relay	Omega	SSRL240DC10	6 Solid state relays

Control over the gas lines

In Chapter 2, the objectives and need for an accurate control over the injected mixture is discussed as well as a flexibility allowing staging and study of dissymmetry influences on stability. Indeed, it was planned to separately control the composition of the four injectors. The first reason is the ability to run on a staged combustion regime on the long term, where two injectors run rich and two injectors run lean. In that case the two rich injectors can be oriented toward the back of the combustion zone and the two other toward the front of the combustor. In addition, one can study the effect of a perturbation of one injector on the global reaction regime, especially at low residence times. The last reason is the flow of air and fuel being fairly small; it would be difficult to have the composition fairly equal between the four injectors using some manual vanes. This is particularly true for the low rate of fuel flow, so that using a manifold will not provide a fair accuracy on both the global and local equivalence ratio.

Implementing a certain number of different gaseous fuels is considered in this study, which are methane, hydrogen and carbon monoxide, such as running in a diluted regime with mixtures of carbon dioxide, nitrogen and water vapor. The controllers will have to be chosen so that one can minimize the total number of controllers, and give at the same time the maximum flexibility over the composition of the four injectors. The gas mass flow controllers chosen for this project are calibrated for all the different pure gases presented above. A manual switch could move from one calibration to the other. For this reason, one could have a very large number of control strategies with a few flow controllers in order to optimize the flow range and also the accuracy. On Table 5-6, some fuel implementations of interest are shown along with the different control

strategies depending on the operation range. The diagrams of the instrumentation are presented on Figure 5-4.

Table 5-6. Range of gases and control configurations, 4 injectors independently controlled (4), 2 injectors independently controlled (2), global mixture controlled (1). The combustion air is assumed to be always in level 4.

Fluid	Function	Control	Flows	Flow rates	Controllers
Air	Combustion	4	2-30g/s	1500SLPM	4 MC500SLPM
	Cooling central	N/A	0-10g/s	500SLPM	1 MC500SLPM
	Cooling annular	N/A	0-20g/s	1000SLPM	1 MC1000SLPM
Methane	Fuel	2	0-1.5g/s	150SLPM	2 MC50SLPM 2 MC250SLPM
	Fuel	4	0-0.5g/s	50SLPM	2 MC50SLPM 2 MC250SLPM
Carbon monoxide	Dilution	1	0-3g/s	50SLPM	1 MC50SLPM
	Fuel (H_2 0%)	4	0-12g/s	200SLPM	2 MC250SLPM 2 MC50SLPM
		2	0-18g/s	600SLPM	2MC250SLPM 2 MC50SLPM
	Fuel (H_2 50%)	2	0-6g/s	100SLPM	2 MC50SLPM
	Fuel (H_2 5%)	2	0-15g/s	500SLPM	2 MC250SLPM
	Mixed (H_2:5-50%)	1	0-18g/s	300SLPM	1 MC50SLPM 1 MC250SLPM
Hydrogen	Fuel (H_2 100%)	2	0-0.85g/s	600SLPM	2 MC250SLPM 2 MC50SLPM
		4	0-0.28g/s	200SLPM	2 MC250SLPM 2 MC50SLPM
	Fuel (H_2 50%)	2	0-0.7g/s	500SLPM	2 MC250SLPM
	Fuel (H_2 5%)	2	0-0.14g/s	100SLPM	2 MC50SLPM
	Staged or mixed	2	0-0.42g/s	300SLPM	1 MC250SLPM 1 MC50SLPM
Carbon dioxide	Dilution	1	0-0.8g/s	50SLPM	1 MC50SLPM
		1	0-4g/s	250SLPM	1 MC250SLPM
Nitrogen	Dilution	1	0-10g/s	500SLPM	1 MC500SLPM
Water vapor	Dilution	1	1-1.5	0-22sccpm	1 Peristaltic pump
N heptane	Fuel	1	0-1.5	0-175sccpm	4 Peristaltic pumps

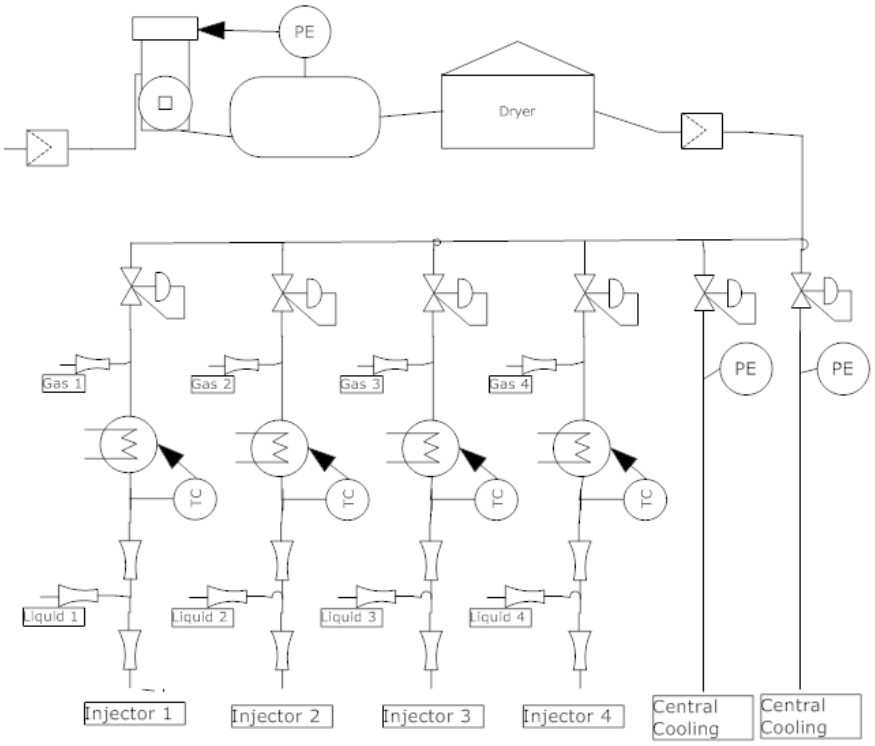

Figure 5-3. Air supply Process diagram

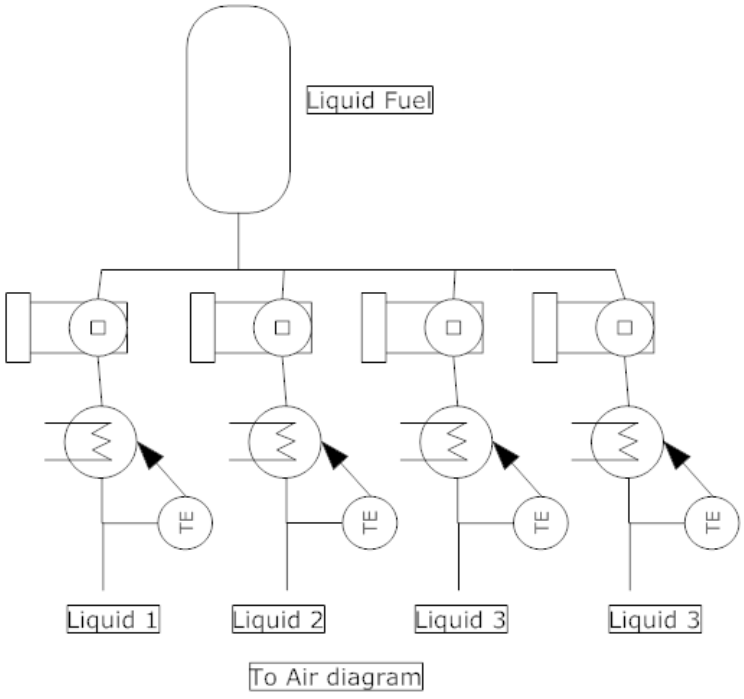

Figure 5-4. Process diagram of liquid fuel

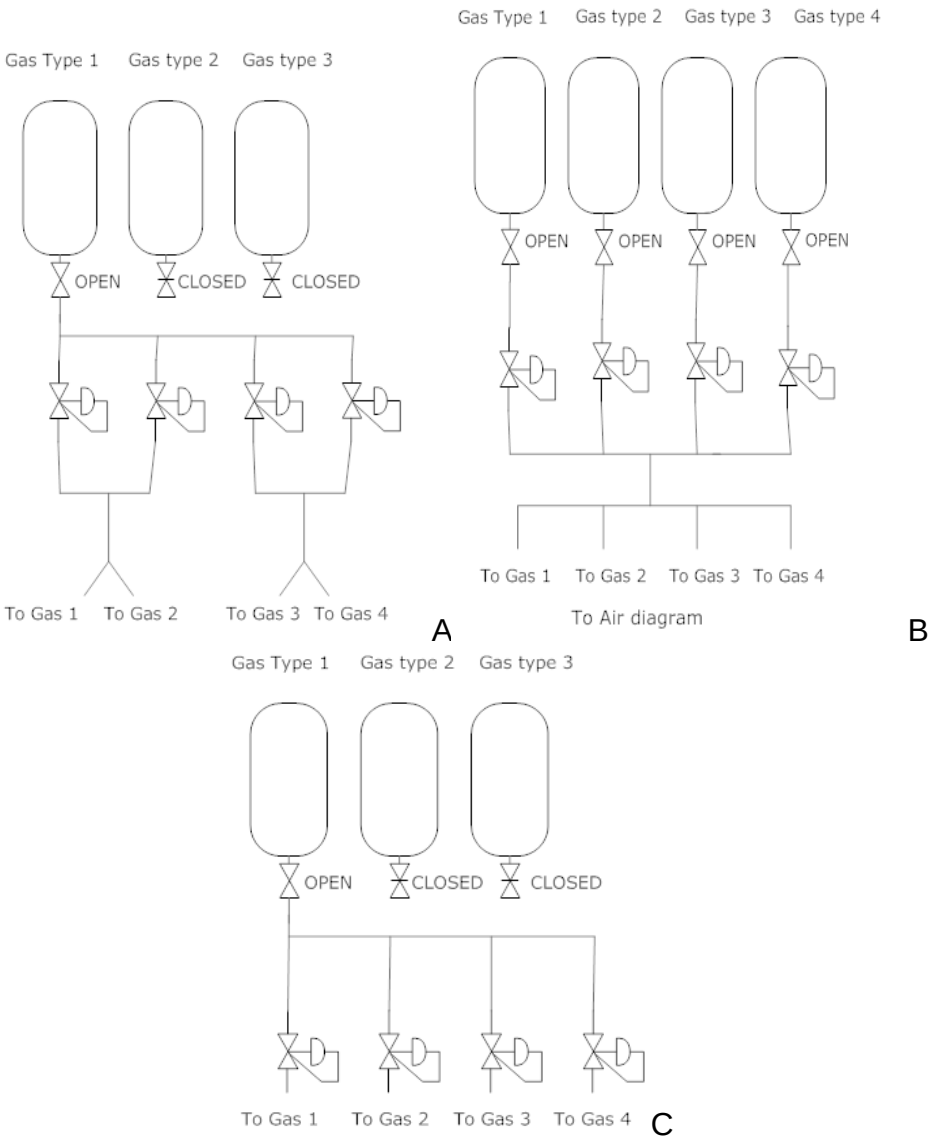

Figure 5-5. Process diagrams of gas in level 4 A), 2 B) and 1 C)

All these regimes are possible with the 12 controllers present in Table 5-6. Three degrees of control are presented above. The lowest level is 1s in which the control is only made over the total flow injected and so the four injectors present the same composition. For the level 2, the injectors are controlled two by two, this means that two compositions of the opposed injectors will have to be identical, but will be independent of the composition of the two others. The highest level is noted 4, since the four

injectors are independently controlled, and so offer the highest accuracy over the combustor composition.

Concerning the study of vitiated combustion, there are different plans. First, one can dilute with pure nitrogen to obtain an oxygen rarefied combustible mixture. Indeed, with 500 SLPM of nitrogen, one can get up to 91% of dilution at LP=1 and 85% at LP=0.5. There is also particularly an interest in characterizing the effect of CO2 in the flameless combustion regime. Indeed, it is desired to investigate both the thermal effects and the chemical effects of dilution. Here one can achieve from 0 to 250 SLPM with two ranges of accuracy for CO_2. According to equilibrium calculations using Cantera and the n heptane mechanism described in Chapter 3, stoichiometric air-n heptane mixture for 0.07g/s of total combustion air flow would create 20 SLPM of CO_2 in the exhaust for an open cycle. One can see here the large range of CO_2 dilution available here. Water injection is also of interest as it might play a primary role in flameless combustion chemistry by increasing the amount of highly reactive OH radicals.

Table 5-7. List of flow controllers

Item from Alicat Scientific	Quantity.	Accuracy (reading/full scale)
MCR-1500SLPM	1	0.8%/0.4%
MCR-500SLPM	1	0.8%/0.4%
MCR-500SLPM	5	0.4%/0.2%
MCR-50SLPM	3	0.4%/0.2%
MCR-250SLPM,	2	0.4%/0.2%
Total	12	

As mentioned in the statement of scope, we are interested in running some sort of synthesis gases as well as hydrogen. In Table 5-7, are presented the flow needed to run different synthesis gas at stoichiometry for several flow rates of air. In shaded are the mixtures that could be implemented within at least one of the control configurations of Table 5-8. Zhang et al. investigated laminar flame speeds for CO/H_2/air mixtures, presenting different CO-to-H_2 ratios, but given a constant adiabatic temperature of 1500K [5]. Flame speeds were measured at 1.6 atmospheres and 300K of reactant temperature. It appears than from a pure H_2 to a low H_2/CO (5% H_2 in mass), the chemical time, defined as the ratio of the flame thickness to the flame speed goes from 0.5ms to 5ms. Running this low mixture will be a challenge for the stability of the combustor, hence interest increases in investigating them and comparing the residence time at blowout for different hydrogen contents. In addition, running pure hydrogen is also considered. Indeed, hydrogen presents a fairly simple mechanism (12reactions) and it could be used for the combustor calibration in parallel with a CFD simulation. Indeed, Conaire et al. made a recent comprehensive study of hydrogen oxidation for conditions ranging from 0.05 to 87 bars and from 298 to 2700K and provided with a 19 reactions-mechanism [53]. A reactor network model could be developed with a higher resolution due to the larger number of CSTR reaction zone that could be modeled within a reasonable computation time in comparison to the GRI 3.0 mechanism.

Table 5-8. Flow rates of H_2, CO and global combustible mixture (air and fuel) for stoichiometric mixtures of CO/H_2/Air containing from 5-50% of H_2 in mass of fuel. The green shaded area corresponds to the conditions that can be achieved with a level 2 of control, and in blue, those achieved with a level 1. The areas not shaded correspond to conditions that cannot be implemented using the controllers presented above.

	Gases in SLPM (298.15K and 1atm) at Φ=1								
H_2 (in mass of fuel)	5%			20%			50%		
Gases	H_2	CO	A+F	H_2	CO	A+F	H_2	CO	A+F
f_a=3.5 g/s	**95**	**130**	**401**	**210**	**60**	**445**	**276**	**20**	**471**
f_a=7.0g/s	*191*	*261*	801	*420*	*120*	890	**552**	**40**	946
f_a=20.0g/s	545	744	2289	1200	343	2543	1577	114	2696

CHAPTER 6
DIAGNOSTICS AND FUTURE IMPLEMENTATIONS

The combustion system designed in this thesis is a flexible research tool for different types of experimental studies. The implementation of diagnostics to investigate the combustion alternative fuel as well as vitiated combustion is a long term process and many different steps may be considered. In a first iteration, the techniques that would help us to understand the combustion behavior of the burner are implemented to help characterize this novel design.

The combustion rig, presented in Chapter 4, possesses different *in situ* measurements ports. An optical line of sight is created by two opposing windows in the vicinity of the combustion zone exit. These ports can also be used for any kind of cooled, extractive probe, or direct flame measurement by a Platinum/Rhodium thermocouple. In addition, five ports have been incorporated to probe the liner temperature at different axial locations, and one to probe the air temperature at the exit of the cooling passages.

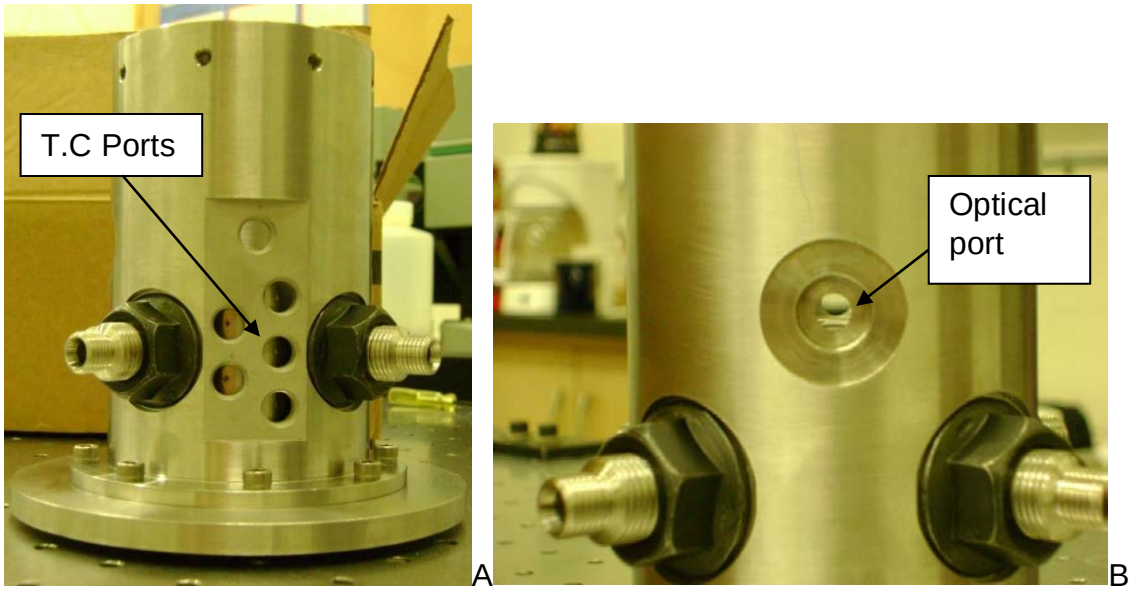

Figure 6-1. Picture of the thermocouple ports A) and an optical access port B)

Combustor characterization

The first experimental investigation planned concerns the stability loop of this system. This parameter influences directly the fuel flexibility performance of this burner. Different mixtures of air and n heptane will be tested in order to characterize the stability limits for a range of flow rates going from 3.5 to 20g/s. The mixture will be ignited with a spark or glow plug implemented through a port in the exhaust tube. A sudden drop of the liner temperature occurs when the flame blows out. Therefore, the outer surface of the liner will be probed by 5 type-T thermocouples. In addition, one can observe the flame right at the exit of the primary zone through the UV windows. This will tell if a luminous reaction occurs outside of the primary zone. To get information on the composition the combustion intermediates and products, a commercial portable gas analyzer probe, Lancom III, currently used in a research micro-gas turbine system can also probe the exhaust gases in this system. This gas analyzer can probe CO, NO, NO2, SO2, and H_2S using electrochemical cells, CO_2 by infrared spectroscopy, and hydrocarbons using a pellistor-catalyser. The electrochemical cells offer a resolution of 1 ppm for the corresponding species, and the volume fraction of CO_2 is assumed to be predicted with an accuracy of 0.1%. The flue gas temperature can also be probed from 0 to 1000°C with an error of 5°C. An additional port in the rig has been implemented so that a cooling thermocouple could probe the cooling air leaving the annular space between the liner and the casing. The temperature rise of the cooling air can provide an estimate of the heat transfer from the liner to the cooling air, and so estimate part of the heat losses from the combustion zone.

An investigation of the mixing in this design can also be performed under a cold flow regime. Nenniger used a Plexiglas version of the toroidal jet stirred reactor fed with

water to characterize the cold flow aerodynamics [11]. Dye was seeded on the water so that the flow patterns could be visualized. Cold flow techniques on air can also be used to characterize a combustor and has been implemented on actual combustion systems. Madhiyanon measured mean and fluctuating absolute velocities in a vortex combustor firing rice husks, using a hot wire anemometer under cold flow conditions [54]**.** In the current case, since this system is pre-vaporized, a cold flow regime can be reached with air only and a hot wire anemometer can provide estimation of the turbulence intensity in the combustor, and give an idea of the amount of mixing present.

Species and Temperature characterization in the primary zone

In Chapter 3, a first model of the primary zone of this reactor has been established using a sequence of well-stirred reactors. Based on a detailed mechanism for n heptane, and assuming a given flow split, the product composition and temperature were simulated. The analysis of the products formed in the primary zone, using gas sampling coupled with a commercial gas analyzer, or, if possible, with a gas chromatograph-mass spectrometer, will provide experimental results to be compared with this reactor model. In addition, experimental stability limits can also be compared to those of a reactor network model. A comparison will not lead to the absolute flow split and reactor zones, since an infinite number of reaction zones would be needed for that, but is essential for kinetic investigation of different fuels and levels of dilution. The technical challenge is this part is to be able to characterize the temperature and composition of the combustion gases at the primary zone exit temperature. Indeed, temperatures above 1500K are expected at this point, as predicted by the reactor network model developed in Chapter 3. At this level of temperature, direct probing could be done using a thin Pl/Pl/10%Rh (type S) thermocouple probe with a non-catalytic

coating made of a mixture of YCl_3 and Be0 [55]. Radiation effects have also to be accounted and corrected as described by Kaskan [56].

Different highly resolved laser-based techniques have been developed for flame temperature measurements. Most of them are based on non-linear wave mixing. Coherent anti-Raman stokes spectroscopy is based on the complex interaction between two incident waves and a free vibrational mode of the molecule probed, so that a strong resonant signal is generated at the anti-Stokes frequency. In this technique, two lasers are used: a fixed frequency w_1 laser such as a Nd-YAG, and another frequency tunable dye laser at w_2, such that resonance could be obtained when $\omega_2-\omega_1=\omega_{21}$, where ω_{21} is the frequency of the vibrational mode. This technique is complex and requires a strong spatial and temporal coherence. However, it can provide very accurate information on both major species concentrations and temperature. In addition, as the wave generated in strongly monochromatic, line of sight implementation is commonly employed. However, it is also limited to concentrations of the order of 1000ppm [57]. Another wave interaction technique has been developed: the degenerate four-wave mixing (DFWM). This technique can provide minor species concentrations and requires fairly simple optical implementation.

Finally, spontaneous emission phenomena are also widely used in combustion diagnostics. It involves the emission of a photon from an upper energy level. Different sources could raise the molecule to an upper electronic energy level such as collisions with photon, electron, or another molecule in the case chemical reaction. In chemiluminescence, a chemical reaction results in addition to the products formation in the emission of a photon. Indeed, a molecule is formed in an excited electronic state,

which then decays, and emits a photon. Chemiluminescence signals of OH^*, C_2^*, or CH^* are widely used for i*n situ* diagnostics, to detect ignition delays for example. The reaction primarily responsible of OH^* formation in hydrocarbon oxidation is:

$$CH + O_2 \rightarrow OH^* + CO. \quad (0.60)$$

The light could be collected and filtered around the specific fluorescence wavelength and so its time-resolved intensity could provide information on the chemical rates and the heat release. Even though the spontaneous fluorescence signal is non-directive, so that it emits into a 4π solid angle, the collected fluorescence signal by the optical port could tell about the eventual reactions taking place at the exit of the primary zone. When the excitation is produced by a laser, the term of laser-induced fluorescence (LIF) is used. In this case, the energy level reached will depend on the wavelength of the incident light. Excitation in the visible or UV range, which requires the simplest optical devices compared with the Infrared region, could provide one with major and minor diatomic species in combustion, such as CH, OH, C_2, CN, NH, and NO. Spectroscopic data of these molecules are provided by Eckbreth [57]. These advanced optical techniques have to be studied in detail in terms of limits of detection, sensitivity, and sources of noise. Some more straightforward incoherent techniques could be quickly implemented in the system. In fact, the line of sight optical access enables extinction measurements, spontaneous Raman, and elastic light back-scattering. In Raman scattering, the incident light interacts with the vibrational mode of the particle, and a photon is emitted as a shifted frequency known as the Raman shift. Different hydrocarbons present resonance peaks in the Raman spectrum as described

by Zhang and co-workers [58]. However the weakness of the Raman signal requires a high fluence laser as excitation source.

Some simple incoherent optical technique such as extinction, back-scattering, and 90° scattering techniques are based on the elastic light scattering theory developed first by Rayleigh for small particles and then generalized by Mie. When an electromagnetic wave of frequency v_0 encounters an obstacle such as a particle, it interacts with the particle electric charges, creating a dipole momentum that oscillates so electromagnetic radiation is generated. The interaction could be elastic, where the emitted wavelength is also λ_0 (Rayleigh scattering), or be inelastic, where the incident EM wave interacts with a vibrational mode of the particle, and emits at a different wavelength (Raman scattering). The wavelength emitted could be longer (stokes) or shorter (anti-Stokes). In elastic light scattering, the interraction between the incident electromagnetic radiation field and the particle are governed by the Maxwell equations in a medium. Mie in 1908 provided with an exact solution for the interaction of a electromagnetic field and a single homogeneous sphere [59]. In Figure 6-2, a sperical particle is represented and a coordinate system is defined according to the direction of propagation of the electromagnetic radiation and of its polarization. Therefore the direction of the scattered signal is represented using the angle Φ and θ with respect to the scattering plane.

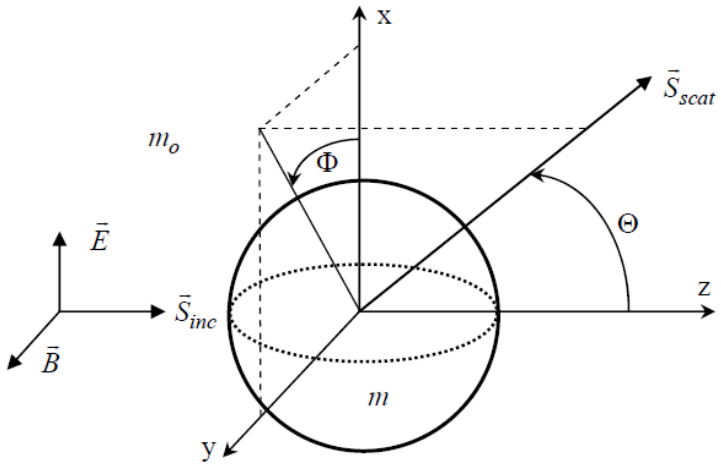

Figure 6-2. Spherical coordinate system in elastic light scattering

Given a monochromatic incident radiation of intensity I_0 and wavelength λ, the intensity of scattered radiation vertically or horizontal polarized with respect to the scattering plan could be expressed by for each scattering angle Φ and Θ:

$$I_\phi = I_0 \frac{\lambda^2}{4\pi^2 r^2} i_1 \sin^2 \phi \tag{0.61}$$

$$I_\Theta = I_0 \frac{\lambda^2}{4\pi^2 r^2} i_1 \cos^2 \Theta, \tag{0.62}$$

where r is the distance from the particle, and i_1 and i_2 two intensity functions.

On the larger size of particles, Mie scattering converges to the geometric optics laws, and for small particles it agrees with the theory developed by Rayleigh in 1871 [60]. This simplifies Mie's complex intensity function into simpler expressions under the assumption of non-absorbing molecules. The Rayleigh theory is based on the assumption that the particle sees a uniform external electric field, and that this field penetrates the particle faster than the time period of the incident electromagnetic wave. These two assumptions may be illustrated by the expressions below:

$$\alpha = \frac{2\pi a}{\lambda} \ll 1, \tag{0.63}$$

$$|\bar{m}|\alpha \ll 1, \tag{0.64}$$

where m is the complex index of refraction of the particle, and a its radius. This theory provides the scattering and absorption total cross section expressed as:

$$C_{scat} = \frac{2\lambda^2}{3\pi}\alpha^6 \left|\frac{\bar{m}^2 - 1}{\bar{m}^2 + 2}\right|^2, \tag{0.65}$$

$$C_{abs} = \frac{-\lambda^2}{\pi}\alpha^3 \,\mathrm{Im}\left\{\frac{\bar{m}^2 - 1}{\bar{m}^2 + 2}\right\}, \tag{0.66}$$

Using the equations above, one can discuss the dependency of the collected signal intensity over the size of the particle and the laser wavelength. The scattering cross-section varies with the 6th power of α, while the absorption cross section varies only with the 3rd power. Given that the extinction cross section is the sum of these two cross sections, one can see that the absorption contribution will be predominant for small particles over the scattering term. However the differential extinction parameter will scale with the 6th power of particle size so that the scattered signal of large aromatic structure will completely overwhelmed that of a diatomic molecule. This technique gives a very strong signal for soot particle from the inception regime to the surface growth regime, corresponding to sizes from 10 to several hundreds of nanometers. The soot formation mechanism will be discussed in more detail below. The scattering-cross section of soot being several orders of magnitude higher than those of nitrogen, a very strong scattered signal could be emitted. However, for a polydisperse system of

particles, the soot volume fraction could be obtained only if one assumes the value of a complex index of refraction. Scattering signals being highly dependent on both the size particle (i.e. cross section) and the number density, the interpretation of the signal could lead to high uncertainties considering the wide range of diameters covered from the early soot precursors to the large particles (from nanometers to hundred of nanometers). While accurate soot number density and volume fraction measurements could not be obtained without precise calibration and sampling, this technique is very interesting to detect the transition from a non-sooting regime to a sooting regime as the back scattered intensity emitted will increase suddenly or the transmitted signal will drop.

Another technique has been developed in the last decade to provide soot volume fractions: the laser induced incandescence (LII). A high energy laser beam will cause the soot particle temperature to rise to about 4000K and then the blackbody radiation from this soot is observed. Several papers showed that the emitted intensity is proportional to the soot volume fraction. Approaches to calibrate the LII signal using other techniques have been developed for soot volume fraction measurements. Elastic light scattering was used in combination with LII in the RAYLIX technique developed by Geitlinger et al. [61] .In addition, on-line extinction calibration has been created by Axelsson using two beams from a Nd YAG laser: one at the fundamental frequency (1064nm) for the LII shot, and a less energetic at the double frequency (532nm) for extinction measurements [17]. These two types of calibration suffer also from the same dependence on the soot refractive index. Wander Wal used gravimetric sampling calibration [62], thereby avoiding the need for refractive index. In this technique, the

soot particles created in the flame were mixed in a gravimetric chimney using a swirling flow of nitrogen in order to get spatial homogeneity before sampling. Knowing the gas flow and the density of the sample, the soot volume fraction can be estimated to calibrate the LII Signal. This approach could be of interest for the current system, where a homogeneous spatial distribution in soot particle could be expected due to the high level of mixing in the combustion zone, so that there is no need for the gravimetric chimney used by Wander Wal. Moreover, time-resolved LII has a main strength as being able to provide the soot particle sizes by measuring the decay time of the emitted radiation. Another advantage of LII is that it shows a rapid rise in LII signal with laser fluence and then a plateau. If one operates in this plateau by using sufficient fluence of laser, the laser beam absorption will not affect the emitted signal. However, vaporization effects could occur when the soot is raised to the vaporization temperature under large laser fluences as investigated by Yoder and co-workers. [63]. They used LII in line with light scattering to investigate the vaporization effect, and did not notice vaporization effects for a excitation laser fluence under $0.1 mJ/cm^2$.

Finally, the line of sight optical access is very suitable to absorption measurements. The absorption spectroscopy consists of tuning a laser beam in order to match one or several electronic/vibrational transitions of the probed molecules. A spectrally resolved signal is collected and compared to a beam which does not travel into the combustion zone. The analysis of the spectral absorption profile can provide different information depending on experimental setup. One can obtain the number density of species such as O_2, H_2O, CO, CO_2, NO, NO_2, OH, NH_3, HF, H_2S, and CH_4, or the temperature and the velocity of the flow through the Doppler shift and profile

broadening [64]. Diode lasers are convenient light sources for absorption measurements since they are inexpensive for the applications concerned in combustion and can be tuned based on the injection current. Most of the molecules of interest have transitions in the infra red around 1.55 μm [64], so that the grating optics should be set for this domain. Finally, tunable diode lasers offer the ability to tune on and off the absorption line, allowing real-time compensation for laser transmission and therefore accurate, real-time species profile measurements.

Stability studies

Once the stability of n heptane has been characterized by reaching stability limits over different loadings, the current system can be used to investigate the intrinsic stability performance of exotic mixtures. Two different types of investigation are of interest for this system. First, the use in low-hydrogen content syngas flames in gas turbine combustors could be prevented by its poor stability performance. The flexibility of the current system enables the variation of two parameters to study the stability performance of syngas. First, the residence time could be varied with the air flow rate so that different reactant concentrations and temperatures affect the oxidation chemistry. Then, the hydrogen-carbon monoxide ratio could be varied on the flight so that stability limits could also be reached on this dimension.

Another investigation is motivated by the challenge of curbing emissions abatement in gas turbine combustors. The technology called flameless combustion regime or mild combustion offers a promising opportunity to curve simultaneously NOx, CO, CO_2 and soot. The flameless regime is characterized by a non-luminous regime, a homogeneous temperature and distributed reaction zone. This regime is obtained with a

high inlet temperature and a low adiabatic flame temperature as a result of an oxygen rarefaction due to dilution. In practical systems, this is achieved by means of internal or external recirculation. The transition to the flameless regime on a semi closed cycle system has been observed with a sharp decrease in luminosity [31]. This could be interpreted by a lower soot yield of the flame. The investigation of the high temperature vitiated regime could be made through the stability limits characterization for different dilution gases. Indeed, divergences have been observed between experimental and numerical studies concerning the enhancement of the operability limits with an increase in the exhaust gas recirculation between Singh et al. [65] and Marek [66]. The investigation could be performed by fixing the flow of air and dilution gases, and by varying the mass flow of fuel before reaching blowout. The present system offers two dimensions to reach a regime in which significant soot particles are formed in order to study the dilution effect on the soot formation process. First, in a premixed regime, the fuel to air ratio can be adjusted in order to reach the soot inception regime of the fuel generally for equivalence ratios above 1.9. The second dimension concerns the degree of premixing of the fuel and air mixture. Indeed the temperature of the liquid fuel injected into the air stream could be adjusted to decrease the amount of pre-vaporization. In this case, a local flamelet regime could be achieved in the reaction zone increasing the soot formation process.

Soot characterization

The drop of luminosity at the transition with the flameless regime may be investigated with the current system through soot characterization over different regimes. As mentioned earlier, optical techniques to obtain soot volume fraction, size and number density are very sensitive to the size of the molecule and particles probed.

Therefore, prior to implementing one or an optical scheme, an insight in the soot particle formation is necessary. Indeed, we can formulate the question:

- Could soot precursors be generated in a controlled manner on this system?
- What type of molecule would be present at the current optical access?

Soot particles are generated in gas turbine combustor under certain conditions. They are often undesirable, as they represent an environmental and health hazard in the one hand, and decrease the combustion efficiency in the other hand, due to an enhanced radiation, and as a byproduct with respect to water and carbon dioxide. The mechanism which rules the early formation of this particle and their further oxidation is very complex and includes gas phase chemistry, surface gas chemistry and particle agglomeration. They include a wide range of particles size from a nanometer to hundreds of nanometer. The early stages of formation involve the formation of aromatic rings from various fuel radicals, such as acetylene and propargyl radicals to form benzene or phenyl. Benzene leads to higher polycyclic aromatic hydrocarbons (PAH) by the H-abstraction, acetylene addition described by Frenklach. [67].The surface of the PAH molecule will grow by this way until it reaches the inception regime, and then coagulation and agglomeration between particles takes place. Finally under solid-gas phase chemistry, the soot particle is oxidized by O atoms, OH radical, and O_2.

Different stages in this mechanism have been studied using different means. Here, the current work will focus on the premixed flame configurations. Early gas chemistry with few aromatic rings has been studied using fuel pyrolysis in shock tubes, coupled with extinction measurements by Alexiou and Williams for blends of toluene and n-heptane [68]. Pyrolysis involves mixture of fuel and diluents so that there is no fuel oxidation reaction.

Table 6-1. Selected experimental studies on soot formation. J.S.R: jet stirred reactor, P.F.R plug flow reactor, DMA: differential mobility analyzer, T.E.M: transmission electron microscopy, G.C: gas chromatograph, EX: extinction, M.S: mass spectrometer, F.I.D: Flame Ionization Detector, amu: atomic mass unit., N.S low angle neutron scattering.

Author (Particle)	Fuel	Device	phi	Temperature	res time	size	Soot level	Exp
Manzello 2007 [14] (Soot inception)	C_2H_4/Air	JSR/PFR	1.9-2.2	1540-1620K	5-42ms	4-70nm	0-50 mg/m^3	DMA TEM
Nenniger 1983 [11] (Soot and PAH)	C_7H_8/Air C_2H_2/Air	JSR/PFR	1.37-2.14 0.8-2.94	1560-1670K 1280-1640K	4-6ms		0-140 µg/g	GC
Wang et al. 2002 [69] (PAH)	C_2H_2/O_2/Ar	Premixed laminar	0.6-2.5	Ti: 330-424K Tm: 1698-1787	0-230ms	5-7nm	N: 0-107 cm^{-3}	NS
Alexiou 1994 [67] (PAH and HC)	C_7H_8/C_7H_{16} C_7H_8/C_8H_{18}	Shock tube	0-1 %mol Ar	1500-2400K	0-0.5ms		0.7 %mol	EX
Macadam 1997 [70] (PAH/C2H2)	C_2H_2/Air /CO_2/N_2	JSR/PFR	2.2	1580-1650K	0-30ms	128-398 amu		GC-MS GC-FID

Different studies have been done on the soot inception and particle growth using laminar premixed flames or well-stirred reactor-plug flow reactors. A setup in which a well-stirred reactor is followed by a plug flow reactor has been demonstrated to have many advantages when investigating the soot inception regime [71]. Using a toroidal jet stirred reactor terminated with a plug flow reactor, Manzello and co-workers measured soot particle size distribution in rich mixtures of ethylene [14]. Probing at different distances from the exit of the WSR provides with exhaust composition after different residence times, and so the different steps of the reaction following the soot precursor generation inside the well stirred reactor can be investigated. Wang and co-workers investigated PAH formation in premixed laminar flames using low-angle neutron spectroscopy [69]. In laminar premixed flames, the conditions are different from the

ones in a jet stirred reactor, as the main heat transfer mechanism is heat conduction. This results in much larger residence times of the chemical process, as they occur at lower temperature. The reported PAH particles ranges from 5-7nm, which corresponds to the high sensitivity range for small angle neutron spectroscopy. Indeed, one considers the Arrhenius form of a reaction rate for an elementary step between two products A and B, one gets the reaction rate:

$$\frac{d[A]}{dt} = -k_0[A][B]e^{-\frac{E_a}{RT}}, \tag{0.67}$$

where E_a is the activation energy and k_0 a constant.

Residence times in combustion could be compared only at similar conditions in terms of temperature and reactant concentration. The current implementation of the burner has been motivated by stability limit characterization, so that it involves very small residence times. In Chapter 3, the kinetic simulation provided with an estimate of the residence time in the primary reactor of the combustion. The total residence time range could be estimated as going from 0.5 to 4ms for the global reaction zone contained in the liner. The temperatures will range from 1300 to 2200K. In the actual configuration, one cannot really consider the zone downstream of the primary zone as a plug flow reactor since there is dilution by the cooling air. At high loadings and within stability limits, the residence time of the mixture in the primary zone is low but the concentration of reactants being high, the overall reaction rate will be faster. In this configuration, one can intuitively think that only the early stages of the soot mechanism could be investigated, as they concern hydrocarbons and PAH.

Brown and co-workers modeled the kinetics of ethylene air mixtures in a perfectly-stirred reactor for various reactor residence times and temperature [72]. Their simulations are based on the soot formation mechanism developed by Frenklach. Based on these results, if one runs mixtures of ethylene and air with rich equivalence ratio from 2 to 3 in the current implementation (0.5-4ms), one can expect to observe mainly small PAH in the system, where size is on the order of a nanometer to several nanometers. Another study has been carried by Singh based also on a Frenklach mechanism, but in which particle sizes are modeled on a different scheme [73]. Based on his model, for a reactor residence time of 1ms, the particle sizes ranged from 2 to 12nm for a flame temperature between 1500 and 2000K. Particles over 50nm should be observed for residence time between 5 and 10ms. These two considerations have to be taken into account for the choice of the optical device.

Futures studies and implementations:

The design of this novel combustion system has been thought to offer certain flexibility for a parametric study and a continuous development of this system. With the actual implementations, the effect on the stability performance of the following different parameter can be studied:

1. Rotation of the injector to change the jet impingement angle and the flow split in the primary zone (Figure 2-4).
2. Modification of the local equivalence ratio of the injected fuel air mixture. One injector could run under a different composition to create an asymmetry in the flame.
3. Staged combustion with two injectors running rich and oriented toward the rear plate and two injectors running lean and oriented toward the exhaust (figure 6.4). This sequential combustion scheme could be of interest for stabilizing techniques in aero-combustors.

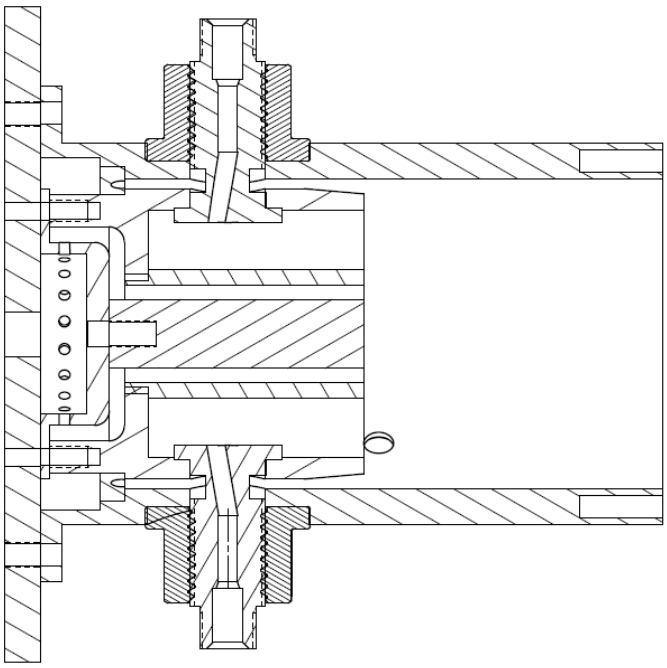

Figure 6-3. Staged combustion configuration where the two rich injectors are shown

Further geometrical changes could be done with the following modifications:

4. To simplify the first design, no nozzles have been implemented on the injector. The presence of a slight elbow close to the injection, this may lead to a disturbed jet velocity profile. Some inserts can be pressed afterward on the injectors to include a converging nozzle in the flow. This can be done after some first experimental observations on the combustion regime.

5. Modification of the inner tube (Figure 6-4 A) to act on the size of the primary reaction zone.

6. Machining of blank injector with smaller or larger diameter, depending whether the interest is in higher flow rates (stability) or lower flow rates (soot) while still providing a good mixing

7. Implementation of 8 secondary air holes in the primary reaction zone for staged combustion implementation (Figure 6-4 B).

8. Modification of the fuel preparation system to increase the pre-vaporization time with a longer premixing section, or to evolve in a diffusion combustion scheme with a smaller tube.

9. Implementation of a tube downstream of the liner so that the primary reaction zone could be continued with a reaction zone close to a plug flow reactor for soot inception regime investigation.

Some additional diagnostics to combustion species and temperature can be possible with additional implementations:

10. Implementation of an additional window as shown in Figure 6-5 or downstream of the reaction zone to provide access for a 90° scattering.

11. Implementation of a transverse nitrogen guided probe to perform real time sampling toward a GC-MS (Gas Chromatograph-Mass spectrometer) or a SMPS (Scanning Mobility Particle Spectrometer). This would enable accurate species analysis (GC-MS), and particle size distribution (SMPS).

In addition to these plans, the design of an afterburner downstream of this multiple injector combustion chamber would be very beneficial in terms of emitted species. Indeed, at high flow rates close to the stability limits, the combustion is incomplete in the primary reaction zone, and the dilution with the cooling may not completely oxidize the intermediates and unburned hydrocarbons created in the primary zone.

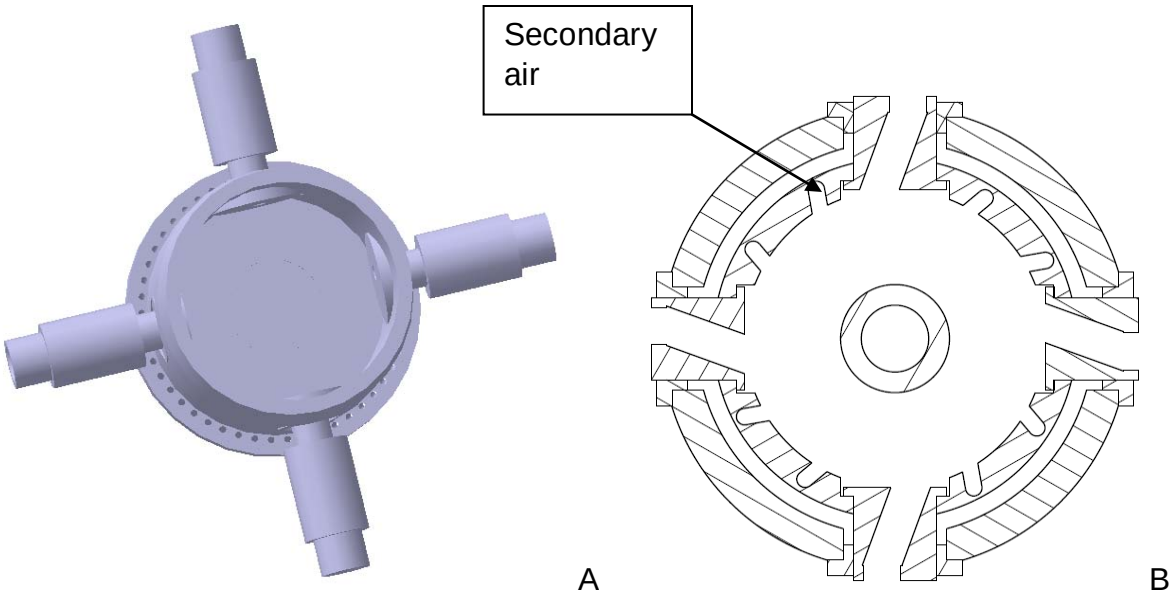

Figure 6-4. Different geometric modifications: removal and change of the inner tube A), addition of 8 secondary air holes B).

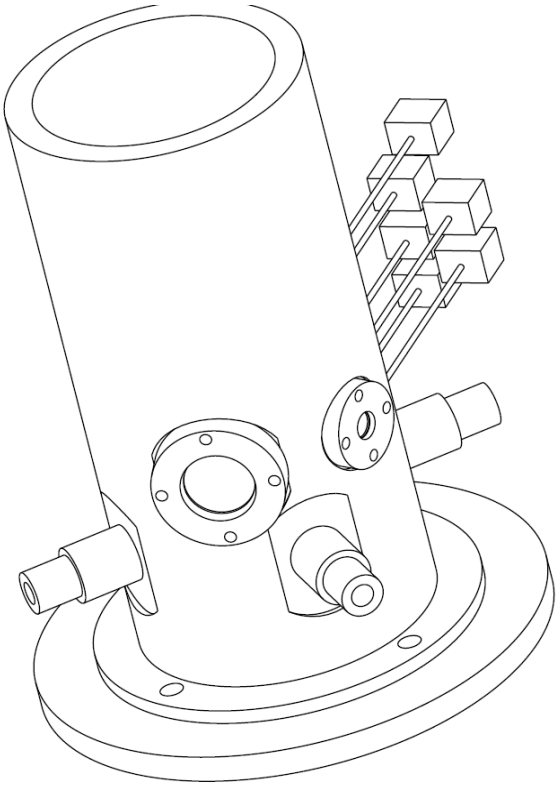

Figure 6-5. Additional UV window port for 90° optical access.

Finally, an advanced reactor model is of primary importance to understanding of the combustion behavior of this burner and to implement adequate diagnostics.

Reacting turbulent flow simulations are an unavoidable step toward a more accurate reactor network approach. An analysis has to be performed in order to choose the adequate simulation in terms of computing time, complexity and predictions between different model such as the LES, DNS, or other turbulent reacting flow model coupled with simple chemistry. (See Chapter 3, Kinetic Modeling)

Based on this simulation, a much more complex reactor neural network model could be created and used to compare with the reference fuel performances for retro-feeding. The current model using 3 reactors and implemented with n-heptane

mechanism could be upgraded with an additional soot formation mechanism and a resolved reactor network including a larger number of CSTR. A good matching between the kinetic simulation and the experimental results is a necessary step to provide qualitative data on fuel oxidation kinetics.

Conclusions

A novel burner design has been created for combustion research. Based on different simulations, the surrounding combustion system has been designed in order to fulfill different functions, such as cooling the wall of the reaction zone, supplying, metering, and controlling the air, and finally mixing, atomizing and vaporizing the liquid fuel. The flexibility criterion in terms of flow rate of air, mixture composition, and temperature has been of primary importance during the whole design process. The combustor rig has been machined and its implementation has started. This system is expected to operate at residence times in the primary zone between 0.5 and 4ms, with a reactor temperature from 1300-2400K, and an expected maximum total power of 40kW. The feed temperature can be varied between 400 and 700K. This rig is implemented with a wide possibility of mixture composition including air, n heptane, methane, different levels of syngas, and under dilution by CO_2, water vapor, and nitrogen. A line of sight type optical access has been implemented for species and temperature probing at the exit of the primary zone. This system has been designed to provide a laboratory-scale research tool to investigate the stability limits and combustion efficiency of different types of fuel, as well as characterizing the transition to a flameless regime

APPENDIX A
EQUATIONS OF GAS DYNAMICS MODEL

These equations are used in the gas dynamics model presented in Chapter 3. The isentropic coefficient γ is defined by:

$$\gamma = \frac{C_p}{C_v},$$

where C_p and C_v are the specific heats, at constant volume and constant pressure respectively.

Isentropic flow

$$\frac{A}{A^*} = \frac{1}{M}\left[\left(\frac{2}{\gamma+1}\right)\left(1+\frac{\gamma-1}{2}M^2\right)\right]^{\frac{\gamma+1}{2(\gamma+1)}}$$

$$\frac{p}{p_o} = \left(1+\frac{\gamma-1}{2}M^2\right)^{\frac{\gamma}{1-\gamma}}$$

$$\frac{T}{T_0} = \left(1+\frac{\gamma-1}{2}M^2\right)$$

$$\frac{\rho}{\rho_0} = \left(1+\frac{\gamma-1}{2}M^2\right)^{\frac{1}{1-\gamma}}$$

Fanno flow

$$\frac{fL_{\max}}{D} = \frac{\gamma+1}{2\gamma}\ln\left(\frac{\frac{\gamma+1}{2}}{1+\frac{\gamma-1}{2}M^2}\right) - \frac{1}{\gamma}\left(1-\frac{1}{M^2}\right) - \left(\frac{\gamma+1}{2\gamma}\right)\ln\left(\frac{1}{M^2}\right)$$

$$\frac{T}{T^*} = \frac{\gamma+1}{2+(\gamma-1)M^2}$$

$$\frac{p}{p^*} = \left(\frac{1}{M}\right)\left[\frac{\gamma+1}{2+(\gamma-1)M^2}\right]^{1/2}$$

$$\frac{\rho}{\rho^*} = \frac{1}{M}\left[\frac{2+(\gamma-1)M^2}{(\gamma+1)}\right]^{1/2}$$

$$\frac{p_0}{p_0^*} = \frac{1}{M}\left[\frac{2+(\gamma-1)M^2}{(\gamma+1)}\right]^{\frac{\gamma+1}{2(\gamma-1)}}$$

Rayleigh Flow:

$$\frac{T}{T^*} = \frac{(1+\gamma)^2 M^2}{(1+\gamma M^2)^2}$$

$$\frac{p}{p^*} = \frac{1+\gamma}{1+\gamma M^2}$$

$$\frac{\rho}{\rho^*} = \frac{1+\gamma M^2}{(1+\gamma)M^2}$$

$$\frac{T_0}{T_0^*} = \frac{(1+\gamma)M^2\left[2+(\gamma-1)M^2\right]}{\left(1+\gamma M^2\right)}$$

$$\frac{p_0}{p_0^*} = \left(\frac{1+\gamma M^2}{1+\gamma}\right)\left[\frac{2+(\gamma-1)M^2}{\gamma+1}\right]^{\frac{\gamma}{\gamma-1}}$$

Singularities (from the incompressible flows theory)

In the equation below K is defined as the pressure drop coefficient in the equation:

$$P_{02} = P_{01} - K\left(\frac{\rho U^2}{2}\right),$$

where 1 and 2 correspond respectively to the upstream and downstream size and U to the flow mean velocity.

- Sudden section widening:

$$K = 1 - \frac{A_1}{A_2}$$

- Sudden section restriction:

$$K = \left(\frac{1}{C_c} - 1\right)^2 \frac{A_1}{A_2}$$

With C_c from 0.6 to 1, depending on the radius, 1 for an infinite radius

- Sharp elbow of angle θ (Weisbach):

$$K = 0.457\sin^2\frac{\theta}{2} + 2.047\sin^4\frac{\theta}{2}$$

APPENDIX B
MACHINING DRAWING

The drawings presented in this Appendix B are not necessarily at the scale described in Figure B-1. The reader should refer to the dimensions noted on the drawings.

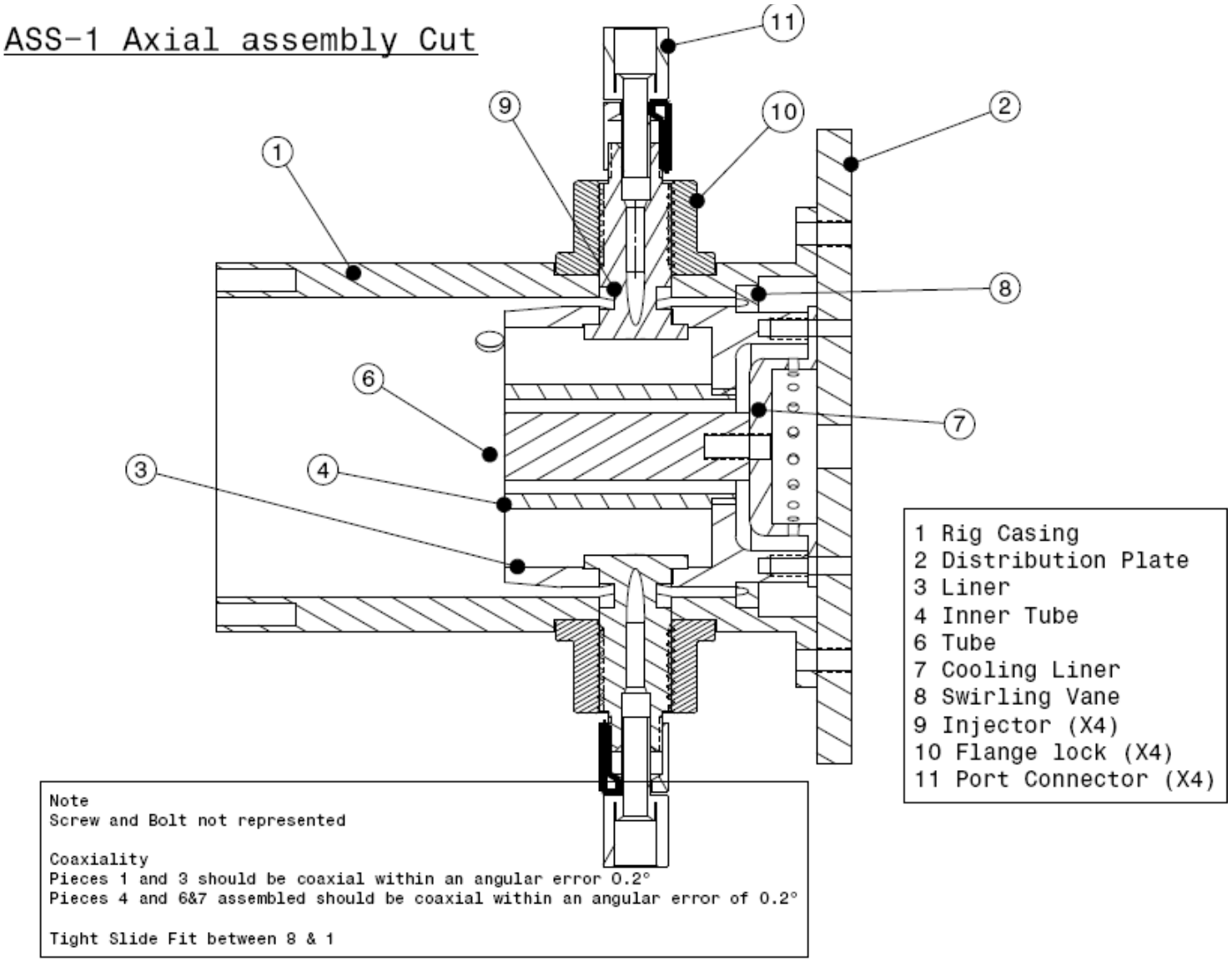

Figure B-1. Machining drawings

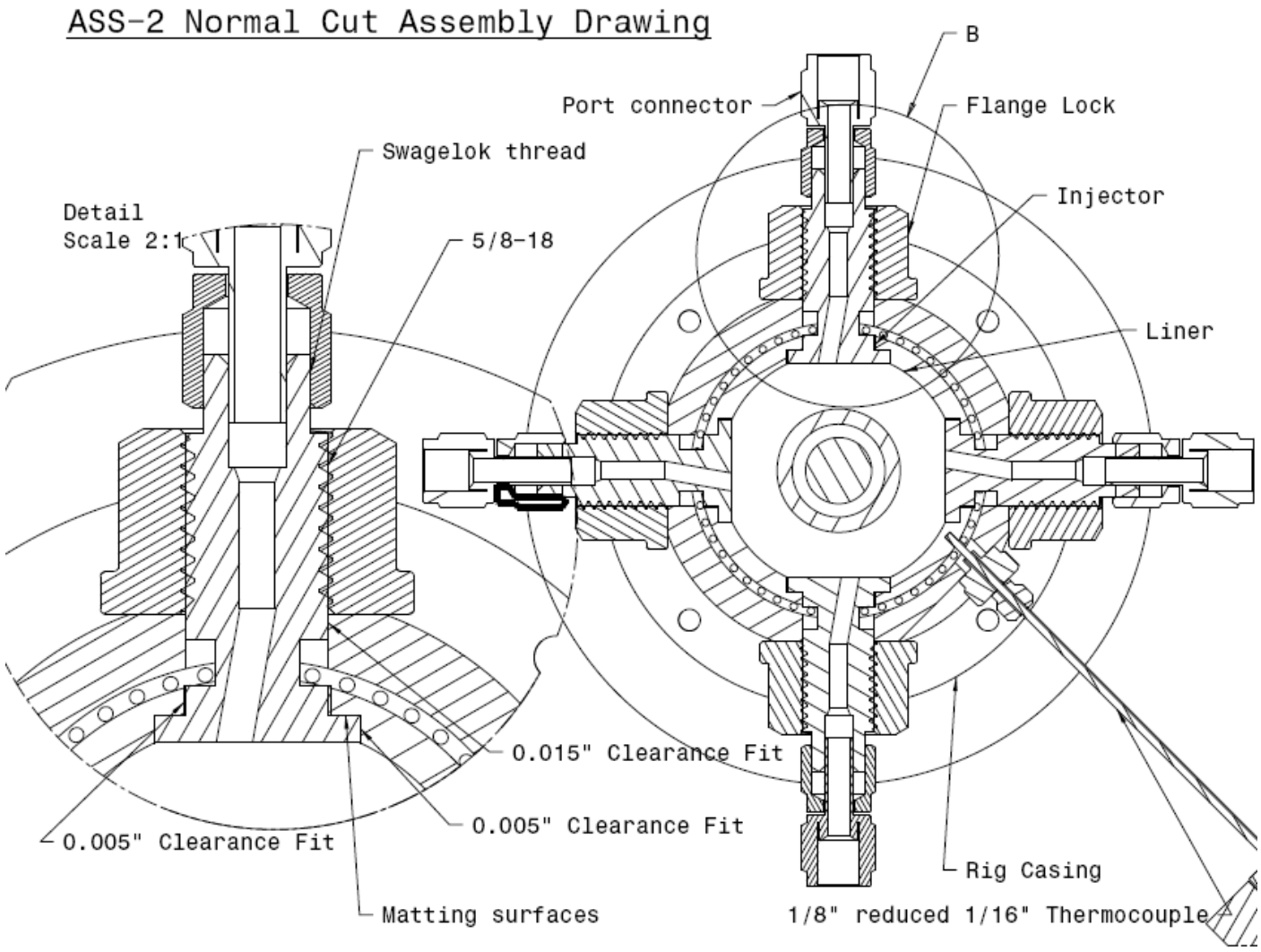

Figure B-1. Machining drawings (continued)

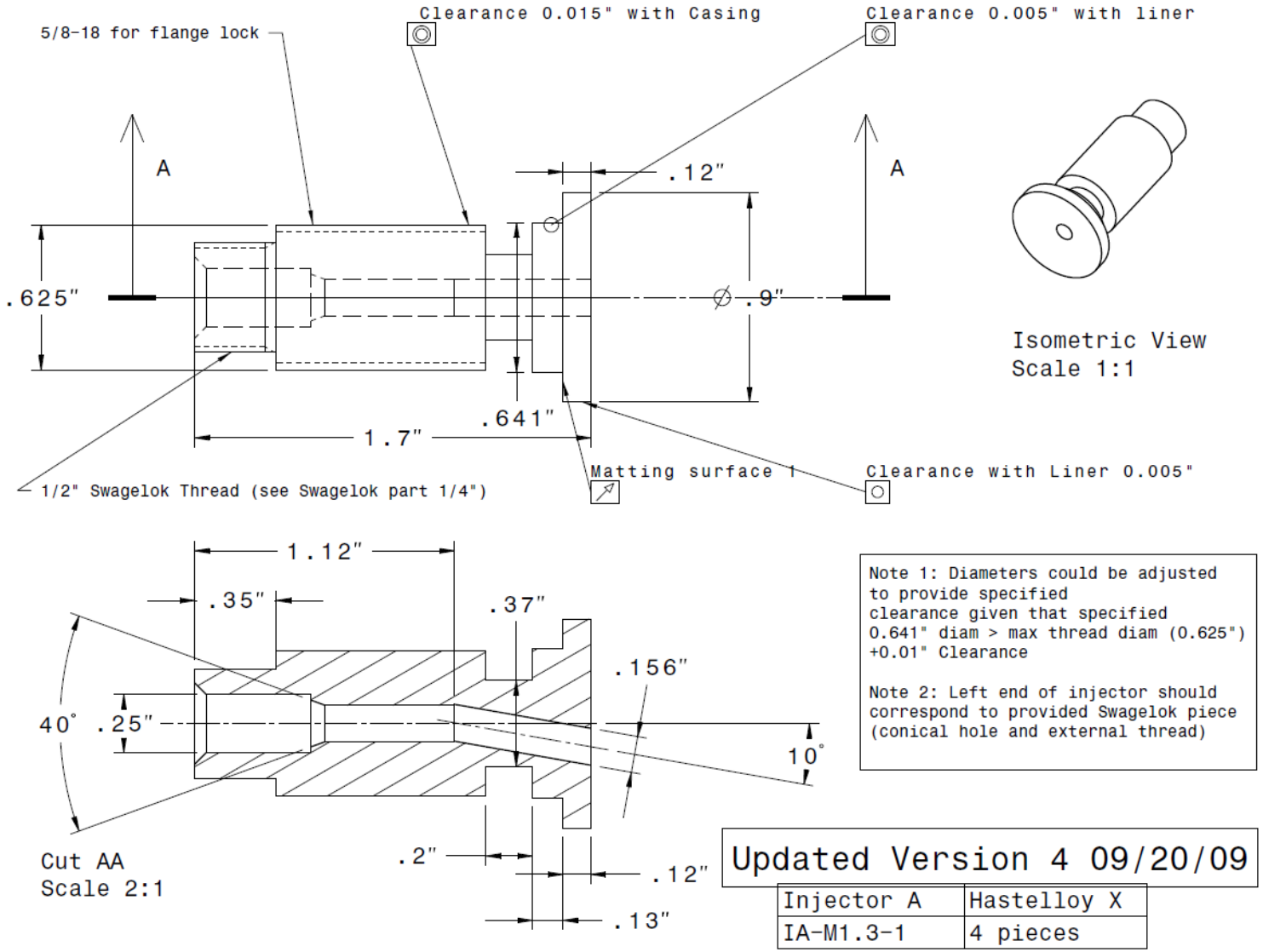

Figure B-1. Machining drawings (continued)

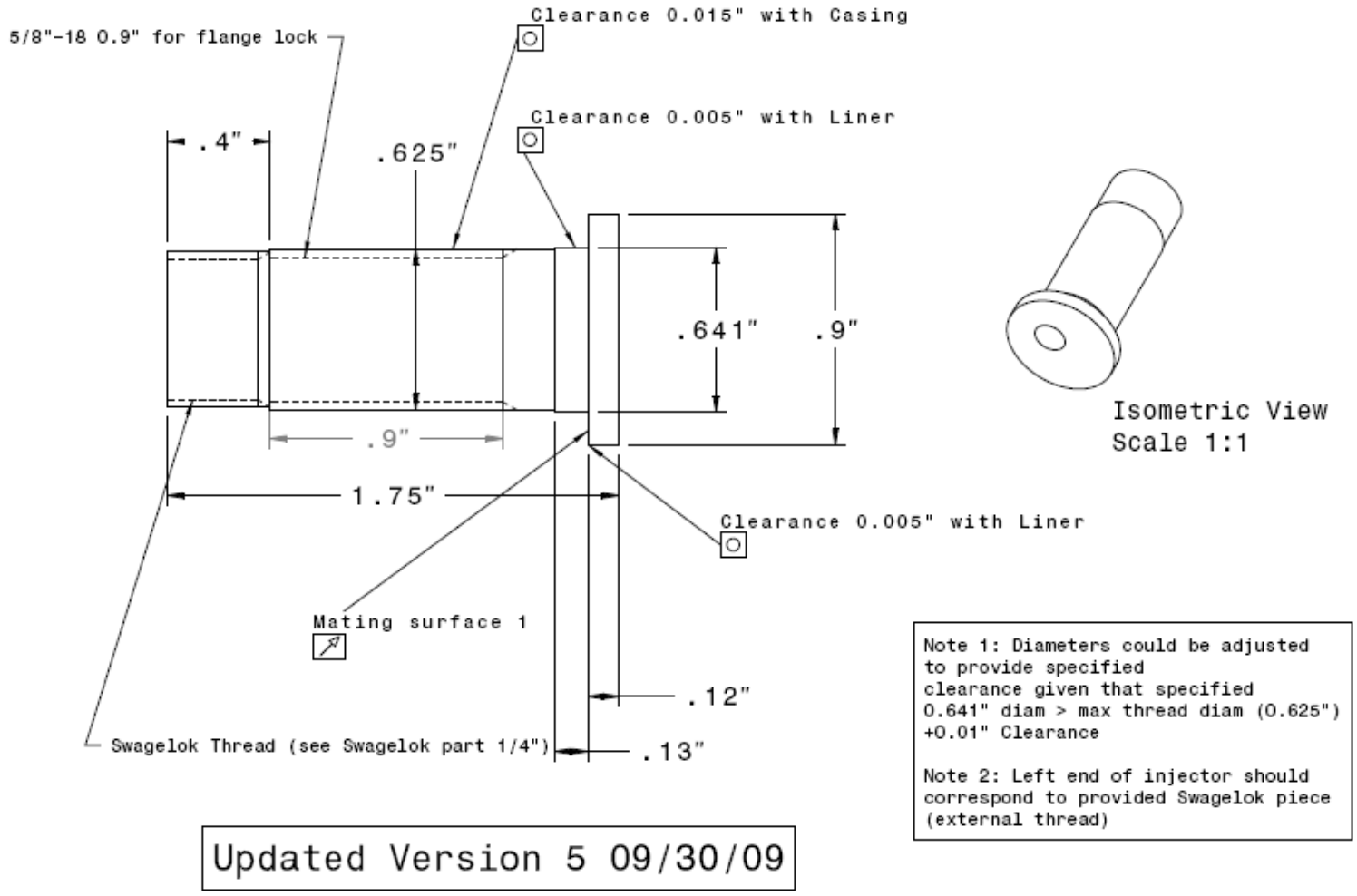

Figure B-1. Machining drawings (continued)

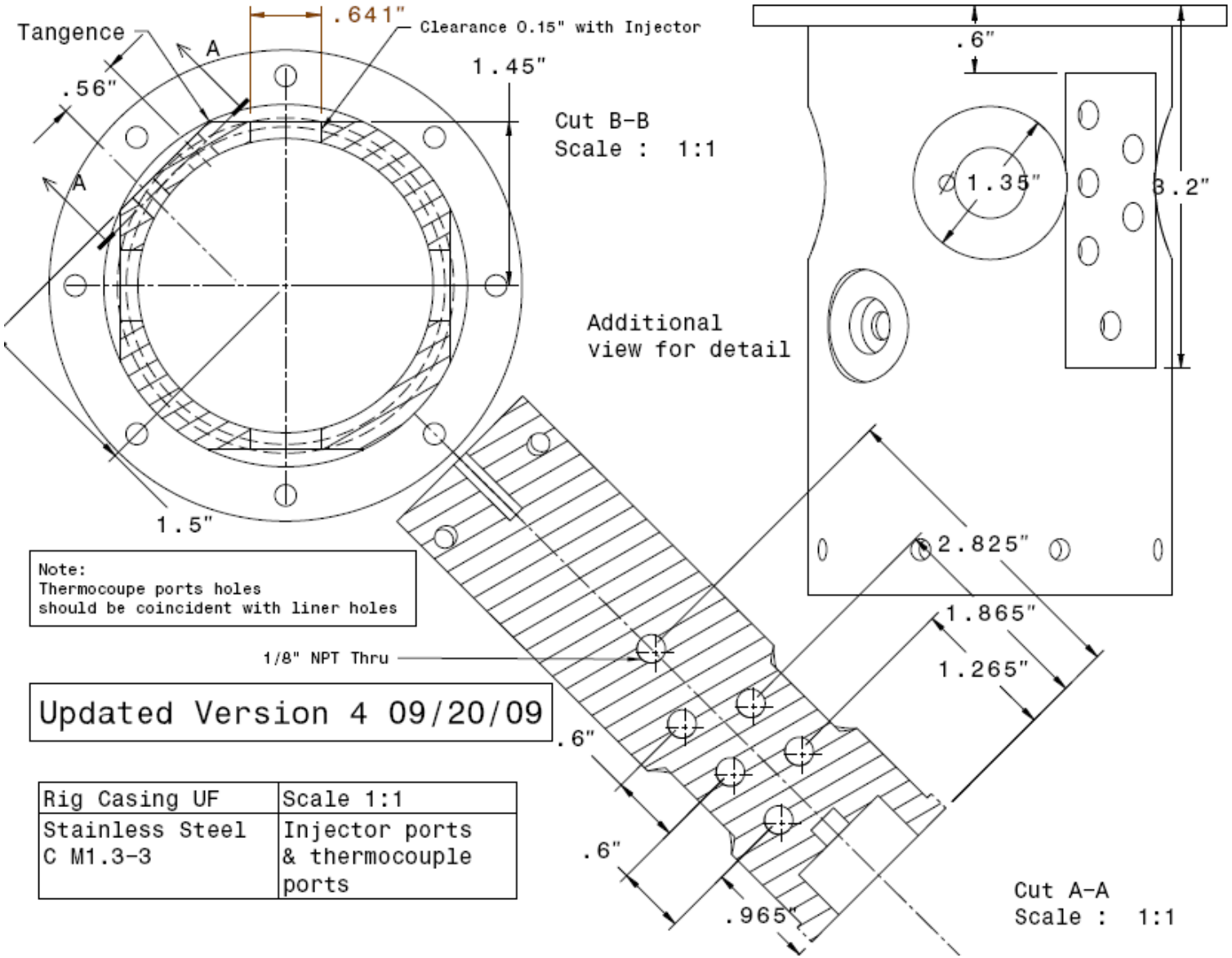

Figure B-1. Machining drawings (continued)

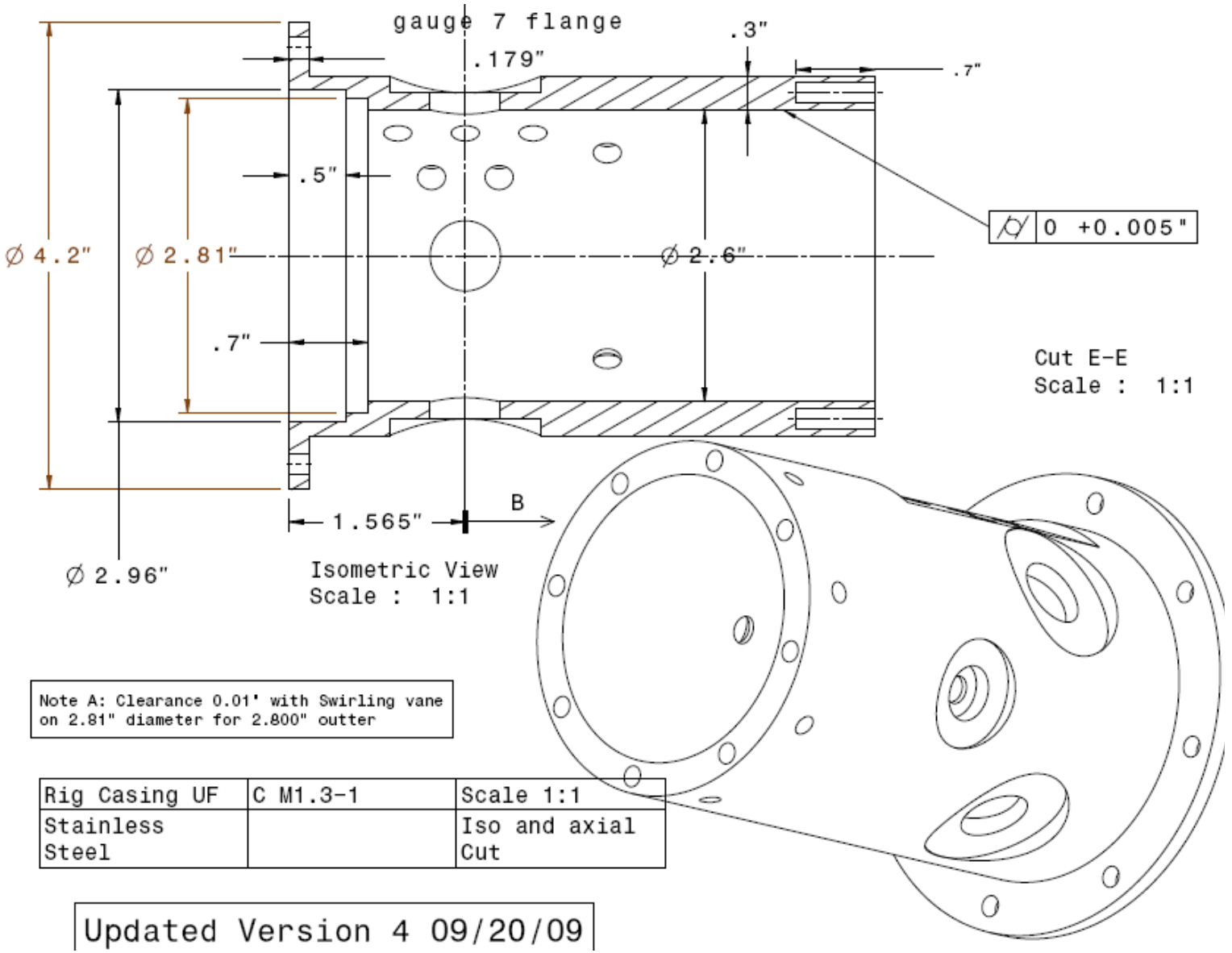

Figure B-1. Machining drawings (continued)

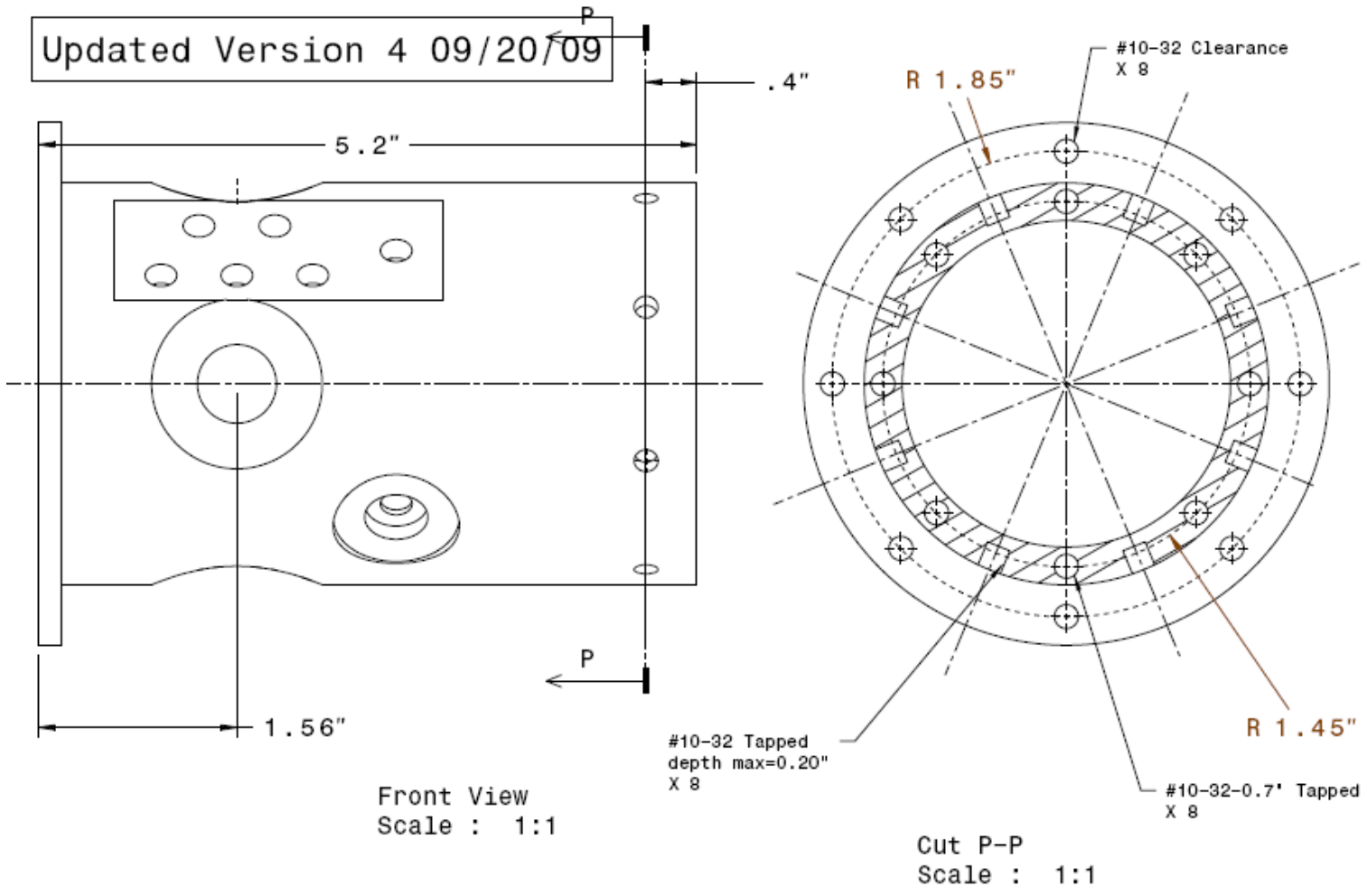

Figure B-1. Machining drawings (continued)

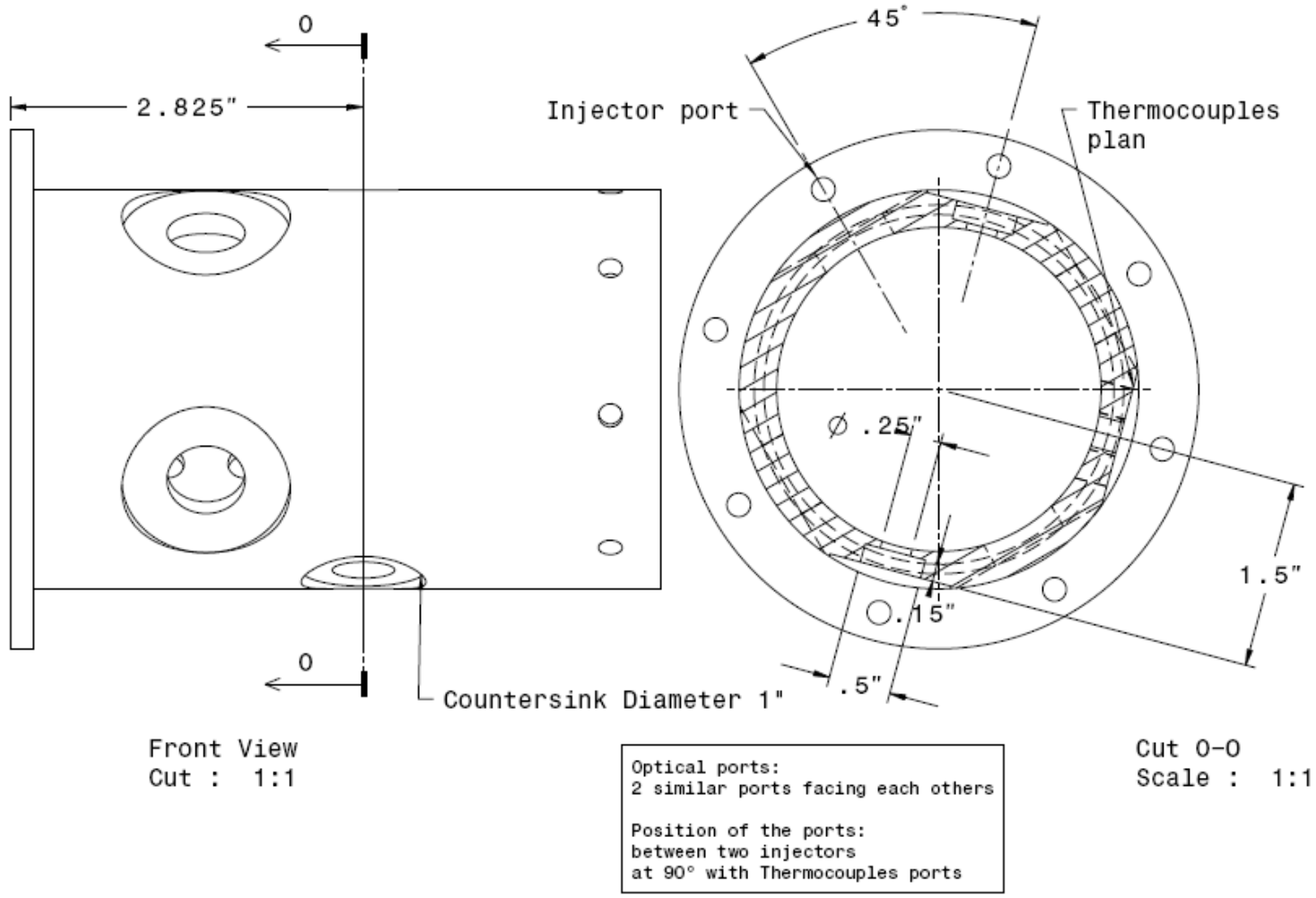

Figure B-1. Machining drawings (continued)

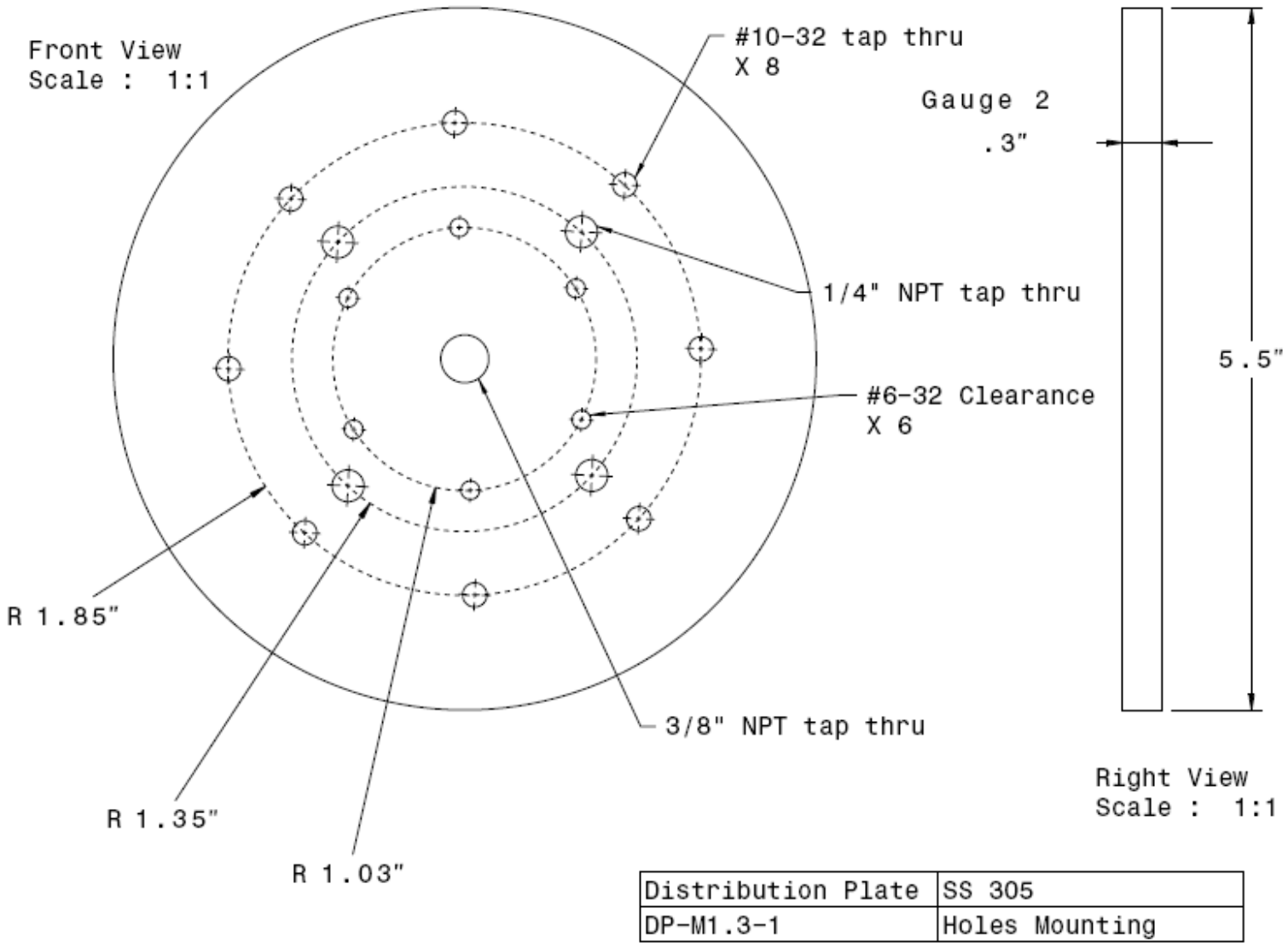

Distribution Plate	SS 305
DP-M1.3-1	Holes Mounting

Figure B-1. Machining drawings (continued)

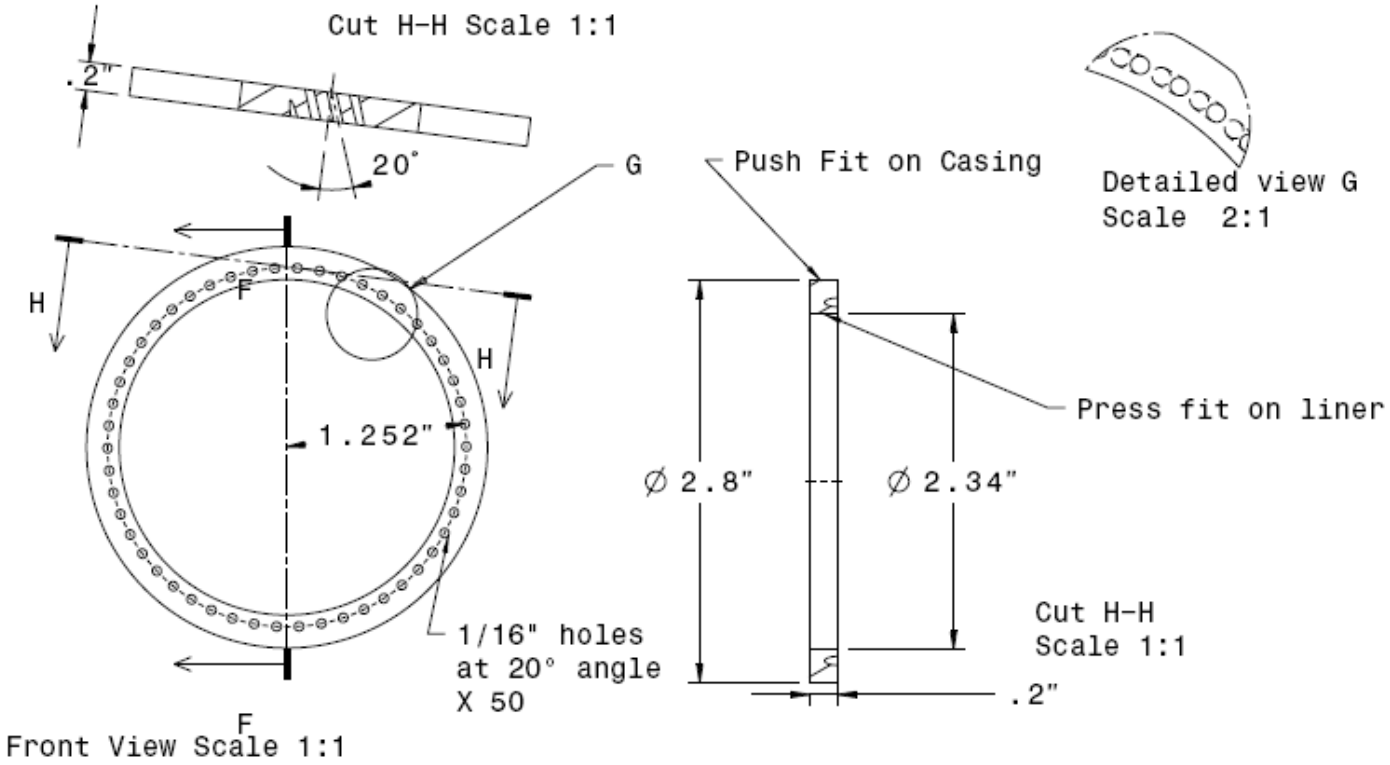

Note A: This part is to be pressed on liner See ASS-1 for position Note B: Clearance 0.010 with Rig casing 2.8"

Swirling vane	SS 305
SV-M1.3-1	

Figure B-1. Machining drawings (continued)

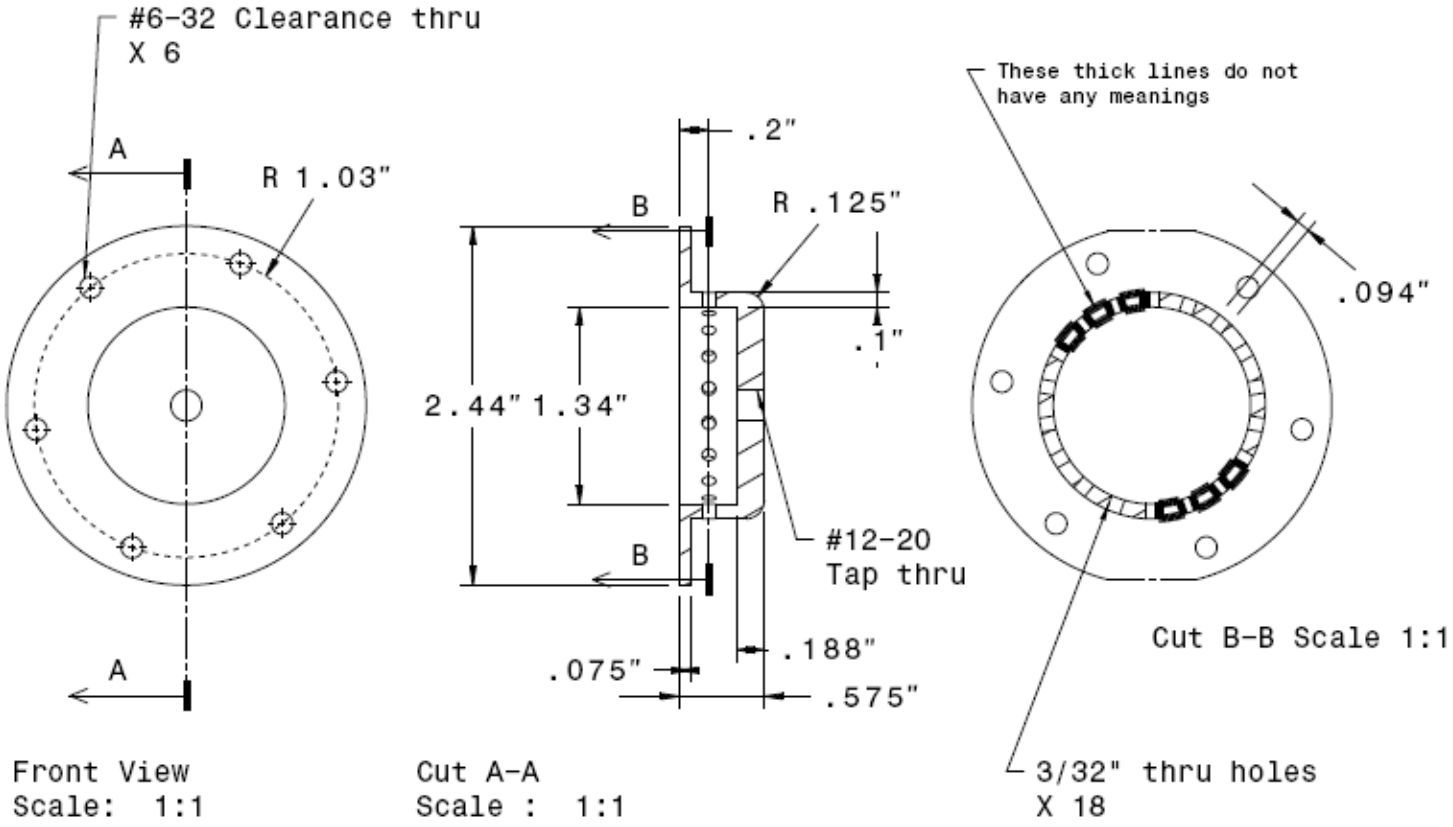

SS 305	Scale 1:1
Stainless Steel	CL-M1.3-1

Figure B-1. Machining drawings (continued)

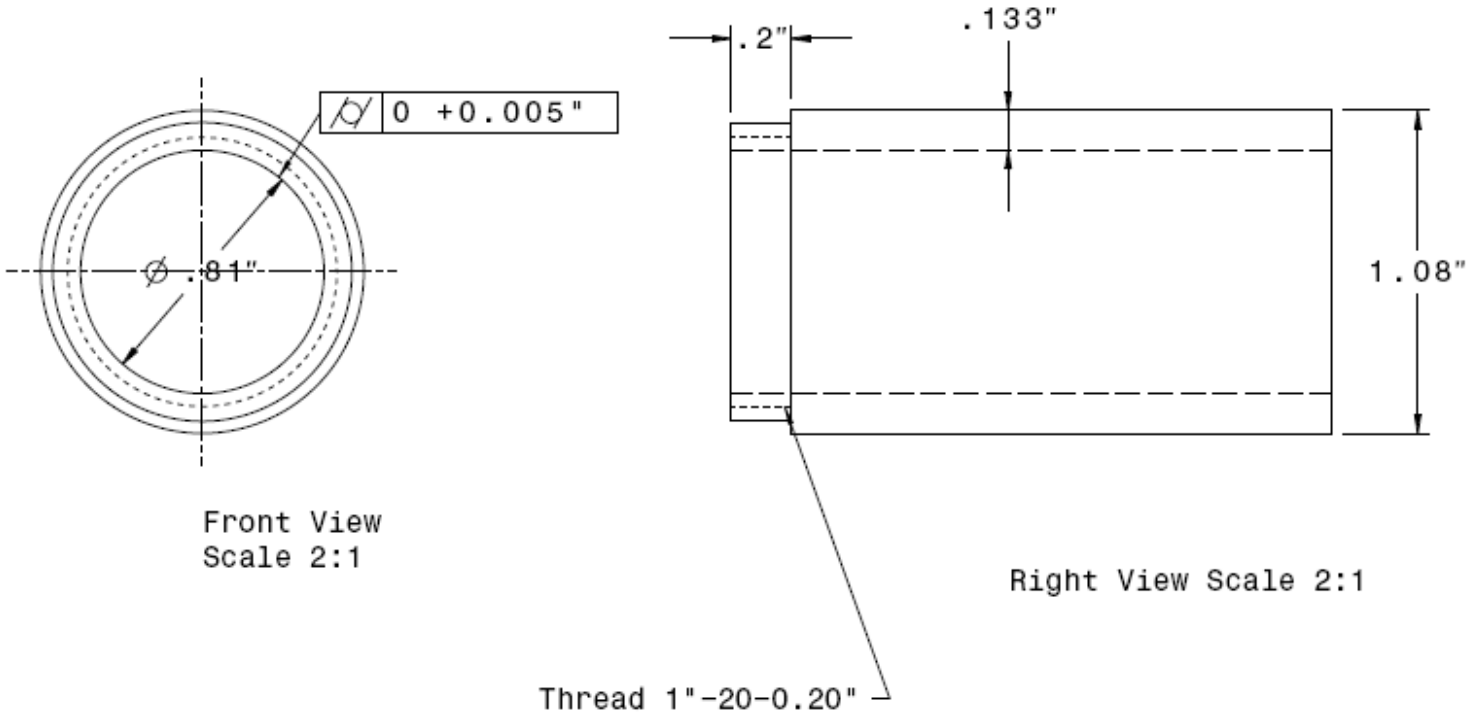

Inner Liner	Scale 2:1	Molybdenum
IL-M1.3-1	1 piece	

Figure B-1. Machining drawings (continued)

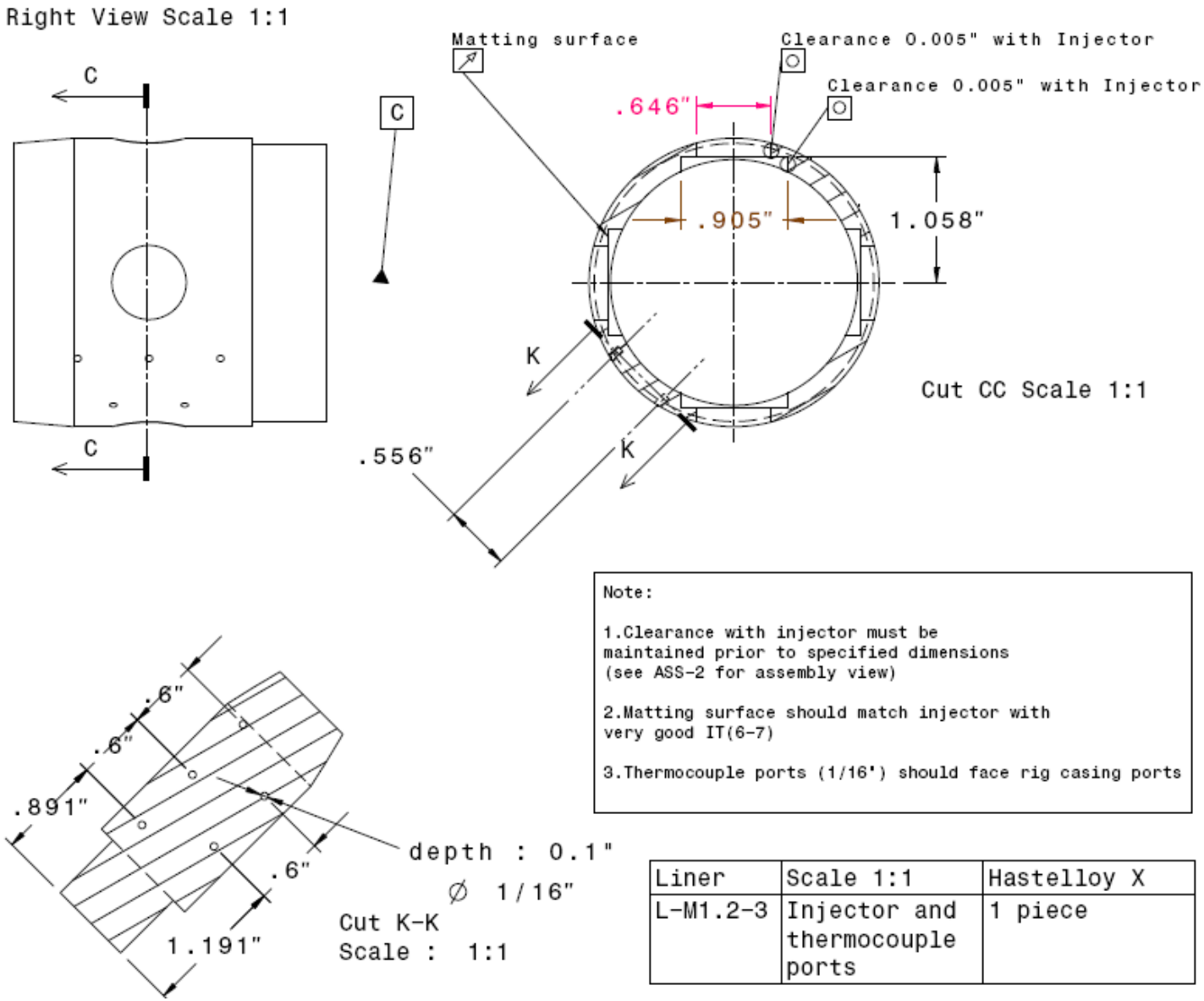

Liner	Scale 1:1	Hastelloy X
L-M1.2-3	Injector and thermocouple ports	1 piece

Figure B-1. Machining drawings (continued)

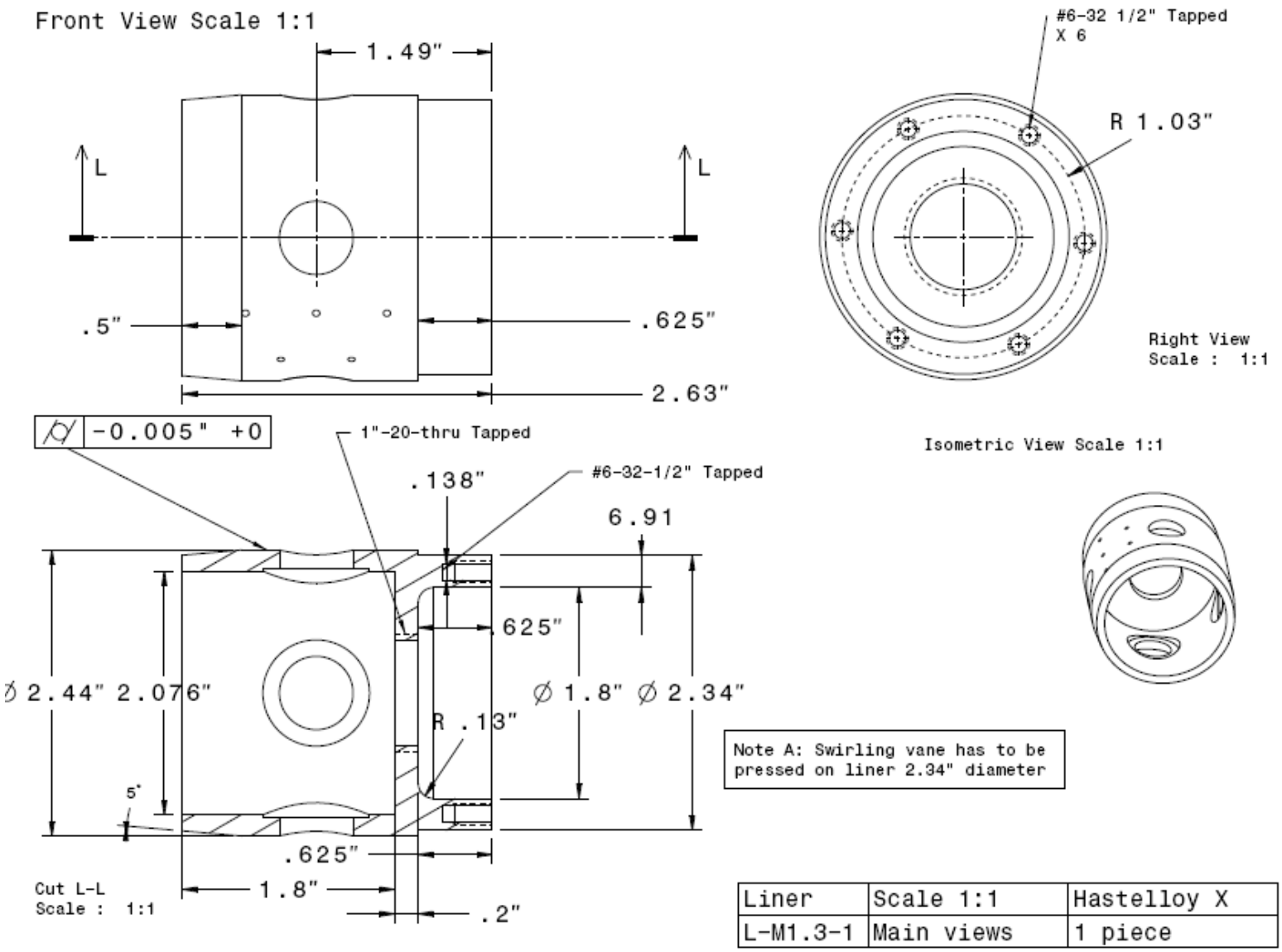

Figure B-1. Machining drawings (continued)

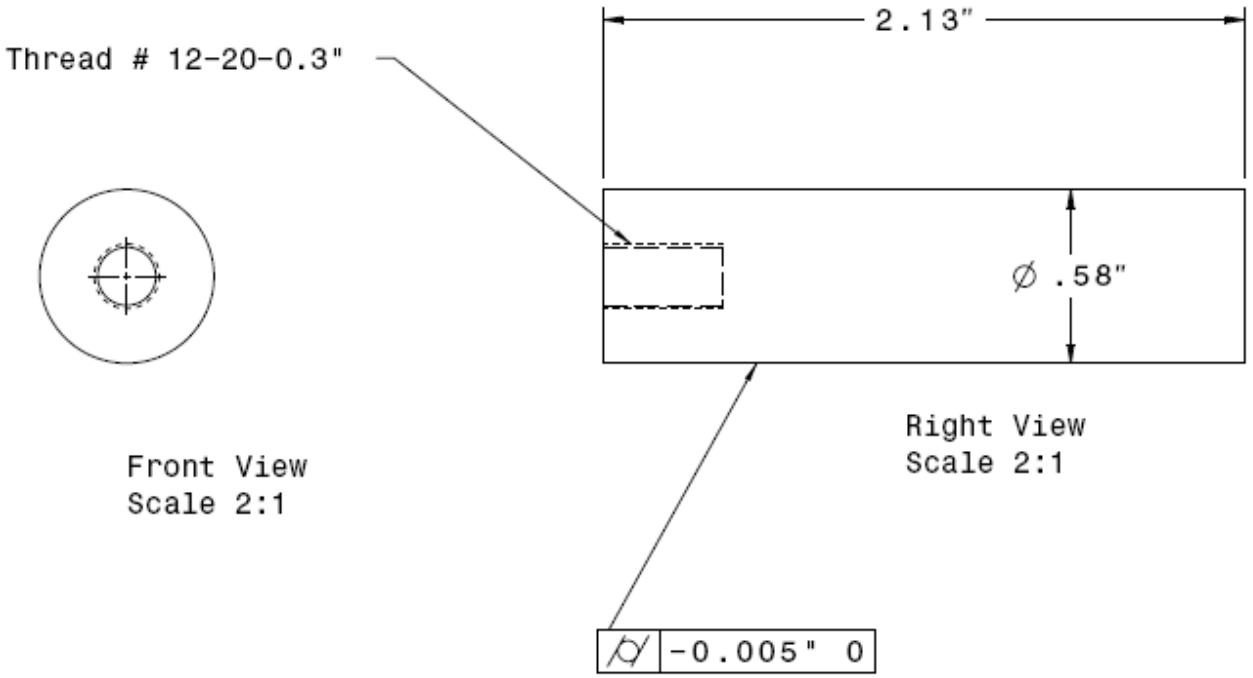

Tube	SS305
T-M1.3-1	1 piece

Figure B-1. Machining drawings (continued)

LIST OF REFERENCES

1. Y. Huang and V. Yang, Prog. Energy Combust. Sci. 35 (2009) 293–364.

2. D. M. Kalitan, J.D Mertens, M.W. Crofton, E. L. Petersen, J. Propulsion and Power, 23 (2005) 1291.

3. J. Natarajan, T. Lieuwen, J. Seitzman, Combust. Flame 151 (2007) 104–119.

4. G. P Smith, D. M. Golden, M. Frenklach, N. W. Moriarty, B. Eiteneer, M. Goldenberg, C. T. Bowman, R. K. Hanson, S. Song, W. C. Gardiner, Jr., V. V. Lissianski, Z. Qin http://www.me.berkeley.edu/gri_mech/.

5. Q. Zhang, D. R. Noble, T. Lieuwen, Trans. ASME 129 (2007) 688-694.

6. J. P. Longwell, M. A. Weiss, Indust. Eng. Chem. 47 (1955) 1634-1643.

7. F.J. Wright, 12th Symposium (International) on Combustion, the Combustion Institute, Pittsburgh, 1969, pp 867.

8. W. S. Blazowski, R.B. Edelman, and E. Wong, Summary Technical Progress Report, Exonn Research and Engineering, 1980

9. B. R. Bowman, D. T. Pratt and C. T. Crowe, 16th Symposium (International) on Combustion, The Combustion Institute, Pittsburgh, 1977, pp 819.

10. D. Bradley, S. B. Chin, M. S. Draper and G. Hankinson, 16th Symposium (International) on Combustion, The Combustion Institute, Pittsburgh, 1977, pp 1571.

11. Nenniger J. E., PhD dissertation, Massachussetts Institute of Technology, Cambridge, 1983.

12. J. Zelina, D. R. Ballal, Transactions of the ASME 119 (1997) 62-67.

13. J. Zelina, J.W. Blust, D.R. Ballal, ASME Paper, GT-47, (1996) 43-58.

14. S.L. Manzello, D.B. Lenhert, A. Yozgatligl, G.W. Mulholland, M.R. Zachariah, W. Tsang, Proc. Combust. Inst. 31 (2007) 675-683.

15. T. Lieuwen, V. McDonell, E.Petersen, D. Santavicca, J. Eng. Gas Turb. Power 130 (2008) 011506-1-9.

16. M.A. Weiss, R.J. Lang, J.P Longwell, Indust. Eng. Chem. 50 (1958) 257-264.

17. B. Axelsson, R. Collin, P.E. Bengtsson, Appl. Phys. B Lasers and Optics, 72, (2001), 367–372.

18. H. J. Curran, P. Gafluri, W. J. Pitz C. K. Westbrook, Combust. Flame 114 (1998) 149-177.

19. J. Herzler, L. Jerig, P. Roth, Proc. Combust. Inst. 30 (2005) 1147–1153.

20. N. M. Marinov, W. J. Pitz, C. K. Westbrook, A. M. Vincitore, M. J. Castaldi, S. M. Senkan, *Comb. Flame* 144 (1998) 192-213.

21. N. M. Marinov, W.J. Pitz, C.K. Westbrook, M. Hori, N. Matsunaga, Proc. Comb. Inst. 27 (1998) 389-396.

22. A. Demirbas, Energy Sources, Part A: Recovery, Utilization, and Environmental Effects 29 (2007) 1507–1512.

23. Srinivasan, W. Ellis, J. F. Crittenden, W. E. Lear, B. Rotavera, E. L. Petersen, Proceedings of ASME Turbo Expo 2008: Power for Land, Sea and Air, June 9-13, Berlin, Germany, 2008, GT 51447.

24. A.K. Gupta, J. Eng. Gas Turb. Power 126 (2004) 9-19.

25. K. Maruta, K. Muso, K. Takeda,T. Niioka, Proc. Combust. Inst. 28 (2000) 2117–2123.

26. J.A. Wunning, J.G. Wunning, Prog. Energy Combust. Sci., 23 (1997) 81–94.

27. P.J. Coelho, Comb. Flame, 124 (2001) 503-518.

28. T. Plessing, N. Peters, J.G. Wünning, Twenty-Seventh Symposium (Int.) on Combustion, The Combustion Institute, Pittsburgh, 1988, pp 3197–3204.

29. A.Cavaliere, M. de Joannon, Prog Energy Combust. Sci. 30 (2004) 329-366.

30. T.S. Nemec, W.E. Lear, ASME Paper, 96-GT-434 (1996) 1-7.

31. W. Ellis, W. E. Lear, S.A. Sherif.47th AIAA Aerospace Sciences Meeting Including The New Horizons Forum and Aerospace Exposition, 5-8 January, Orlando, Florida, 2009, pp 255-262.

32. Singh W. E. Lear, Proceedings of ASME Turbo Expo 2009: Power for Land, Sea, and Air, June 08-12, 2009, Orlando, USA, 2009, GT2009-60272.

33. J. P. Longwell, E. E. Frost, M. A. Weiss, J. Indust. Eng. Chem. 45 (1953) 1629-1633.

34. R. Ballal, A. H. Lefebvre, J. Eng. Power 101 (1979) 343-348.

35. Y.D. Wang, Y. Huang , D. McIlveen-Wright, J. McMullan, N. Hewitt, P. Eames S. Rezvani, Fuel Processing Tech. 87 (2006) 727–736.

36. M Harris., Small Engine Group, Florida Turbine Technology, Jupiter, Florida, 2009, personal communication.

37. V. W. Greenhough, A.H. Lefebvre, 6th Symposium (International) on Combustion, Reinhold, New York, 1957, pp858-869.

38. A.M. Eaton, L.D. Smoot, S.C. Hill, C.N. Eatough, Prog. Energy Combust. Sci. 25 (1999) 387–436.

39. M. Falcitelli, S. Pasini L. Tognotti, Computer and Chem. Eng. 26 (2002) 1171–1183.

40. A.B. Lebedev, A.N. Secundov, A.M. Starik, N.S. Titova A.M. Schepin, Proc. of the Combust. Inst. 32 (2009) 2941–2947.

41. A. H. Lefebvre, M.V. Herbert, Proc. Inst. of Mech. Eng. 174 (1960) 463-473.

42. Reeves, National Gas Turbines Establishment, England, NGTE Memo M285, 1956.

43. M. Fishenden, O.A Saunders, Oxford University Press, New York, 1950.

44. Lefebvre A. H., Gas Turbine Combustion, 2nd edition, Taylor & Francis, 1999, pp 50-57.

45. W. Kays, M Crawford, B. Weigand, Convective Heat and Mass Transfer, 4th Edition, McGraw-Hill, 2005, pp 302-305.

46. W. Kays. E. Leung, Intern. J. Heat Mass Transfer, 6 (1963) 537-557.

47. G.A. Greene, C.C. Finfrock, T.F. Irvine Jr, Exp. Therm. Fluid Sci. 22 (2000) 145-153.

48. W. Thiele, K.J Kundig, D.W. Murphy, G. Soloway, B. Duffin, SAE Technical Paper 900365.

49. S. R. Turns, An introduction to Combustion, 2nd Edition, McGraw-Hill, 2000, pp 441-444.

50. R.P Tye, D.R Salmon, Proceedings of the 27th International Thermal Conductivity Conference and the 15th International Thermal Expansion Symposium, 2005, pp 372-381.

51. S. Kumar, P.J. Paul, H.S. Mukunda, Proc. Combust. Inst. 30 (2005) 2613-2621.

52. Y. Mori, K. Kutagami, Intern. J. Heat Mass Transfer 10 (1967) 1801-1813.

53. M. Ó. Conaire, H. J. Curran, J. M. Simmie, W. J. Pitz, C. K. Westbrook, Intern. J. of Chem. Dynamics, 36 (2004) 603-622.

54. T. Madhiyanon, N. Piriyarungroj, S. Soponronnarit**,** Energy Conv. and Manag. 49 (2008) 1202-1210.

55. R.A. *Shandross*, J.P Longwell, J.B. Howard, Combust. Flame, 85 (*1991)* 282-284.

56. W.E. Kaskan, Proc. Combust. Inst. 6 (1957) 134–143.

57. A. C. Eckbreth, Laser Diagnostics for Combustion Temperature and Species, 2nd edition., Combustion Science and Technology Series, vol. 3, Gordon and Breach Publishers, New York, 1996

58. N. Zhang, Z. Tian, Y. Y. Leng, H. T. Wang, F. Q., J.H. Meng, Science in China Series D-Earth Sciences 50 (2007) 1171-1178.

59. G. Mie, Ann. Physik, 25 (1908) 377-445.

60. L. Rayleigh, Philos. Mag., 41, (1871) 274-279 reprinted in Scientifics papers by Lord Rayleigh, Vol 1, No.8, Dover, New York, 1964.

61. H. Geitlinger, Th. Streibel, R. Suntz, H. Bockhorn, Proceedings of the 27th International Symposium on Combustion, The Combustion Institute, Pittsburgh,1998, pp1613-1621.

62. L. Vander Wal., Z. Zhou, M. Y. Choi, Combust. Flame 105 (1996) 462-470.

63. G. D. Yoder, P.K. Diwakar, D.W. Hahn, Appl. Optics 44 (2005) 4211-4219.

64. M. G Allen, Meas. Sci. Technol. 9 (1998) 545–562

65. B. Singh, W.E. Lear, 7th International Energy Conversion Engineering Conference, AIAA, Denver, Colorado, Aug. 2-5, 2009, AIAA 2009-4570.

66. C. J. Marek, R.R. Tacina, National Aeronautics and Space Administration, Springfield, Va, 1976, NASA technical memorandum 3464.

67. M. Y. Frenklach, Phys. Chem. Chem. Phys**.** 4 (2002) 2028 -2037.

68. A. Alexiou, A. Williams, Fuel 74 (1995) 153-158.

69. H. Wang, B. Zhao, B. Wyslouzil, K. Streletzky, Proc. Combust. Inst. 29 (2002) 2749-2757.

70. S. Macadam, PhD Dissertation, Massachussetts Institute of Technology, Cambridge, 1997.

71. F.W. Lam, J.P. Longwell, J.B. Howard, Twenty-Third Symposium (International) on Combustion, The Combustion Institute, Pittsburgh, 1990, pp 1477-1484.

72. N. J. Brown, K. L. Revzan, M. Frenklach, Twenty-Seven Symposium (International) on Combustion The Combustion Institute, Pittsburgh, 1997, pp 1573-1580.

73. B. Singh, PhD candidate, Department of Aerospace and Mechanical Engineering, University of Florida, Gainesville, 2009, personal communication.

BIOGRAPHICAL SKETCH

Benoit Fond was born in Angouleme, France, the fourth of a six-child family. After two years of preparatory program in mathematics and physics at the Lycee Montaigne in Bordeaux, he passed the entrance examination of Arts et Metiers Paristech where he pursued the 3-years *diplome d'ingenieur*. This degree is equivalent to a Master of Science in the French Graduate Schools of Engineering also called "Grandes ecoles". He studied mechanical and industrial engineering from 2006 to 2008 and enrolled at the University of Florida in August 2008 to pursue a Master of Science in mechanical engineering as part of a double diploma.